Summer 2010

A multi-scale observation-modeling study of summertime California air quality

Min Huang
University of Iowa

A MULTI-SCALE OBSERVATION-MODELING STUDY OF SUMMERTIME CALIFORNIA AIR QUALITY

by

Min Huang

A thesis submitted in partial fulfillment
of the requirements for the Master of Science degree
in Chemical and Biochemical Engineering in the
Graduate College of The University of Iowa

July 2010

Thesis Supervisor: Professor Gregory R. Carmichael

Graduate College
The University of Iowa
Iowa City, Iowa

CERTIFICATE OF APPROVAL

_____

MASTER'S THESIS

_____

This is to certify that the Master's thesis of

Min Huang

has been approved by the Examining Committee
for the thesis requirement for the Master of Science
degree in Chemical and Biochemical Engineering at the July 2010
graduation.

Thesis Committee: _____
Gregory R. Carmichael, Thesis Supervisor

_____
Charles O. Stanier

_____
Thomas M. Peters

To My Family

ACKNOWLEDGEMENTS

I would like to thank my graduate advisor Dr. Gregory Carmichael for introducing me the graduate study on atmospheric modeling at the University of Iowa, and for his guidance and support on this research. I thank Dr. Charles Stanier and Dr. Thomas Peters for teaching interesting and informative atmospheric-related classes and being helpful thesis committee members. I thank Dr. Vicki Grassian for having co-advised me on experimental research. I thank all the faculty members in the department of Chemical and Biochemical Engineering for offering me the opportunity to be part of the program. I also appreciate the comments and suggestions from atmospheric experts working in other universities, research institutions/agencies, and government.

I would like to thank Bhupesh Adhikary, Scott Spak, Sarika Kulkarni, Yafang Cheng and Chao Wei for helping me with STEM and WRF models, analysis tools and writing. I thank Aditsuda Jamroensan and Pallavi Marrapu for helping me start with the ARCTAS-CARB project. I thank Linda Wheatley, Jane Frank, Jeremie Moen and the Engineering CSS staff for their administrative and technical support. I also enjoy working with Jaemeen Baek, Sang Rin Lee, Sinan Sousan, Alicia Pettibone, Pablo Saide, Man Yu, Robert Bullard, Anand Sharma, Courtney Hatch, Jennifer Schuttlefield, John Pettibone, Juan Navea, Julie Park, Hongbo Fu, Sherrie Elzey, Pragati Galhotra, Kelly Gierlus and Gayan Rubasinghege.

I would like to thank my parents Shijian Huang and Jianhua Shen for their encouragement and support on my graduate study through the years. Both as engineers, they show me good examples of hard working and critical thinking.

ABSTRACT

Multi-scale tracer and full-chemistry simulations with the STEM atmospheric chemistry model have been used to analyze the effects of both transported and local production of pollutants on California air quality during the ARCTAS–CARB experiment conducted in June 2008.

During this summer experiment, simulated and observed Ozone (O_3) transport patterns from the coast to inland northern California are shown to vary based on the meteorological conditions and the oceanic O_3 profiles, which are strongly episodically affected by Asian inflows. During a specific period (June 21–June 24), high coastal O_3 air-masses at altitudes ~2–4 km can be transported inland and can significantly influence the surface O_3 20–30 hours later over the northern Sacramento valley and the southern California can be indirectly affected by in-state transport. The model performance was improved by using lateral boundary conditions (LBCs) downscaled from RAQMS global model that assimilated satellite data, as well as the LBC based on NASA DC-8 airborne observations during the experiment. The effects of oxidized sulfur (SO_x) in these transported Asian air-masses over California are relatively less strong than O_3 and its precursors. Local emissions are the major contributor to the elevated sulfur concentrations below 5 km. Several SO_x emission inventories (EI) are compared and the simulated SO_x are validated with various observational datasets, with special focus on three regions–South Coast, San Francisco and Central Valley. The resolutions and the spatial and/or temporal variations of SO_x emissions in all EIs remain to be further improved. Both terrestrial and maritime emissions are found to be important to coastal SO_x distributions. Their percentile contributions to coastal SO_x spatial distributions for the experiment week are estimated, and their absolute contributions during flight periods are then quantified with observational-based scaling factors. The California-Mexico pollutant interaction mainly occurred between two sister city pairs–the coastal city pair

(San Diego–Tijuana) was heavily affected by both California and Mexico maritime emissions through both directions, due to the northwesterly winds during daytime and the opposite winds through the nights. This effect was extended to the inland city pair (Mexicali–Calexico) by dominant inland westerly winds, where was also shortly impacted by southerly winds from Mexico, during which time limited areas over the southeast of California were also affected.

TABLE OF CONTENTS

LIST OF TABLES viii

LIST OF FIGURES ix

CHAPTER 1 INTRODUCTION 1

1.1 Background 1
1.2 Regional-scale chemical transport model and input data 3
1.2.1 Model 3
1.2.2 Meteorology 5
1.2.3 Emissions 6
1.2.4 Lateral Boundary Conditions 7
1.3 Research objectives and thesis outline 8
1.4 Summary of contributions 9

CHAPTER 2 IMPACTS OF TRANSPORTED BACKGROUND OZONE ON CALIFORNIA AIR QUALITY 16

2.1 Introduction 16
2.2 Observational data 19
2.3 Results and discussions 20
2.3.1 O_3 concentrations and air-mass movement during ARCTAS-CARB 20
2.3.2 Coastal-inland O_3 transport 22
2.3.3 Model LBC sensitivity studies 27
2.3.4 Model performance improvement 29
2.3.4.1 Methodology 29
2.3.4.2 Model performance improvement at the surface 30
2.3.4.3 Model performance improvement along the flight path 32
2.4 Summary and conclusions 33

CHAPTER 3 EFFECTS OF EMISSIONS AND TRANSPORT ON SULFUR DISTRIBUTIONS OVER CALIFORNIA 59

3.1 Introduction 59
3.2 Observational data 62
3.3 Results and discussions 63
3.3.1 Emission inventory comparisons 63
3.3.2 Model results validation 65
3.3.2.1 Comparison with surface observations 65
3.3.2.2 Comparison with flight observations 68
3.3.2.3 Comparison with OMI columns 70
3.3.3 Long-range and regional SO_4 transport events 71
3.3.3.1 Asian inflows and Mexico effects 71
3.3.3.2 Local contributions 73
3.3.3.3 Shipping effects on air quality at coastal and downwind areas 75
3.4 Conclusions 77

CHAPTER 4 SUMMARY AND FUTURE WORK 112

4.1 Summary 112

4.2 Future work.....114
REFERENCES 116

LIST OF TABLES

Table 1.1 State and national O_3 and SO_2 standards 11

Table 1.2 Summary of STEM inputs for base cases in two resolutions 12

Table 1.3 Summary of STEM lateral boundary condition sensitivity studies 13

Table 2.1 Comparisons between observed and modeled O_3 at three northern California sites, better model simulations are in bold (OBS-observations) 36

Table 2.2 Comparisons between observed and modeled O_3 at the southern California site JOT, better model simulations are in bold (OBS-observations) 37

Table 3.1 CARB surface sites monitoring hourly SO_2 79

Table 3.2 Summary of the 24 – hour average emissions (in molecules/cm^2/s) from surface sites in three cases, highest and lowest amounts are in bold and italic respectively 80

Table 3.3 Observed and modeled SO_2 at surface sites over multiple regions.....81

Table 3.4 Observed and modeled fine SO_4 ($\mu g/m^3$) at sixteen IMPROVE sites over California 82

Table 3.5 R^2 between modeled and observed SO_x and OH along all flight tracks over three regions, highest correlations are in bold. 83

Table 3.6 Ratios of Observed/modeled SO_x at < 500 m, based on vertical profiles figures, bold numbers were used to scale shipping emission figures in section 3.3.3 84

Table 3.7 Air masses properties below 1 km AGL along four flight paths, summarized by regions 84

LIST OF FIGURES

Figure 1.1 SO_x emission trends during 1975 – 2020 14

Figure 1.2 State O_3 designations based on both 1-hour and 8-hour standards 15

Figure 2.1 Three domains of the STEM modeling system. 38

Figure 2.2 The identification of air-mass sources during June 22 DC-8 flight time 39

Figure 2.3 12 km WRF wind fields at two altitudes AGL over California at 18 UTC on three days of June, 2008.....41

Figure 2.4 12 km modeled surface CO and O_3 over California at 18 UTC at 18 UTC on three days of June, 2008.....42

Figure 2.5 Vertical profiles of O_3, its precursors and reservoirs at THD, California. 43

Figure 2.6 Time-height (AGL, m) curtain plots of China CO contributions across four sites.....45

Figure 2.7 O_3 time-height (AGL, m) curtain plots from the 12 km base case across four sites.....46

Figure 2.8 Reconstructed O_3 concentrations along three-day back trajectories based on 12 km meteorology fields originating at four sites on June 23.....47

Figure 2.9 The coastal-inland transport pattern 48

Figure 2.10 Trajectories during the specific period. 49

Figure 2.11 Trajectories out of the June 21-24 period.....50

Figure 2.12 Two-dimensional plots of LBC sensitivity study in 60 km grids.....51

Figure 2.13 Time series plots of LBC sensitivity study in 60 km grids 52

Figure 2.14 Assessment of LBCs: RAQMS and 60 km STEM base results were used as LBCs for 60 km and 12 km STEM base cases, respectively. 53

Figure 2.15 Wind fields along the June 22 DC-8 flight path, and the downwind areas 54

Figure 2.16 Impacts of using observational-based LBC on predicted California surface O_3 and CO at 18 UTC on three days of June, 2008 in 60 km grids.....55

Figure 2.17 Impacts of using observational-based LBC on predicted California surface O_3 and CO at 18 UTC on three days of June, 2008 in 12 km grids.....56

Figure 2.18 Observed O_3 time series in comparison with STEM simulations at four sites during the flight week 57

Figure 2.19 Impacts of using observational-based LBC on predicted O_3 along the June 22 and June 24 DC-8 flight tracks below 1km 58

Figure 3.1 DC-8 flight 12-15 (June 18, 20, 22, 24, 2008) paths during the ARCTAS-CARB period. The domains of SC, SF and CV were defined in the boxes. 85

Figure 3.2 The average surface SO_2 emissions during 06/18-24 over the SC area during weekdays, Saturday (June 21) and Sunday (June 22), for three EIs. 86

Figure 3.3 The average surface SO_2 emissions during 06/18-24 over the SF area during weekdays, Saturday (June 21) and Sunday (June 22), for three EIs. 87

Figure 3.4 The average surface SO_2 emissions during 06/18-24 over the Fresno area during weekdays, Saturday (June 21) and Sunday (June 22), for three EIs. 88

Figure 3.5 The average surface weekday SO_4 emissions during 06/18-24 from two EIs over three regions 89

Figure 3.6 The weekday-weekend variations of average surface SO_4 emissions over three regions, during June 18–24 90

Figure 3.7 Time series of surface SO_2 emissions from the three emission inventories during 06/18-24 over multiple regions 91

Figure 3.8 The 24-hr average surface SO_x distributions during 06/18-24 from three model simulations 92

Figure 3.9 12 km WRF wind fields at surface, at multiple times on 06/20. 93

Figure 3.10 Time series plots for observed and modeled SO_2 and SO_4 over four surface regions. Data at multiple sites over SC and SF areas are averaged 94

Figure 3.11 Time series plots for observed and modeled surface SO_2 at SC individual sites 95

Figure 3.12 Weekly-averaged (June 18 – June 24) SO_4 at six California CASTNET sites 96

Figure 3.13 Daily-averaged fine SO_4 (0 – 2.5 μm) at sixteen California IMPROVE sites from observations and model simulations 97

Figure 3.14 Observed SO_x distributions along all DC-8 flight paths (below 5 km ASL), over three regions 98

Figure 3.15 Vertical profiles of observed and modeled total sulfur along all DC-8 flight paths, over three regions 99

Figure 3.16 Vertical profiles for observed and modeled SO_x over three regions along all DC-8 flight paths.....100

Figure 3.17 Weekly-averaged (June 18 – June 24) OMI and 12 km modeled PBL SO_2 column.....101

Figure 3.18 Effects of Asian SO_x on California air quality. 102

Figure 3.19 12 km WRF wind fields at ~500 m AGL, at 19 UTC (noon, LT), on four days of June.....104

Figure 3.20 Time series for DC-8 observed and modeled wind fields and SO_x over California – Mexico border on June 24 105

Figure 3.21 Back trajectories originating along flight paths, based on 12 km WRF meteorology fields, below 1 km AGL, shown by days and regions. 106

Figure 3.22 Back trajectories originating along flight paths, based on 12 km WRF meteorology fields, at 2 – 4 km ASL, shown by days and regions.....107

Figure 3.23 24-hr averaged contributions (%) of maritime and terrestrial SO_x emissions on SC surface air quality in 12 km grids, during 06/18-24.....108

Figure 3.24 24-hr averaged contributions (%) of maritime and terrestrial SO_x emissions on SF surface air quality in 12 km grids, during 06/18-24. 109

Figure 3.25 Contributions (after scaling) of maritime and terrestrial SO_x emissions on SC surface air quality in 12 km grids, during the 06/18, 22, 24 flight time 16 – 24 UTC.....110

Figure 3.26 Contributions (after scaling) of maritime and terrestrial SO_x emissions on SF surface air quality in 12 km grids, during the 06/20 flight time 16 – 24 UTC.....111

CHAPTER 1

INTRODUCTION

1.1 Background

The state of California has a wide range of terrain types including mountains, valleys, water (oceans, rivers and lakes) and deserts, and also has varied climate because of the wide span of latitudes and complexity of terrain. It is the most populous state and the third largest state in area in the U. S. (Annual Estimates of the Population for the United States, Regions, States, and Puerto Rico: April 1, 2000 to July 1, 2009, U.S. Census Bureau, 2009). The California population increased by 33 % in the past 20 years and the economy has grown rapidly (Cox et al., 2009). In response to the effects of development, California has taken good effort to study and improve its air quality from the perspective of human health and welfare, taking the diverse meteorological conditions and geography into account. Similar as federal standards, the California Air Resource Board (CARB) has adopted health-based standards for the criteria pollutants. For most of these pollutants the state standards are more stringent than the national standards. Table 1.1 shows the Ozone (O_3) and Sulfur Dioxide (SO_2) standards as examples. Even with the substantial economic development, the emissions for most of primary pollutants have been reduced by a large extent in the last 20 years (for example, NO_x by 34 %, VOC by 57%, CO by >70 %, respectively), and the entire state now meets the state and national standards for most of these pollutants. However, unlike the continuous decreasing trend in statewide NO_x, VOC, and CO emissions through the past decades, the reduction of anthropogenic SO_x emissions stopped since 1995 and the emission is estimated to rise in the next 10 years, partially due to the emissions from the "other mobiles" categories, majorly resulted from the significant growth in shipping activities and the high-sulfur fuels that ocean-going vessels typically use (Figure 1.1). The recently adopted regulation for fuels used in ship auxiliary engines is expected to help offset this trend. Furthermore,

the marine sulfur emissions from biogenic and geogenic sources have been poorly known and documented, which may respond to the anthropogenic nutrient enhancement (VanCuren, 2010). In addition to the SO_x pollution, the only two pollutants to date that have not met the state and federal standards are O_3 and Particulate Matters ($PM_{2.5}$ and PM_{10}), and nearly all Californians live in areas that are designated as nonattainment for the state (about 99 %) and national (about 93 %) health-based O_3 and/or PM standards (Figure 1.2, Cox et al., 2009). Little improvement in O_3 has been observed over the last decade despite the continued emission reductions. Local production, together with inter-continental and in-state transport contributes to the O_3 levels over both urban and rural areas.

In order to address regional issues of air quality over California, the California portion of the Arctic Research of the Composition of the Troposphere from Aircraft and Satellites (ARCTAS-CARB) was conducted in June 2008 by the National Aeronautics and Space Administration (NASA) (http://www.espo.nasa.gov/arctas/). The NASA DC-8 aircraft platform sampled trace gas and aerosol concentrations through four scientific flights over California for ~25 daytime hours in total on June 18, June 20, June 22, and June 24, 2008. These flights were sponsored by CARB. This mission had multiple scientific objectives, including improving the state emission inventories, characterizing off-shore shipping emissions, quantifying the import of pollution from Mexico and Asia and characterizing the upwind boundary conditions necessary to model inland O_3 and aerosols. In addition to the flight measurements, ground, satellite and sounding measurements were conducted during the same period. Global and regional-scale models simulated meteorological conditions and chemical distributions spatially (three dimensional) and temporally. They assisted the flight planning during the campaign, and also interpreted the observational data to better understand the atmospheric characteristics.

1.2 Regional-scale chemical transport model and input data

1.2.1 Model

We simulated the period from June 18 to June 28, 2008 using the Sulfur Transport and dEposition Model (STEM) – Version 2K3, one of the regional models that assisted in flight planning during the ARCTAS-CARB campaign. The advantages of modeling analysis after the experiment include: 1) provide the four-dimensional context of the observations; 2) evaluate the individual chemical and physical processes; 3) assess bottom-up and top-down emission inventories (EIs) and test emission control strategies. The STEM model solves the equation to calculate the concentration of a given chemical species from an eulerian view point as shown in (1.1):

$$\frac{\partial C_i}{\partial t} = \left[\frac{\partial C_i}{\partial t}\right]_{TRANSPORT} + \left[\frac{dC_i}{dt}\right]_{LOCAL} \quad (1.1)$$

Where

Transport operator (advection; turbulence): $\frac{\partial C_i}{\partial t} = -\mathbf{U} \bullet \nabla C_i + \frac{1}{\rho} \nabla \bullet \mathbf{K} \nabla C_i$

Local (chemistry) operator: $\frac{dC_i}{dt} = P_i - L_i$

P_i and L_i represent local source and sink, respectively.

The tracer and full-chemistry versions of STEM have been used during a number of field experiments in the past decade. Their performance has been evaluated and relies largely on domain design, model resolutions and the quality of input data. The modeling system applied here (Adhikary et al., 2010) includes three components:

1) A hemisphere tracer model to study long range transport of pollutants and dust with 60 km horizontal resolution and 30 vertical layers to the stratosphere, and a 6-hour time resolution;
2) A continental scale gas-phase and aerosol chemical transport simulation on a subset of the hemispheric grid with a 60 km horizontal resolution and 18 vertical layers with the same intervals as the tracer model (i.e., the 18 lowest layers), and a 6-hour time resolution;

3) A regional-scale gas-phase and aerosol chemical transport domain centered over California with a 12 km horizontal resolution and 32 vertical layers at smaller intervals than in 1) and 2), and a 1-hour time resolution.

The northern hemisphere calculation utilized a tagged tracer version of STEM. This model calculates a variety of aerosols, as well as several air mass markers (such as CO, SO_2, BC, OC, SO_4, dust and Hg). The calculations are based on simple decay rates, and include dry deposition and wet scavenging. Because of its long atmospheric life-time of 1 - 2 months, carbon monoxide (CO) is one of the primary tracers used to estimate the contributions of geographic areas to hemispheric-scale transport. For this study, we included anthropogenic CO tracers for eight regions in the hemispheric domain: the U.S. mainland, Alaska, Canada, Greenland, Europe, Russia, China and other Asia nations. The biomass burning CO tracers include North America, North America and South America. All initial conditions and inflow boundary conditions of CO are set to zero. The tracer calculations also include estimates of air mass age, which represents a combination of transport time, source intensities and diffusion, using ethane emission and decay rates as a proxy (Tang et al., 2007).

The STEM full-chemistry model calculates 225 gas phase chemistry reactions based on SAPRC 99 gaseous chemical mechanism (Carter, 2000), with thirty different photolysis rates calculated by the online Tropospheric Ultraviolet-Visible radiation model (TUV) (Madronich, 2002). The TUV model needs total ozone column to calculate the absorption of UV radiation by ozone molecules. Since the STEM model is a regional model simulating the troposphere, satellite column ozone data is used. For this study, we used the column O_3 data from the Ozone Mapping Spectrometer (OMI) instrument on board the NASA Aura spacecraft. STEM also includes a four-bin aerosol module (0.1-0.3 μm, 0.3-1.0 μm, 1.0-2.5 μm and 2.5-10.0 μm) with thermodynamics calculated using the Simulating Composition of Atmospheric Particles at Equilibrium (SCAPE II) model (Kim and Seinfeld, 1995). A detailed description of the current STEM-2K3 model can be

found in a recent paper by Adhikary et al. (2010). The STEM full-chemistry calculations were performed using 60 km and 12 km resolutions in this study and the model setups are summarized in Table 1.2. The 60 km cases represent the general picture of pollutant distributions over the eastern Pacific and the continental U. S., while the 12 km cases concentrate on detailed pollutant spatial and temporal distributions under the impacts of transport and local productions over California.

1.2.2 Meteorology

As equation 1.1 indicates, meteorological data are required to simulate chemical transport in the atmosphere. STEM does not require a uniform horizontal grid and can be mapped to any map projection and resolution based on the meteorological model. In this study, meteorology fields for all three grids were generated by the Advanced Research Weather Research & Forecasting Model (WRF-ARW) Version 2.2.1 (Skamarock et al., 2007) with forecast and reanalyzed meteorological inputs (Mesinger et al., 2006) for the 60 km and 12 km simulations, respectively. The 60 km WRF grid included 30 layers and the 12 km grid included 40 layers. The tracer model used the simulated meteorological fields from all 30 layers; while the 60 km and 12 km full chemistry simulations only used the lowest 18 and 32 layers, respectively. The WRF-ARW simulations at both resolutions utilized the same physics and dynamics schemes. The primary physics options include Goddard shortwave (Chou and Suarez, 1994) and Rapid Radiative Transfer Model (RRTM) long wave scheme (Mlawer et al., 1997), the NOAH land and surface model (Chen and Dudhia, 2001), Monin-Obukhov similarity theory (Monin and Obukhov, 1954) with the Mellor-Yamada-Janjic planetary boundary layer closure scheme (Janjic, 2002), WSM 5-class microphysics (Hong et al., 2004) and the Betts-Miller-Janjic scheme (Janjic, 2000). The STEM preprocessor was used to extract topography and other land use variables along with the meteorological parameters. Other model inputs, such as

emissions, initial and boundary conditions were gridded for the same map projection and grid resolution, which will be discussed in detail in the following sections.

1.2.3 Emissions

Emission inputs for each of the three modeling systems differed slightly, based on respective demands for resolution and completeness. In the hemispheric tracer model, we used a bottom-up global gridded inventory prior to the ARCTAS mission (Streets et al., http://mic.greenresource.cn/arctas_premission, 2008). This inventory is driven by regional-specific information on fuels and activity from various economic sectors, including anthropogenic, biomass and global shipping. In the 60 km continental simulation, anthropogenic emissions for North America were taken from the 2001 National Emissions Estimate Version 3 (NEI 2001), an update of the 1999 U.S. National Emissions Inventory with growth factors applied by Source Classification Code, and augmented with national inventories for Canada (2000) and Mexico (1999). The NEI 2001 misses the shipping emissions over the ocean. Daily biomass burning emissions from the Real-time Air Quality Modeling System (RAQMS) (Pierce et al., 2007) were provided by the Cooperative Institute for Meteorological Satellite Studies (CIMSS). Biogenic emissions of terpene and isoprene were taken from the twelve-year-averaged data from the Orchidee model (Lathiere et al., 2006). For the sulfur emission study in Chapter 3, a sensitivity case in 60 km grids (DS case) was conducted with SO_2 emissions replaced by the most updated ARCTAS inventory (Version 3.2) by Streets' with no weekday/weekend variations (http://www.cgrer.uiowa.edu/arctas/emission.html). In this case, SO_4 emissions remained the same as the base case. For the 12 km simulations the anthropogenic and biogenic emissions were re-gridded from a contemporary CARB 4 km EI. The anthropogenic emissions out of the CARB domain (including Mexico, states of Nevada, Washington and Idaho) were also taken from NEI 2001, same as in the 60 km base simulation. Biomass burning emissions were generated by the prep-chem-source

model (WRF/Chem Version 3.1 users' guide, 2009), which used the MODIS - detected point fire information at 1 km ground resolution (Giglio et al., 2003) and was adjusted at each time step to match total emissions rates from RAQMS.

1.2.4 Lateral Boundary Conditions

Temporal and spatial variations in top and lateral boundary conditions (LBCs) downscaled from global models enhance model performance, especially for long-live species and over areas less impacted by local pollution (Tang et al., 2007). From sensitivity studies using the Community Multi-scale Air Quality (CMAQ) model, Tang et al. (2009) concluded that the use of global model predictions for LBC improved the correlation coefficients of surface O_3 prediction over the U.S. west coast, but may also increase the O_3 mean bias.

In Chapter 2, to study the impacts of LBCs on model performance, and to better understand the role of distant sources, a variety of western LBCs were tested, as summarized in Table 1.3. In the 60 km base case, LBC for thirty gaseous species and top boundary conditions for ten gaseous species (not listed) were taken from the archived RAQMS real-time chemical analyses data. RAQMS real-time chemical analyses included assimilation of stratospheric (above 250 mb) O_3 profiles from the Microwave Limb Sounder (MLS) and cloud cleared total O_3 columns from the O_3 Monitoring Instrument (OMI) onboard the NASA Aura satellite. The RAQMS O_3 profiles were compared with measurements by Tropospheric Emission Spectrometer (TES) onboard the NASA Aura satellite for Step and Stare observations over the Eastern Pacific (150E - 120E, 30N - 60N) during June 15 - July 15. RAQMS mean biases relative to TES were generally less than 10%, except near 100 mb where the bias was up to 20% lower than TES. The RMS errors ranged from 20 to 40% in the troposphere with peaks near 200 mb and below 800 mb. RAQMS underestimated tropospheric O_3variability by about 20% relative to TES. Comparison with ten Trinidad Head O_3 sondes launched between June 27 and July 06

showed that the RAQMS real-time O_3 analysis had a mean high bias in the troposphere (below 200 mb) which ranged from 10% below 500 mb to 30% at 300 mb (from personal contact with R. B. Pierce) . For the 12 km base case simulations the STEM 60 km base case results were extracted and used as boundary conditions. Several additional western LBCs were used to further study the sensitivity of modeled O_3 to the western LBC in the 60 km model grid. In the Clean WBC case, O_3 and CO concentrations in the western LBC were set to constants (vertically, horizontally and temporally) at 40 ppb and 90 ppb, respectively. This constant 40 ppb background O_3 level is often used as a baseline for O_3 risk assessments by the U. S. EPA. In the Fixed BC case, we temporally fixed the top and all LBCs with the 20-day averaged (June 10 - June 30, 2008) RAQMS boundary conditions. Then in the Reduced WBC case, we reduced the Fixed BC values by 10 ppb of O_3 in every grid cell along the western boundary. Finally, observations from the June 22 DC-8 flight were interpolated to the 60 km and 12 km model grid and used as the western LBC, to explore the impact of using the observations on model performance. Details of the various LBCs used in these studies are summarized in Table 1.3.

1.3 Research objectives and thesis outline

Located at the west coast of the U. S. adjacent to Mexico, California is a receptor of Asian and Mexico pollution. The large amount of local emissions contributes to its air quality problems, especially over urban areas, and most of the urban areas are upwind contributors to the downwind areas based on previous studies (Cox et al., 2009). These factors influence the spatial and temporal distributions of pollutants over California altogether. This modeling-observation study aims at better understanding the contributions of local emissions as well as the impacts of long-range, California-Mexico and in-state transport of pollutants on California's air quality during the ARCTAS-CARB experiment period in June, 2008.

In Chapter 1, background information on California's air quality is described briefly and the general objectives of this research are introduced. The ARCTAS-CARB experiment and the modeling methodology are introduced. Specific scientific questions regarding pollutant transport and local (both terrestrial and maritime) emissions are further discussed in Chapter 2 and 3, using both observational and STEM-modeled chemical concentrations. Chapter 2 investigates the direct and indirect impacts of O_3 transported from the eastern Pacific on California air quality and looks at the effects of model LBCs over the eastern Pacific on predicted surface O_3 concentrations. In Chapter 3, three SO_x EIs are compared and evaluated. The properties of the Asian inflows and the California-Mexico air interactions are analyzed and the impacts of terrestrial and maritime sulfur emissions on coastal air quality are assessed. Chapter 4 summarizes this research and suggests the direction for future work.

1.4 Summary of contributions

This research applies chemical transport model STEM to study atmosphere characteristics during the ARCTAS-CARB experiment period in June 2008. The major contributions have been summarized in this section.

1) Determine a period during ARCTAS-CARB when California was heavily affected by Asian inflows, and compare the direct and indirect impacts of the Asian inflows during this period with the whole experiment week
2) Evaluate the model sensitivity to LBCs, and improved O_3 prediction at lower troposphere by using the observational-based LBC
3) Spatially and temporally compare three SO_x different EIs over three California regions, and evaluate them by comparing modeled SO_x with various observational datasets

4) Quantify SO_x in Asian and Mexico inflows, analyze the air interactions over California-Mexico border, and identify the contribution of local SO_x (terrestrial and maritime) sources
5) Quantify the impact of maritime SO_x emissions on near-shore and inland air quality

Table 1.1 State and national O_3 and SO_2 standards

Pollutant	Averaging Time	California Standards	National Standards	
			Primary	Secondary
Ozone (O_3)	1 hour	90 ppb	120 ppb	Same as Primary Standard
	8 hour	70 ppb	75 ppb	Same as Primary Standard
Sulfur Dioxide (SO_2)	Annual Arithmetic Mean		30 ppb	
	24 hour	40 ppb	140 ppb	
	3 hour			500 ppb
	1 hour	250 ppb		

Source: Cox, P., Delao, A., Komorniczak, A., and Weller, R.: The California almanac of emissions and air quality 2009 edition. http://www.arb.ca.gov/aqd/almanac/almanac09/almanac2009all.pdf, 2009

Table 1.2 Summary of STEM inputs for base cases in two resolutions

Model Inputs	Raw data sources		Raw data resolutions	
	60 km Base	12 km Base	60 km Base	12 km Base
Meteorology, WRF 2.2.1	GFS + one time step SST	NARR + daily SST	6 hrs, 1 º × 1 º	3 hrs, 36 km
Anthropogenic Emissions (point and mobile)	NEI 2001, weekday varied from weekends	CARB 2005, projected from 2002, daily varied. Out of CARB domain filled with NEI 2001	1 º × 1 º, 1 hr	4 km × 4 km, 1 hr
Biogenic Emissions	Orchidee	CARB 2005, projected from 2002, daily varied	1 º × 1 º, monthly averaged	4 km × 4 km, 1 hr
Biomass burning Emissions	RAQMS real time	MODIS-detected hot spots being processed by the prep-chem-source model, mass-conserved normalization	1 º × 1 º, 12 hrs	1 km × 1 km, 24 hrs
Top and Lateral Boundary Conditions	RAQMS real time (gases) + STEM tracer (several aerosols)	STEM 60 km base case	2 º × 2 º, 6 hrs & 60 km × 60 km, 6 hrs	60 km × 60 km, 18 layers, 6 hrs
Ozone column, for TUV	Measured by Ozone Mapping Spectrometer (OMI) instrument on board the NASA Aura spacecraft, daily		1 º × 1 º, 1 day	

Table 1.3 Summary of STEM lateral boundary condition sensitivity studies

Name	Descriptions	Resolution(s) applied	
		60 km	12 km
Clean Western Boundary Conditions (Clean WBC)	Constant 40 ppb O_3, 90 ppb CO as western LBC	✓	
Fixed RAQMS Boundary Conditions (Fixed BC)	Temporally fix top BC and LBCs for all species using averaged 20-day BCs in the base case	✓	
Reduced Western Boundary Conditions (Reduced WBC)	Reduce 10 ppb of O_3 from the western LBC in the Fixed BC case	✓	
Observational-based Western Boundary Conditions (Obs. cases)	Measurements on the June 22 DC-8 flight were interpolated to STEM grids as western LBC for the flight week, species included: NO_x, CO, O_3, H_2O_2, PAN, HNO_3, SO_2	✓	✓

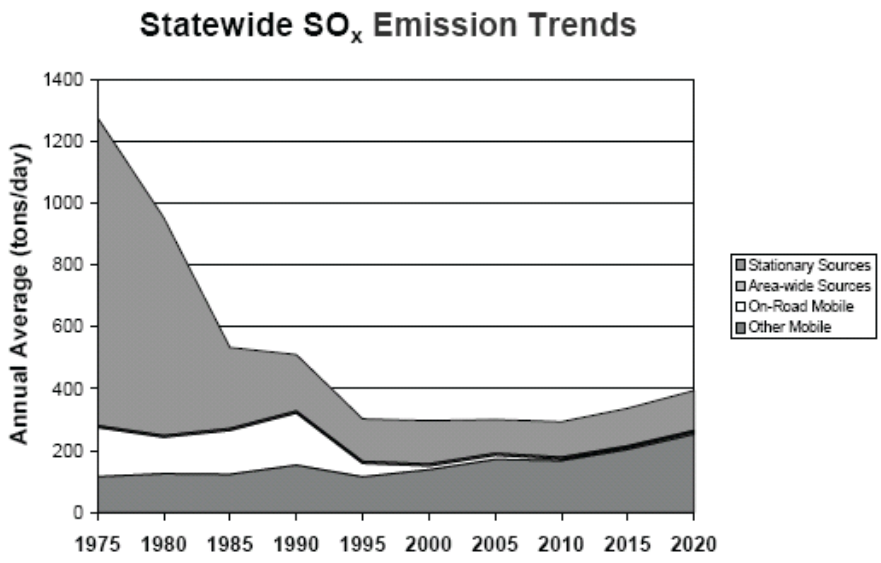

Figure 1.1 SO_x emission trends during 1975 – 2020

Source: Cox, P., Delao, A., Komorniczak, A., and Weller, R.: The California almanac of emissions and air quality 2009 edition. http://www.arb.ca.gov/aqd/almanac/almanac09/almanac2009all.pdf, 2009

Figure 1.2 State O_3 designations based on both 1-hour and 8-hour standards

Source: Cox, P., Delao, A., Komorniczak, A., and Weller, R.: The California almanac of emissions and air quality 2009 edition. http://www.arb.ca.gov/aqd/almanac/almanac09/almanac2009all.pdf, 2009

CHAPTER 2

IMPACTS OF TRANSPORTED BACKGROUND OZONE ON CALIFORNIA AIR QUALITY

2.1 Introduction

Tropospheric ozone (O_3) is an atmospheric pollutant harmful to human health and agriculture, and is also one of the most important green house gases. The U.S. National Ambient Air Quality Standard (NAAQS) for daily maximum 8-hour average O_3 has recently been lowered to 75 ppb, and is likely to be lowered further to between 60 ppb and 70 ppb in future regulatory reviews of its direct impacts on human health. The California Air Resource Board (CARB) currently sets more stringent state 1-hour and 8-hour O_3 standards at 90 ppb and 70 ppb to better address longstanding urban and regional O_3 problems.

The U.S. EPA has defined Policy-Relevant Background O_3 (PRB) as those concentrations that would occur in the United States in the absence of anthropogenic emissions in continental North America (EPA, 2006). The PRB concentration defines the level below which O_3 regulatory standards cannot be set. This includes O_3 formed through photochemical reactions involving precursors originating exclusively from continental biogenic sources, wildfires, and lightning, as well as O_3 transported from outside of North America and from the stratosphere. Current literature indicates an increasing trend of background O_3 due to rising global emission trends, and projects that PRB will continue to rise until the end of the 21st century in North America (Jaffe et al., 2003; Lin et al., 2000; Vingarzan et al., 2004). Previous work has reported a wide range of background O_3 in the northern hemisphere based on modeling studies and observational analysis, with estimates varying from 15 ppb to 60 ppb (Fiore et al., 2003; Lefohn et al., 2001; Jaffe et al., 2003). Many of these studies have analyzed observations at remote sites to determine the contributions of long-range O_3 transport. However,

remote sites of interest are not completely devoid of local anthropogenic impacts (Nolle et al., 2001), and thus these analyses must include techniques to exclude the contributions from regionally polluted air-masses. Modeling studies are also often used, but they contain uncertainties due to coarse spatial resolution and quality of inputs (Fiore et al., 2003). While estimates vary due to differences in season, location, elevation, experimental and modeling methods, there is considerable agreement that less than 40ppb of PRB is due to natural sources in North America, peaking in spring, and 5 - 15 ppb is due to trans-continental transport of O_3 (Fiore et al., 2002; Vingarzan et al., 2004; McKendry et al., 2006).

Transported O_3 from outside the continental U.S., together with locally-formed O_3, contributes to the variability in O_3 observed at inland sites in California. A recent study has reported an increasing trend in background O_3 over the eastern Pacific since the 1980s during springtime, when Asian emissions have their greatest impacts on the western North America (Cooper et al., 2010). Fewer studies have focused on the role of background O_3 in the summertime (Fiore et al., 2003; Parrish et al., 2009), a period with the most frequent and intense episodes of O_3 pollution, in which the impact of long-range transport is believed to reach its annual minimum.

Based on multi-year observations, Parrish et al. (2009) contend that the observed summertime O_3 over northern California is directly proportional to transported background from the eastern Pacific, and estimate a transport time of 20 - 30 hours for coastal O_3 at 1 - 2.5 km altitude over Trinidad Head (THD) to impact surface concentrations over inland O_3 non-attainment areas. Background O_3 in the transported air averaged 58 ppb on the days that O_3 exceeded the current 75 ppb NAAQS at one example site, and was occasionally above 75 ppb. This summertime study associated transported background concentrations with higher local concentrations in several locations heavily influenced by O_3 formed locally from nearby anthropogenic emissions. Oltmans et al. (2008) has found that summertime background O_3 levels over the eastern Pacific in

southern California are similar to those in northern California. In addition, Parrish et al. (2009) pointed out the potential similarity in transport patterns from coastal to inland areas over northern and southern California. However, the impact of transported background O_3 over southern California is more difficult to discern because of the weaker vertical mixing and the higher local production levels.

Assessing the contributions of distant sources on local pollution levels remains a challenging problem and reducing the uncertainty in estimates requires a better understanding of transport patterns that bring together long-range transported air masses and local pollutants (NAS, 2010). Three-dimensional chemical transport modeling is an important complement to observation-based approaches and is critical to fully understand the factors responsible for reported long-time trends (Law, 2010), as well as short-term variations in the properties of transported air masses.

This chapter investigates the impacts of O_3 transported from the eastern Pacific on California air quality using observational data collected during the ARCTAS-CARB experiment. These data are analyzed using results from the STEM regional-scale modeling system, including a tracer model and full-chemistry simulations at two horizontal resolutions. Results from the tracer model and back trajectories are employed to determine days during the experiment when California was strongly influenced by Asian inflows. We show the direct and indirect effects of foreign inflows on measurement sites located at THD, in the northern Central Valley, and in southern California. Based on trajectories from high resolution meteorology fields, and O_3 concentration correlation analysis, transport times from the coast to the valley and their altitudinal relationships are estimated for the specific time period influenced by Asian inflows and over the entire ARCTAS-CARB period. The amount of O_3 transported into northern California from the free troposphere is estimated according to observed O_3 vertical profiles and the inferred transported altitudes. Results are extended to look at the impact of LBC over the eastern Pacific on predicted surface O_3 concentrations over

California. Model sensitivities to western LBC are evaluated. The implication of these results for observation and model approaches to improve O_3 prediction are also discussed.

2.2 Observational data

One of ARCTAS-CARB scientific objectives was to characterize upwind boundary conditions necessary to model inland O_3 (Jacob et al., 2009) and the June 22 flight was designed specifically for this purpose. On this day, the DC-8 took off from Palmdale, CA, flew over the Pacific Ocean to THD, and then circled back to Palmdale along the coast (Figure 2.1c). In addition to airborne measurements, continuous hourly O_3 measurements were made at CARB and Clean Air Status and Trends Network (CASTNET) surface sites (http://www.arb.ca.gov/qaweb/siteinfo.php; http://www.epa.gov/castnet/). Ozone soundings were also launched on June 20, June 22, June 24, and June 26, 2008 at the remote coastal THD site (ftp://ftp.cmdl.noaa.gov/ozwv/ozone/ARCIONS/CARB/).

Within the CARB and CASTNET surface O_3 monitoring network, five California sites were selected for the present analysis (Figure 2.1c). Three of them are located in California's Central Valley: an isolated rural site, Tuscan Butte (TB), which has the highest O_3 design value in the Northern Sacramento Valley (Parrish et al., 2009); a suburban site, Walnut Grove Tower (WGT), 20 miles south of Sacramento; and a remote CASTNET site, Lassen Volcanic National Park (LAV), located to the east of valley. The other two are the CASTNET site at Joshua Tree National Monument (JOT) in southern California, chosen to compare with the northern sites, and a background coastal site at THD, selected for identifying the transport patterns from coast to inland. Elevations of these sites are 572 m, 0 m, 1756 m, 1244 m and 20 m, respectively.

2.3 Results and discussions

2.3.1 O_3 concentrations and air-mass movement during ARCTAS-CARB

The 24-hour average surface O_3 concentrations during June 18 - June 28, 2008 from the 60 km and 12 km base case simulations are shown in Figure 2.1b, c, respectively. The entire 12 km domain is shown but only the U. S. continental portion of the 60 km domain is included. The 12 km case shows the advantages of higher resolutions. Horizontally, the increased resolution captured local features around urban emissions sources and indicated more complicated wind fields over California. Vertically, the 12 km simulation produced mixing layer heights closer to those reported in previous studies than the 60 km results, especially at valley sites (Dillon et al., 2002), ranging from several hundred meters to ~2000 m above ground. Temporally, the 12 km simulations were able to better capture the strong diurnal variations in O_3 seen at some of the surface sites (which will be discussed in more details later).

Meteorological factors play a major role in pollutant production and transport. The weather over California during the mission week was dominated by high pressure centered over the Pacific, with weak mid-latitude cyclonic disturbance (Fuelberg et al., 2010). Asian inflows entered the west coast of the U. S. during the June 21 - June 24, 2008 period (Figure 2.1a), and the June 22 DC-8 flight encountered these long-range transport inflows (Figure 2.2). High VOC ages (100 - 400 hours) along most of the oceanic part of the DC-8 June 22 flight path and over northern California during 17 - 23 UTC indicate inflows with long histories of active chemistry from outside of the U. S. continent. Five-day back trajectories along this day's flight path show that these air masses travelled in the free troposphere from the western Pacific off the coast of Asia before arriving in California, with the largest Asian influence occurring along the northernmost outbound part of the flight. Over the southern California near shore

portions of the inbound flight path, the flow was at lower altitudes, with air-masses coming from the northern California coast (in purple). The regions with the largest influence from Asian sources during this flight are shown in Figure 2.2c and 2.2d, together with the VOC age and back trajectory calculations. To further identify the influence of emissions from specific geographical regions we tagged primary CO emissions in the hemispheric tracer model, which treats primary CO as an inert tracer. Shown in Fig 2c,d are plots of the % contribution to anthropogenic primary CO from China sources. The CO contributions from Chinese emissions at the surface at 18 UTC and 24 UTC (00 UTC, June 23) were the greatest over northern California and offshore areas of southern California, ranging from 20 - 80%, but areas south of San Francisco had a smaller fractional contribution from Asian sources at these times.

Further insights into flow conditions during and after the flight period from 12 km simulations are gained from maps of wind vectors at roughly 1500 m and 3000 m AGL at 18 UTC on June 22, June 23, and June 24, 2008 (Figure 2.3). At 3000 m, onshore westerly winds blew at almost constant speed penetrating inland to California and then extending to Nevada on June 22 and June 23. The wind speed over California decreased on June 24. The offshore winds at 32 - 33 N were from the southwest on June 22, and shifted to northwesterly flows when approaching the shore of southern California. These flows continued for the following two days. Coastal winds at 1500 m were northwesterly, with the Central Valley displaying greater complexity and daily variability due to local orographic features. They became more organized on June 23 and June 24, with northwesterly winds throughout the valley. The southern portions of California were under a low pressure system with southwesterly winds.

Corresponding surface CO and O_3 concentrations from the 12 km model simulations are shown in Figure 2.4. Extensive areas in southern California and the Central Valley were subject to O_3 concentrations exceeding 70 ppb, especially on June 23 and June 24, as a result of hot and dry weather conditions. On these days air-masses

enhanced in O_3 and precursors were transported over the ocean and into the northern portion of the valley. They were mixed together with CO and other precursors emitted during the northern California fire events, and then transported southward where they were mixed with local emissions leading to the high O_3 and CO concentrations.

2.3.2 Coastal-inland O_3 transport

As discussed in 3.1, northern California was impacted by pollution from Asia from June 22 - June 24. The coastal site at THD is a representative station for characterizing variations in background O_3 from the eastern Pacific (Oltmans et al., 2008). Observed O_3 vertical profiles from sondes launched at THD on four days (with launch times between 18 and 22 UTC) are shown in Figure 2.5a. Although O_3 was consistently between 20 - 30 ppb near the surface, significantly higher O_3 (with values ranging from 60 - 80 ppb) was observed on June 22 and June 24, at altitudes between 1500 m and 3500 m. In contrast, on the relatively cleaner days of June 20 and June 26, O_3 concentrations stayed below 50 ppb at altitudes below 5000 m. These results illustrate the large O_3 variability in the air masses transported into California during summertime. Figure 2.5b - e show the vertical profiles of several chemicals sampled by DC-8 near the THD site at approximately the same time as the O_3 sounding was launched on June 22. O_3 concentrations show similar vertical structure as the THD O_3 sonde results. The PAN and NO_2 profiles are highly correlated with the O_3 profiles. The CO profile shows three general segments as identified from the tagged tracer CO results (not shown): marine air below ~1 km; a mid region from 1 to 5 km, where CO structure is the result of a mixture of Asian anthropogenic sources and biomass burning from North America (below ~ 2 km); and an upper segment (above 5 km), which is a mixture of anthropogenic and biomass burning from Asia.

Time-height curtain plots of CO contributions from China at the observational sites calculated by the tracer model are shown Figure 2.6. The THD site was heavily

influenced by Asian emissions, with contributions from China CO sources exceeding 60% from the surface to 5 km above ground. These plots also highlight the episodic nature of the Asian transport events. For example, one of the transport events started on June 21, and strongly impacted inland northern California. The China CO contributions jumped from below 2% to above 40% by the end of June 22 at the TB and LAV sites. China inflows also affected the WGT site, but accounted for less than 10% at the surface. Unlike the TB and LAV sites where the China inflows mixed down from several thousand meters above ground to the surface, this China-impacted air-mass passed over the WGT site above 2 km, and only a small fraction mixed down to the surface. In contrast, the impacts of Chinese sources were very small at the southern California JOT site (not shown).

The influence of transported background O_3 from Asian inflows at four inland surface sites was analyzed, in connection to the tracer results. The time-height O_3 distributions from 12 km simulations (Figure 2.7) clearly show that O_3 transported above the boundary layer can impact the surface as air-masses descend and entrain into the boundary layer. The O_3 vertical structure was complicated, showing the combined impacts of local production in the boundary layer as well as long-range transport at higher altitudes.

To further understand the flow characteristics associated with periods with observed high O_3 values, we estimated O_3 distributions backward in time by combining the corresponding observed values with air–mass back trajectories. In this methodology, we take the observed concentration and propagate its value backwards in time along a wind trajectory. By running multiple trajectories, and assuming that the value does not change along that trajectory we can identify the general flow conditions and upwind regions associate with high O_3 values. In this method the geographic region covered by the trajectories was divided into an array of $1^{\circ} \times 1^{\circ}$ grid cells, and the location of an air parcel at a particular time was represented by the trajectory segment latitude and

longitude endpoints. The average concentration colored on each grid cell was calculated by the mean observed O_3 concentrations associated with each trajectory endpoint that landed in the surface grid at the discrete time intervals specified as shown in equation (2.1) (Kurata et al., 2004).

$$C=\frac{1}{N}\sum_{i=1}^{N} Ci \qquad (2.1)$$

Where N is the number of the trajectories that passed over that grid cell and Ci denotes the observed concentration at the originating point associated with the trajectory. In this way, we colored three-day back trajectories originating from four surface sites on June 23, based on 12 km WRF meteorology fields (Figure 2.8). The starting times used were from 00 UTC to 23 UTC with one-hour interval. Results at LAV and TB sites show that the high observed surface O_3 levels periods were associated with inflows from the eastern Pacific and the coastal area. In contrast, high O_3 periods at the WGT site were associated with flows passing over near-coastal areas of northern California as well as flows directly from the San Francisco Bay area. The high O_3 levels at JOT were associated with flows through the Central Valley, with some flows extending out into the eastern Pacific.

To further characterize the influence of O_3 over the eastern Pacific on surface O_3 over California we examined space-time correlations. Specifically, we calculated correlations between THD O_3 at multiple elevations and surface O_3 at inland sites for different hourly time offsets. We calculated R-square values using both observational and modeled data and the results for the TB site are shown in Figure 2.9. Observed O_3 time series at THD were constructed using O_3 sonde data at THD on June 20, June 22, June 24 and June 26. Soundings for each day were averaged every 500 m up to 5000 m AGL. Averages for each altitude bin were interpolated to hourly values using a univariate interpolation approach (Akima, 1970), and the resulting altitude-specific time series were then correlated with the time series built from hourly surface O_3 observations at the TB site. Resultant correlations between O_3 at three altitude bins (1000 – 1500 m, 2500 –

3000 m, and 3500 – 4000 m) above THD and surface O_3 at TB are shown in Figure 2.9c. High R-square values ranged from 0.67 to 0.75 at these altitudes, indicating strong correlations between surface O_3 at the TB site and O_3 at all three altitudes above THD during June 21 - June 24. Surface O_3 at the TB site was most highly correlated with O_3 at 2500 - 3000 m above THD with a time lag of around 30 hours.

This analysis was repeated using 12 km modeled data, correlating hourly concentrations at THD at the same altitudes with predicted hourly surface O_3 at TB. Predicted O_3 vertical structures on June 22 at THD and the time series at TB are compared with observations in Figure 2.9a and 2.9b. Model-based correlations in Figure 2.9d and 2.9e show correlations across several time offsets, due to the higher fidelity of the time series used in analysis. The highest R-square value was 0.68, found at 2500 m with a time offset of 22 hours, shorter than the 30 hour offset found in the observational data.

To better understand the causes of these O_3 transport correlation relationships, we plot the forward trajectories in Figure 2.10a, b from the 12 km meteorology fields originating on June 22, from 1500 m and 2500 m above THD, respectively. The starting times were from 00 UTC to 23 UTC with a one-hour interval. On this day, the winds blew from ~2500 m above THD directly to northern California (Figure 2.10b). The forward trajectory starting at 2500 m above THD at 01 UTC on June 22 (6pm LT, June 21) is shown in Figure 2.10d. The air-mass descended as it traveled inland into the valley, reaching the east side of the valley after about 17 - 18 hours, where it affected the TB surface concentrations at the end of June 22. Upslope mountain-valley flows in the afternoon lifted the air-masses, and they continued moving east. At 1500 m, the wind directions were more varied leading to the impact being more dispersed, affecting TB, Nevada as well as large areas south of THD. This analysis shows clearly the inland transport and entrainment of the eastern Pacific O_3 into the boundary layer.

The origin of the air masses reaching TB are shown to be a mixture of air from Oregon transported at low altitudes (< ~1500m), as well as air transported from the eastern Pacific at attitudes between 1.5 to 3 km as shown in Figure 2.10c. These back-trajectories of air masses at about 400-500 m above TB area were calculated from 00 UTC to 23 UTC with one-hour intervals on June 22 and June 23. We plot the back trajectory of an air mass at about 400-500 m above TB area at 00 UTC on June 23 (5 pm LT, June 22) in Figure 2.10e. This air-mass was at 3500 - 4000 m above the eastern Pacific 40 hour earlier. It then passed THD at ~ 3000 m ASL and descended east into the valley, taking ~22 hours to travel from the coast to the valley, where the pollutants were finally mixed down to the surface.

The correlation between THD O_3 at multiple elevations and surface O_3 at inland sites varied throughout the ARCTAS-CARB period. Figure 2.9d and 2.9e show the model correlations between THD at 1500 m and 2500 m and the TB site at different time offsets for the June 18 - June 28 period. Over this longer analysis time period, no significant correlations were observed at 2500 m. But at 1500 m, a lower maximum R-square of 0.3 was obtained for a 30-hour transport time. These results are similar to those from the correlation study using 8-hour average O_3 based on multi-year observations (Parrish et al., 2009), and can be also further explained with air-mass trajectories (Figure 2.11).

Similar as Figure 2.10a-c, Figure 2.11 shows the forward trajectories from the 12 km meteorology fields originating from 1500 m and 2500 m above THD, together with the back-trajectories of air masses at about 400-500 m above TB area, for every hour on June 20 (before the long-range transport event). The air-masses on this day at 2500 m above THD blew directly to Oregon and had no direct impact over the TB area. The air-masses at 1500 m above THD blew directly to the northern California including the TB area, but stayed at ~1200 – 1500 m above the valley surface. The pollutants they carried were mixed down to the surface during day time as the boundary layer grew. The back-

trajectories in Figure 2.11c also indicate that the air-masses over the TB area were mainly from below 1500 m above the Eastern Pacific on this day.

These results show that surface O_3 in northern California can be directly influenced by O_3 transported over the eastern Pacific in summer. Near the coast the influence is limited to the MBL O_3, where concentrations are typically below 40 ppb. However, inland, the influence of O_3, transported at higher altitudes is strengthened; there coastal O_3 levels can reach 60 - 80 ppb. The enhancement of O_3 over the ocean at higher altitudes significantly affects downwind surface O_3 concentrations.

The situation in southern California is different. As discussed in the introduction, the O_3 entering southern California directly from the eastern Pacific in the summer is very similar in magnitude and vertical structure to that measured at THD. However, the southern California coastal ranges are not as high and continuous as in northern California. Thus southern California is often under the influence of on-shore marine boundary layer flows, which bring lower levels of background O_3 that then mix with the high emissions regions. Therefore, it is more difficult to detect the influence of this eastern Pacific O_3 on inland surface observations in southern California. During this analysis period, we did not have a situation where air over the southern portion of the eastern Pacific at altitudes from 1.5 to 4 km had a significant direct impact on O_3 at the JOT site in southern California.

2.3.3 Model LBC sensitivity studies

Considering the significance of O_3 transported from the eastern Pacific on California surface O_3, the uncertainties in the model western LBC along with the meteorological conditions can represent a significant source of error in the prediction of surface O_3 over California. To demonstrate the impact of the western LBC on surface O_3 predictions over California, a series of LBC sensitivity simulations were performed in the 60 km model grid.

There are several methods to create LBCs including using constant values, default profile gradients, and real-time profiles downscaled from global model results. Here we show results for simulations using various approaches. The change in surface O_3 for the Clean WBC case (Figure 2.12b) shows that the use of the Clean WBC resulted in a decrease in California surface O_3, with large changes (exceeding 5 ppb) extending over two thirds of the study domain. The averaged O_3 concentration decreases during June 21 - June 24 over northern California are more than twice those over the south. The time series of surface O_3 values and their change due to the use of the Clean WBC at TB are shown in Figure 2.13a and 2.13b. The largest changes in O_3 (> 20 ppb) due to the Clean WBC occurred after June 22, and correspond to the arrival time of Asia-influenced air as discussed earlier (Figure 2.6). These results demonstrate the importance of a better representation of the western LBC in order to improve model predictions.

A better representation of the LBC can be obtained by downscaling results from global chemical transport models. Tang et al. (2007) demonstrated that LBCs derived from global models can capture much of the temporal and spatial variability along the boundary and can enhance air quality predictions. Recall that for the base simulation we took this approach and used results from the RAQMS global model as the LBC in our 60 km base simulations. The RAQMS-predicted O_3 values were directly compared with the O_3 sondes at THD on June 22 (Figure 2.9a) and the observations for the June 22 DC-8 flight are shown in Figure 2.14. The comparison of the THD O_3 shows that RAQMS captured vertical gradients but generally over predicted O_3 by 10 - 20 ppb from surface to 5000 m. O_3 values along the flight path are shown in terms of a vertical distribution and as a function of flight altitude and time (Figure 2.14a, b). For this flight the RAQMS model over-predicted O_3 between 1.5 - 4 km. RAQMS also showed less variability above 1 km. The Base case simulations are also presented in Figure 2.14. The 60 km O_3 values are slightly higher than RAQMS and the observations below 1 km, lower between 1.5 - 4 km (and closer to observations), closer to the RAQM results at 5 - 8 km, and higher

above 8 km. These results show that while the use of global model LBCs can improve model performance, that biases can be introduced. In this case the high bias in the RAQMS LBC at THD and along at 1.5 - 4 km along the June 22 flight path contributed to the over prediction of O_3 at the TB site that is shown in Figure 2.13a.

To further explore the sensitivity of the predictions to the LBC we performed additional simulations. To explore the importance of temporal variability we used 20-day temporal averaged RAQMS boundary conditions in the Fixed BC case. The predicted surface O_3 during June 21 - June 24 dropped 3 - 7 ppb over two-thirds of California as shown in Figure 2.12c. As shown in Figure 2.13c, the use of temporally averaged boundary conditions resulted in a decrease in predicted O_3 relative to the base case by ~10 ppb, during the periods with large Asia influence. This is due to the fact that the episodic enhancements were largely removed by the longer time period used to prepare this LBC. The results for the sensitivity simulations where the western LBC was reduced by 10 ppb of O_3 from the Fixed BC case are also shown in Figure 2.13c and 2.13d. Results from this constant perturbation case helps illustrate how the boundary values are modified within the STEM model. Average changes of surface O_3 over California during June 21 - June 24 vary from 1 - 6 ppb (Figure 2.12d), relative to the fixed BC case. Time variations of changes in O_3 at the TB site are shown in Figure 2.13d and 1 - 8 ppb of O_3 decrease can be seen by reducing 10 ppb of O_3 in the fixed western LBC. The extent to which the O_3 signal was damped (i.e., lower than the 10 ppb perturbation) reflects the degree to which O_3 levels were influenced by local meteorological and chemical processes. The smaller the change is, the larger the influence of the local contributions is.

2.3.4 Model performance improvement

2.3.4.1 Methodology

Further improvements in model prediction will require better constraining of the LBCs. The ARCTAS-CARB experiment devoted one flight to characterizing the LBC

under Asian inflow conditions. We performed an additional simulation where we used the observations over the eastern Pacific as the western LBC in the 60 km model domain. Sampled concentrations for eight gaseous pollutants (NO, NO_2, CO, O_3, H_2O_2, PAN, HNO_3 and SO_2) were averaged every 1000 m. The mean O_3 profile used for this case is also shown in blue in Figure 2.14a. We vertically interpolated these values to STEM grids, and replaced the RAQMS western LBC with these observation-based vertical gradients, in both 60 km and 12 km grids for the flight week. To identify the regions where we would expected to see the biggest changes in model predictions using the observational-based (Obs case) western LBC, we calculated forward trajectories along the flight path using the 12 km WRF meteorology fields. The 12 km WRF meteorology is compared with the aircraft observations along the flight path in Figure 2.15a. In general the 12 km simulation is able to capture the main features of the flow fields. The trajectories for flight altitudes at 2 - 4 km above the eastern Pacific are shown in Figure 2.15b. Air-masses sampled by the aircraft are shown to travel forward in time at multiple vertical layers and then descend into the Sacramento Valley, the west ridge of the Central Valley, and along coastal southern California.

2.3.4.2 Model performance improvement at the surface

The impact of the observational-based LBC on the 60 km predictions is shown in Figure 2.16, where the surface O_3 difference (Base case - Obs case) over California at 18 UTC (11am local time) on June 22, June 23 and June 24 is plotted. At 18 UTC on June 22, O_3 dropped 8 - 10 ppb over northern California in the 60 km Obs case. The effects of the western LBC were first felt over northern California and then were transported to the south and the east in the next 24 - 48 hours.

The impact of the observational-based western LBC on the 12 km predictions is shown in Figure 2.17. In contrast to the 60 km results, the 12 km impacts on June 22 are below 5 ppb all over California, except the border of California and Nevada, and the

spatial patterns are somewhat different. The impacts in the 12 km case travel from north to south and moved out of the study domain after June 24. These differences reflect the fact that the base 12 km simulation did not show as high a bias in northern California as did the 60 km simulation, and also indicate the difference in meteorological fields, which can be implied along with the similar trend of changes in CO at corresponded times (Figure 2.16 and 2.17, d - f). While the 60 km wind fields reflected major aspects of the on-shore flows, the 12 km wind fields better captured the detailed inland air movements and in-valley circulations. This is best seen in the fact that the changes in the 60 km Obs case mostly happened in northern California and in limited areas of central and southern California. In contrast, significant changes in O_3 for the 12 km Obs case are found over both northern and southern California.

To quantify the improvement in model simulations when using the observational-based western LBC, modeled and observed O_3 time series plots for four surface sites are shown in Figure 2.18. For the three sites located in northern California (Figure 2.18a - c), the 60 km base case generally over-predicted O_3 on June 22 and June 23. The Obs case reduced the over-prediction. A detailed comparison of maximum, minimum and average O_3 concentrations between model simulations and observations is summarized in Table 2.1 on June 22 and June 23. The O_3 concentrations from 60 km Obs case were closer to observations except that it missed the peak value at WGT on June 23. In contrast, at the JOT site in southern California, there was no change of O_3 after replacing western LBC with observations in 60 km during the same period (not shown). No significant differences were observed between 12 km base and Obs cases at three northern California sites (not shown), but at the JOT site some small changes were seen (Figure 2.18d). As Table 2.2 shows, maximum, average and minimum values of simulated O_3 in 12 km Obs case decreased and its average and minimum O_3 better captured the observations. The O_3 decrease was larger after June 23, due to the transport within the Central Valley as discussed previously. Table 2.1 and 2.2 show that R-squares between observed and

modeled surface O_3 during June 22 - June 24 were also improved at the surface sites in Obs cases, except for a slight decrease at TB site.

2.3.4.3 Model performance improvement along the flight path

The improvement of O_3 along the June 22 and June 24 DC-8 flights paths was also evaluated. To quantify the reduction of model biases, at all locations below 1000 m above ground, we define the Sensitivity Index (SI) in (2.2)

$$\text{Sensitivity Index\%} = \frac{|O3 \text{ in Obs case} - \text{Observed } O3|}{|O3 \text{ in Obs case} - O3 \text{ in base case}|} \times 100\% \quad (2.2)$$

The ratio of model bias can quantify the extent of model improvement by using the observational-based western LBC. O_3 predictions were improved in Obs cases at locations with SI below 100%. We also define cumulative sensitive data points, as well as the cumulative ratio in (2.3) and (2.4).

$$\text{Cumulative sensitive data points (SI)} = \text{number of data points} < \text{SI} \quad (2.3)$$

$$\text{Cumulative ratio (SI)} = \frac{\text{number of data points} < \text{SI}}{\text{all data points}} \quad (2.4)$$

Figure 2.19a shows that 60% and 70% of data points were improved in the 60 km and 12 km Obs cases. Furthermore, 26% and 17% of all data points in 60 km and 12 km cases, respectively, had SI values below 80%. The model biases for these points were reduced by more than 20% when the observational-based LBC was used. These data points are colored by SI in Figure 2.19b and 2.19c. They are mostly located in northern California, near shore of southern California and downwind areas of the Central Valley. The highest improvements (with SI < 20%) for the 60 km case were over northern California, and over southern California downwind of the Central Valley in the 12 km case. These improvements in 60 km and 12 km model performance along two flight paths on June 22 and June 24 show some similarities to the improvement seen at the surface sites in response to the observational-based western LBC.

These results suggest that the added observations contributed appreciably to improving model predictions. Chemical data assimilation in global models holds the possibility of reducing uncertainties in LBC used in limited-area air quality models. However, the RAQMS first guess boundary conditions used are based on MLS and OMI data that contain low information content in the mid to lower troposphere. Additional information is available from current satellite instruments such as TES, however TES lacks the temporal and spatial coverage needed for LBCs. The measurements from aircraft contain high information content and the observational-based LBC can highly improve regional model performance over downwind areas at lower troposphere. The challenge that remains is to improve our observing system in ways that it can provide the spatial and temporal information needed to improve model predictions of air quality. This should be a priority of our future observing systems.

2.4 Summary and conclusions

Tracer and full-chemistry versions of STEM model at three spatial scales were used to analyze the effects of transported background O_3 from the eastern Pacific on California air quality during the ARCTAS-CARB experiment conducted in June 2008. Two different spatial resolutions and a variety of lateral boundary conditions (LBC) were applied in the full-chemistry model simulations.

Tracer model and back trajectories indicated that during June 21 - June 24 strong Asian inflows affected northern California. Based on the 12 km meteorological fields, we analyzed reconstructed O_3 distributions along air-mass back trajectories originating at five California sites and correlated observed and modeled O_3 between coastal THD and inland TB sites to study O_3 transport patterns. During the entire ARCTAS-CARB study period O_3 levels in the inflow air were less than 40 ppb O_3 below 1.5 km. The time-lag correlations of O_3 at this altitude with a surface site at TB showed maximum correlations of 0.3 and a transport time of less than 30 hours. Under Asia inflow conditions during

June 21 - June 24 the peak R-square value increased to approximate 0.7, and the transport altitude was extended to around 3 km where 60 - 80 ppb of coastal O_3 was observed.

We evaluated the sensitivity of modeled O_3 to various treatments of the boundary conditions and showed that modeled O_3 over downwind areas were highly sensitive to the western LBC during June 21 - June 24. The use of constant values failed to capture the varied O_3 vertical structures over the eastern Pacific during this time period. We showed the results of using top and lateral boundary conditions downscaled from the RAQMS global model, but also showed that they can contain biases. Temporal averaging of these boundary conditions is shown to be one way to reduce such biases.

In addition to model-based real-time LBC, the measurements on the June 22 DC-8 flight provided actual O_3 vertical gradients over the ocean, which were used as LBC. Use of these observation-based LBC was shown to improve O_3 predictions at four California inland surface sites and at altitudes below 1000 m along two DC-8 flight tracks. The extent of model improvement over different areas depended on base case performance, meteorology fields and the discrepancies of model-based western LBC from the flight observations.

We conclude from this study that:

1) The pollutant transport patterns from oceanic background and their effects on California air quality (or other similar regions) depend on the vertical structures over the eastern Pacific and meteorological conditions. Long-range transport of Asian inflows can change the pollutant profiles over the eastern Pacific during summertime significantly. Capturing this variability in the observations is important and challenging as information is needed above the surface.
2) Accurate real-time LBC for long-lived species together with high quality meteorology fields improve model predictions at areas where the background pollutants are transported aloft as well as their downwind regions.

Improvements in our observing systems are needed that provide information on the three-dimensional nature of pollutant distributions are needed to improve our capability to predict pollution levels and to better quantify the influence of these Asian inflows on the U. S. west coast air quality.

Table 2.1 Comparisons between observed and modeled O_3 at three northern California sites, better model simulations are in bold (OBS-observations)

		TB (ppb)			LAV (ppb)			WGT (ppb)		
		OBS	60km base	60km Obs.	OBS	60km base	60km Obs.	OBS	60km base	60km Obs.
06/22	Max.	57.0	57.1	**57.0**	58.0	58.8	**58.6**	51.7	72.0	**67.0**
	Mean	42.8	48.7	**48.2**	39.9	51.1	**50.5**	34.6	51.2	**49.4**
	Min.	31.0	38.9	**38.0**	15.0	43.1	**42.9**	22.4	36.3	**36.2**
06/23	Max.	62.0	75.8	**63.1**	64.0	85.0	**73.0**	82.1	**80.7**	70.9
	Mean	53.9	64.7	**54.7**	53.3	75.3	**64.6**	44.0	70.4	**59.5**
	Min.	34.	52.2	**49.3**	40.0	62.0	**54.6**	21.8	62.4	**50.6**
06/22 - 06/24	RSQ (OBS:Model)		**0.35**	0.31		0.35	**0.37**		0.39	**0.44**

Table 2.2 Comparisons between observed and modeled O_3 at the southern California site JOT, better model simulations are in bold (OBS-observations)

		JOT (ppb)		
		OBS	12 km base	12 km Obs.
06/22	Max.	113.0	**89.8**	88.1
	Mean	64.3	68.3	**67.8**
	Min.	46.0	58.6	**58.4**
06/23	Max.	87.0	**83.7**	79.3
	Mean	59.1	67.8	**63.3**
	Min.	51.0	56.1	**54.8**
06/24	Max.	93.0	101.0	**94.7**
	Mean	63.7	81.6	**74.4**
	Min.	45.0	71.0	**65.3**
06/22 – 06-24	RSQ (OBS:Model)		0.40	**0.44**

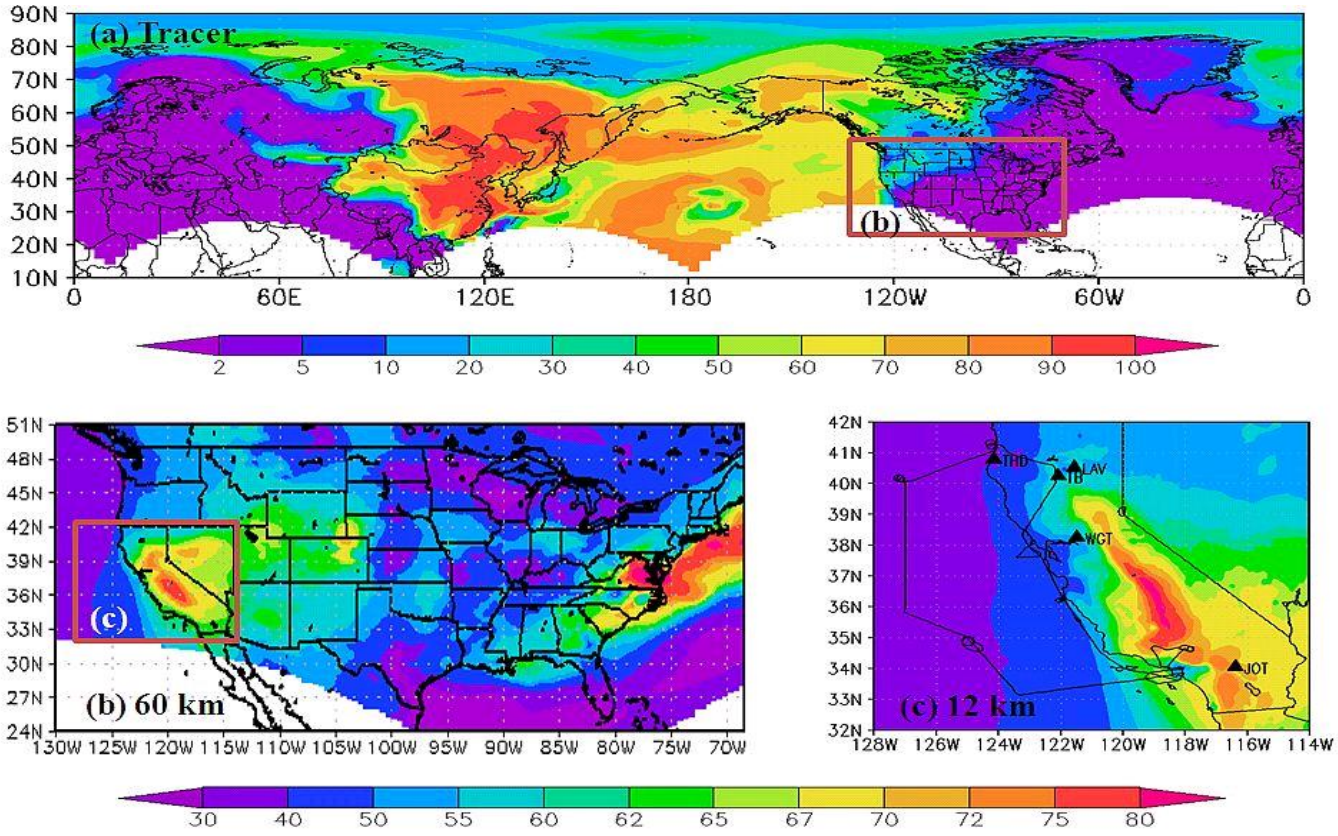

Figure 2.1 Three domains of the STEM modeling system. (a) Averaged (24-hour) surface contribution of China CO as % during 06/21-06/24 in tracer domain; Averaged (24-hour) O_3 concentrations at surface from the (b) 60 km and (c) 12 km (Five surface sites and 06/22 DC-8 flight path included) model simulations during 06/18-06/28, 2008

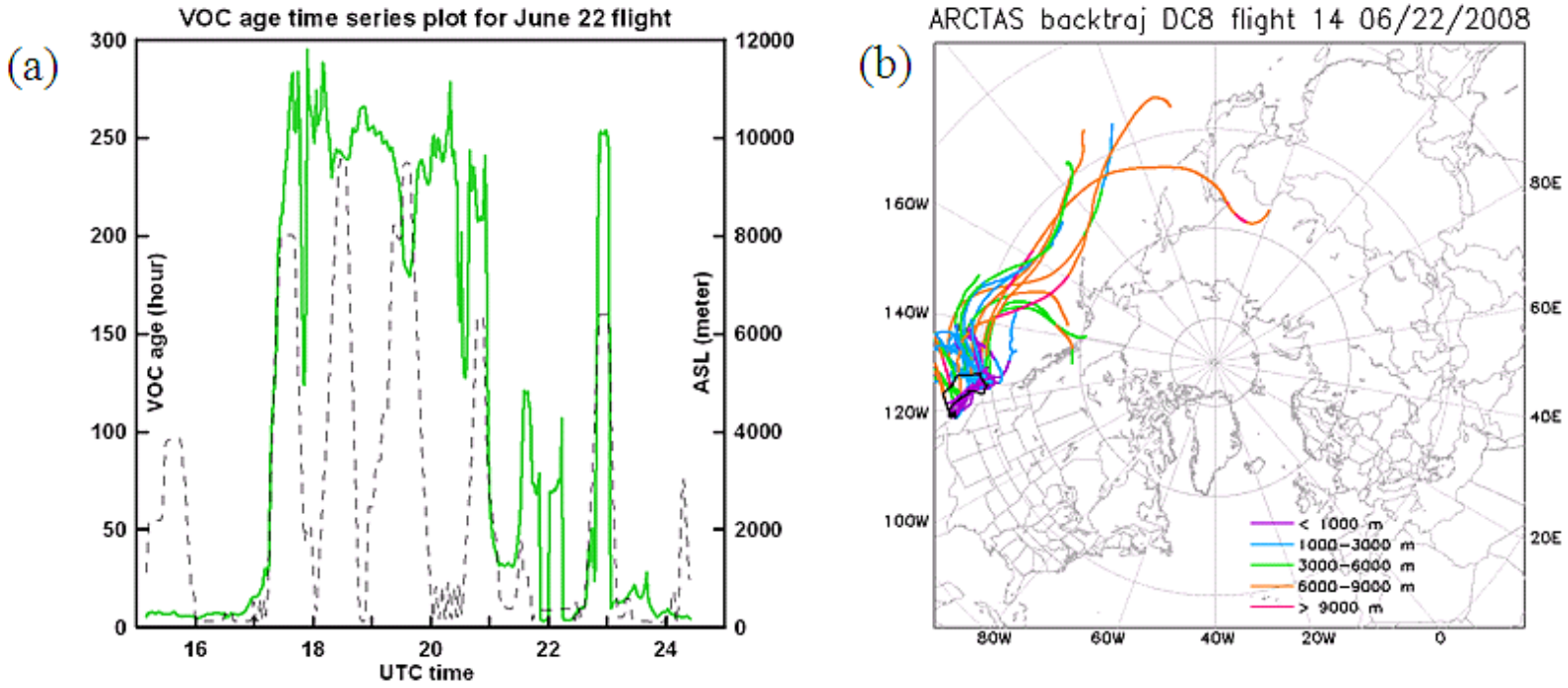

Figure 2.2 The identification of air-mass sources during June 22 DC-8 flight time. (a) VOC ages and (b) Five-day back trajectories along June 22 DC-8 flight path

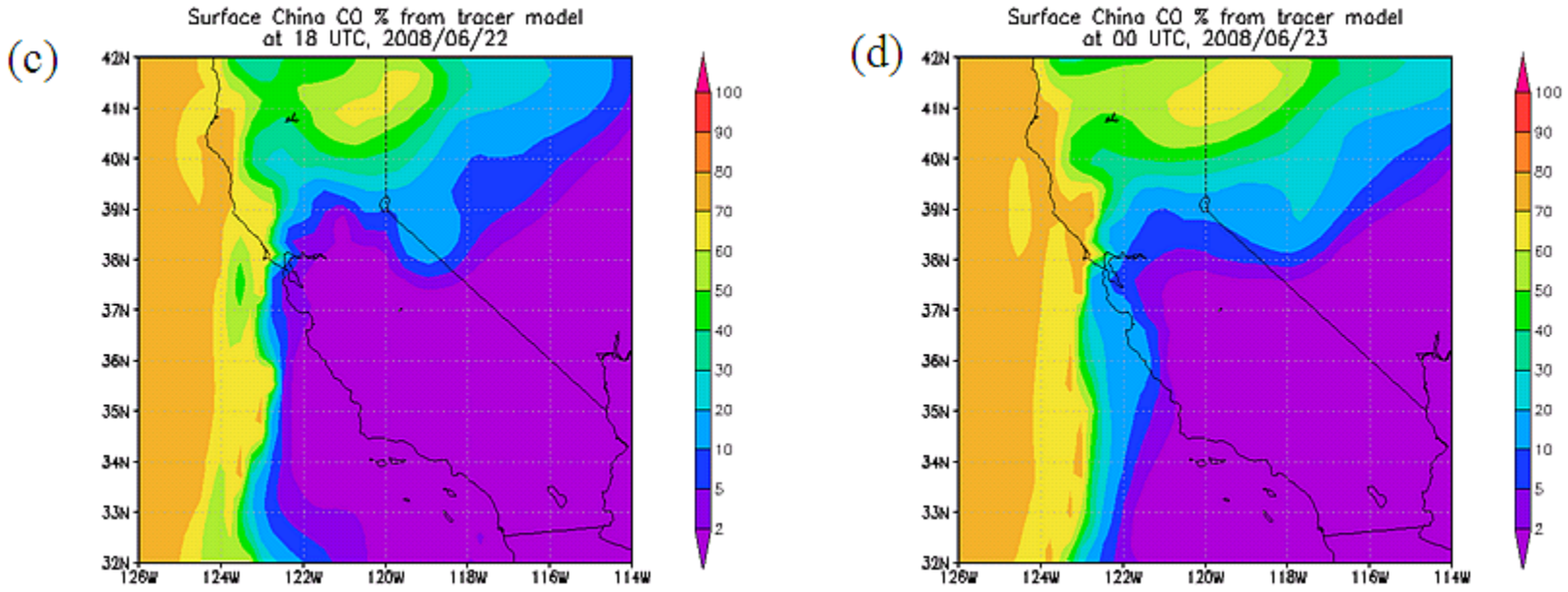

(c, d) Tracer surface contribution of China CO as % over California during flight time
Figure 2.2 Continued

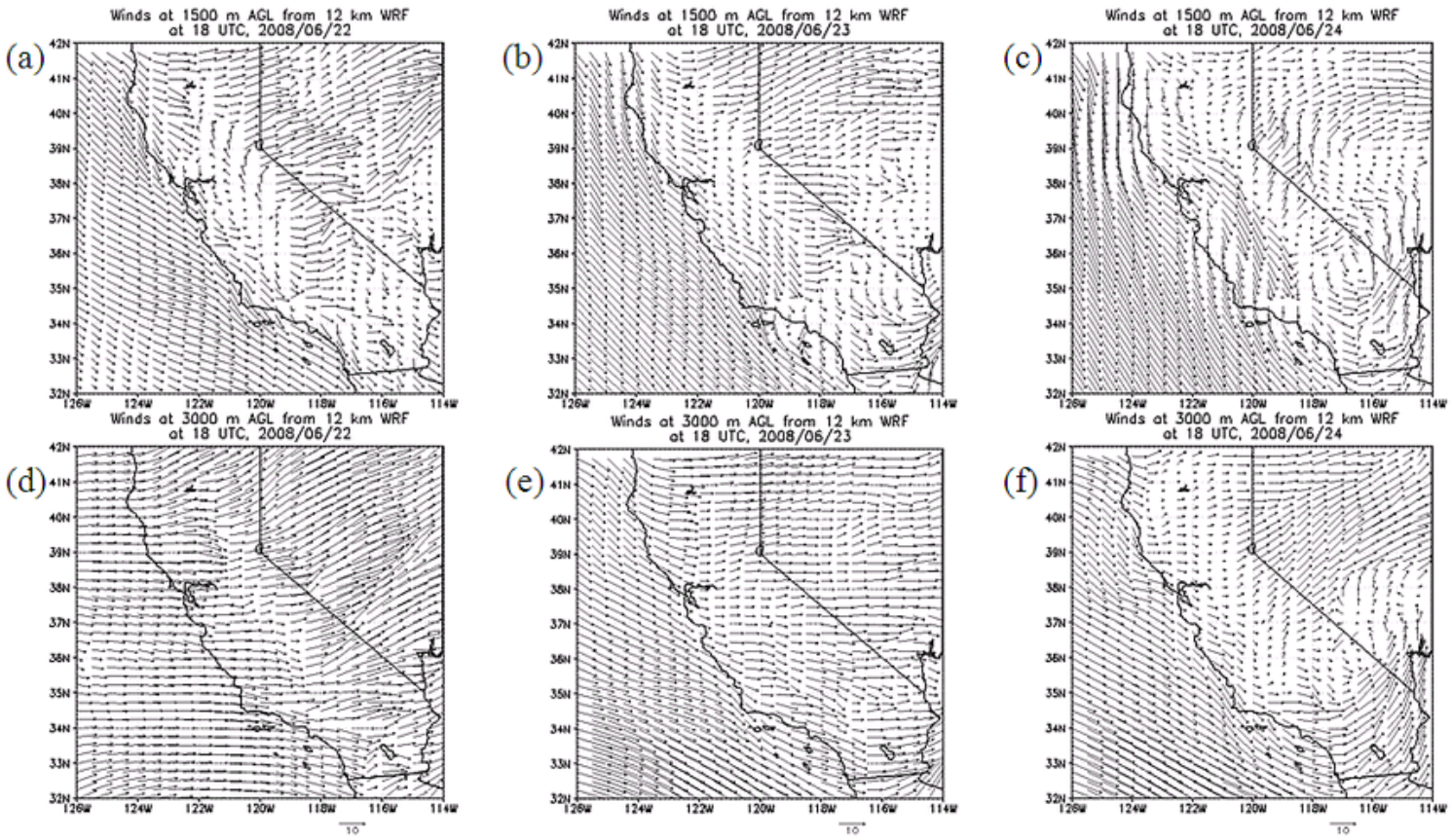

Figure 2.3 12 km WRF wind fields at two altitudes AGL over California at 18 UTC on three days of June, 2008. (a-c) 1500 m; (d-f) 3000 m; (a;d) June 22 (b;e) June 23; (c;f) 24

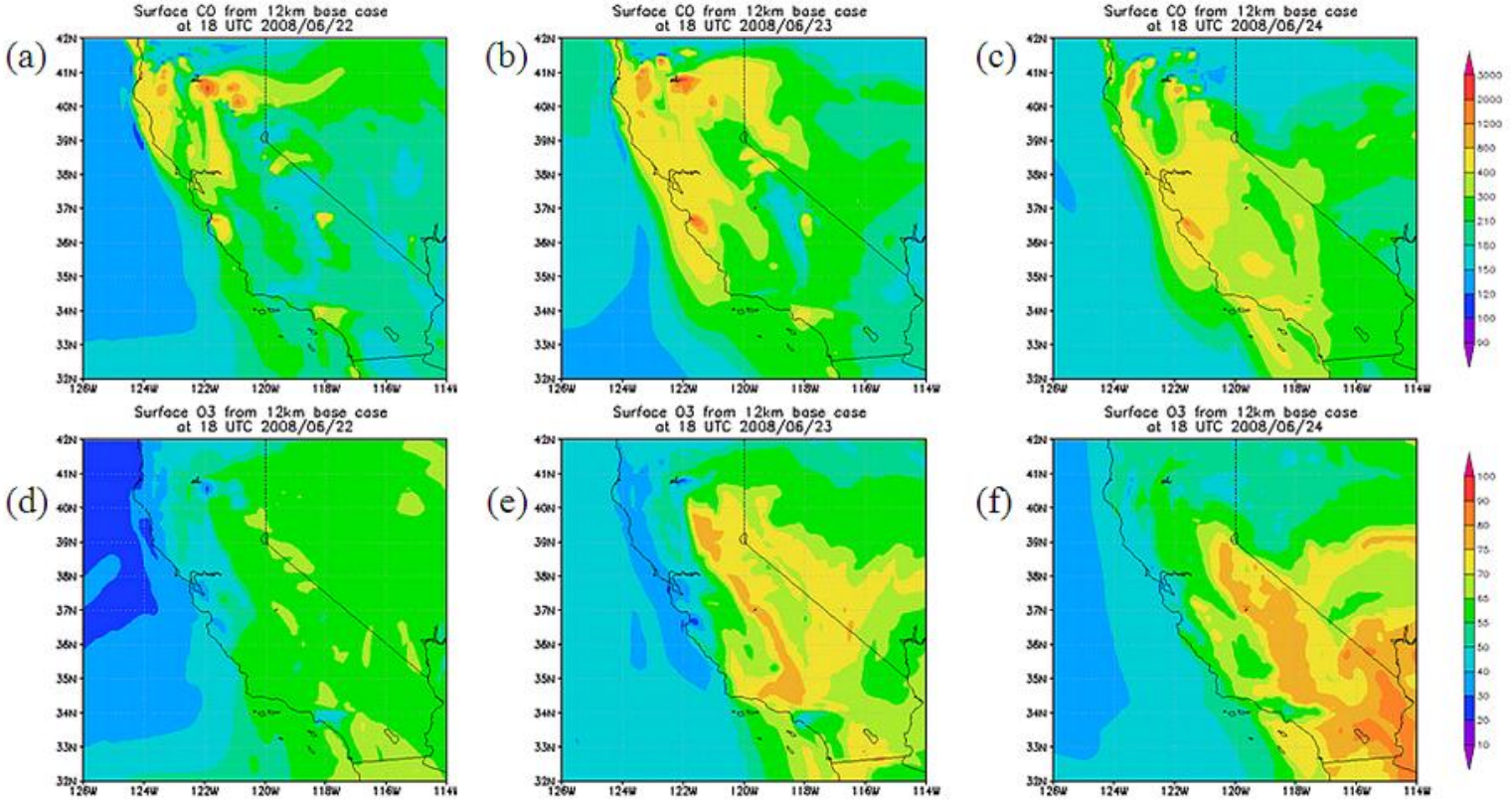

Figure 2.4 12 km modeled surface CO and O_3 over California at 18 UTC at 18 UTC on three days of June, 2008. (a-c) CO; (d-f) O_3; (a;d) June 22 (b;e) June 23; (c;f) 24

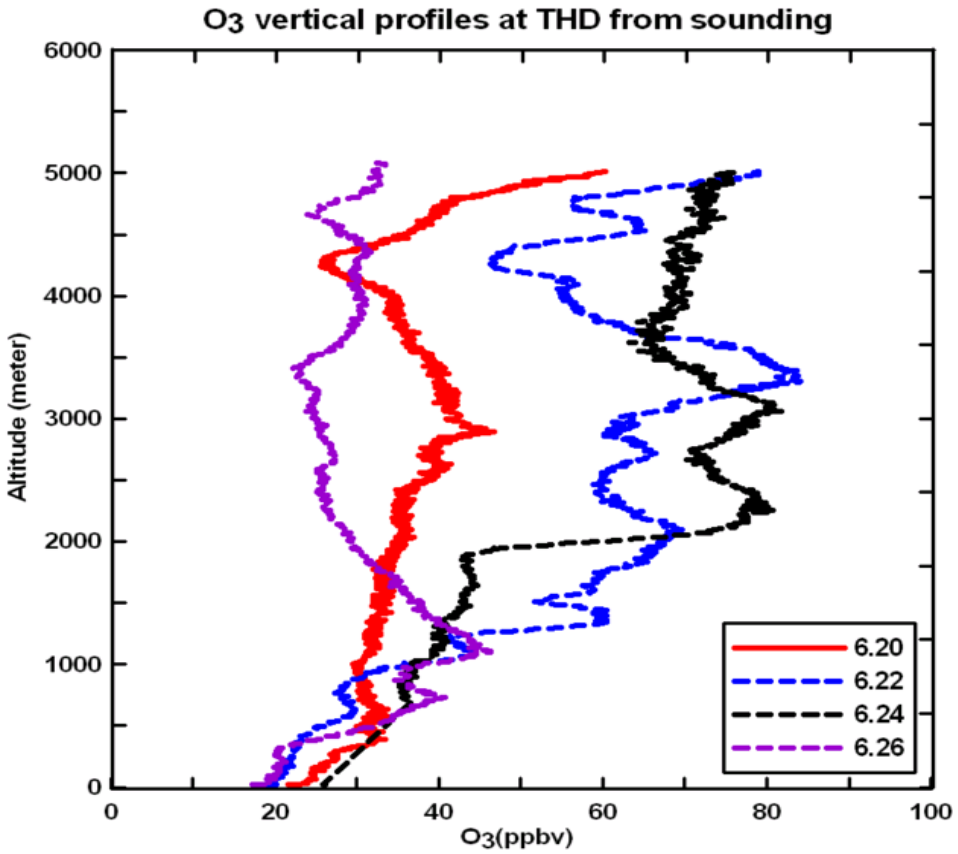

Figure 2.5 Vertical profiles of O_3, its precursors and reservoirs at THD, California. (a) O_3 vertical profiles at THD on four sounding days

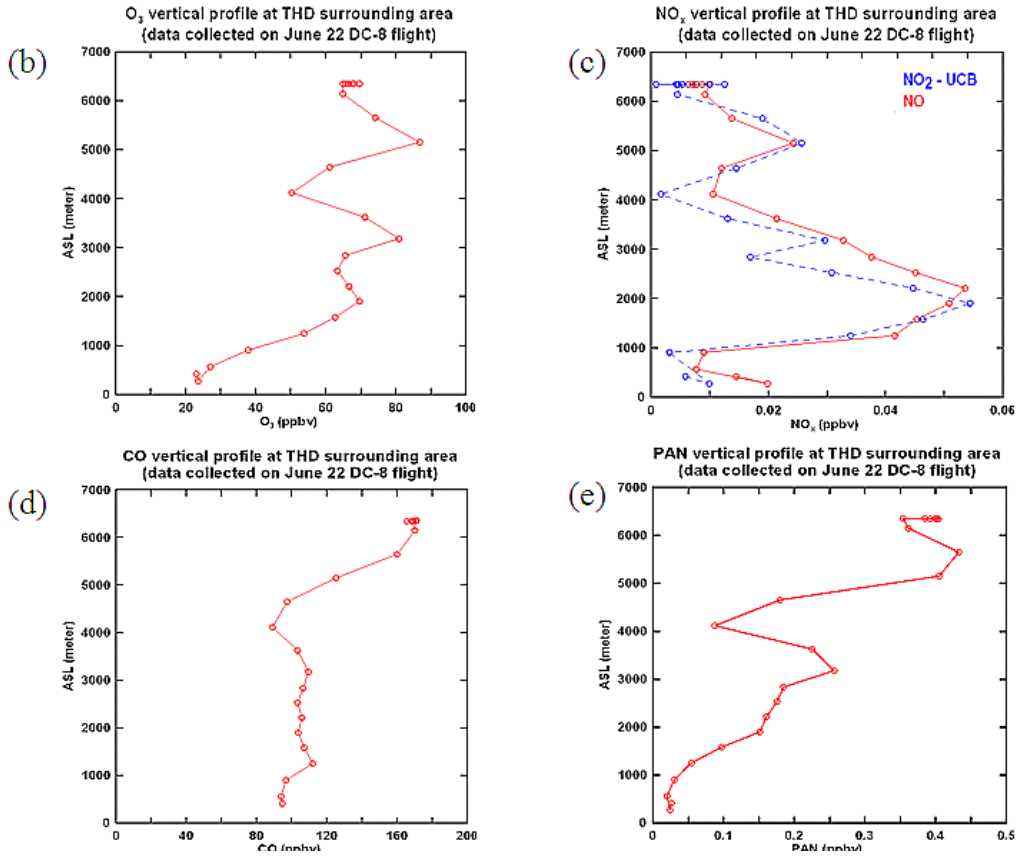

(b) O_3 (c) NO_x (d) CO (e) PAN vertical profiles on June 22 at THD surrounding areas, data collected on DC-8
Figure 2.5 Continued

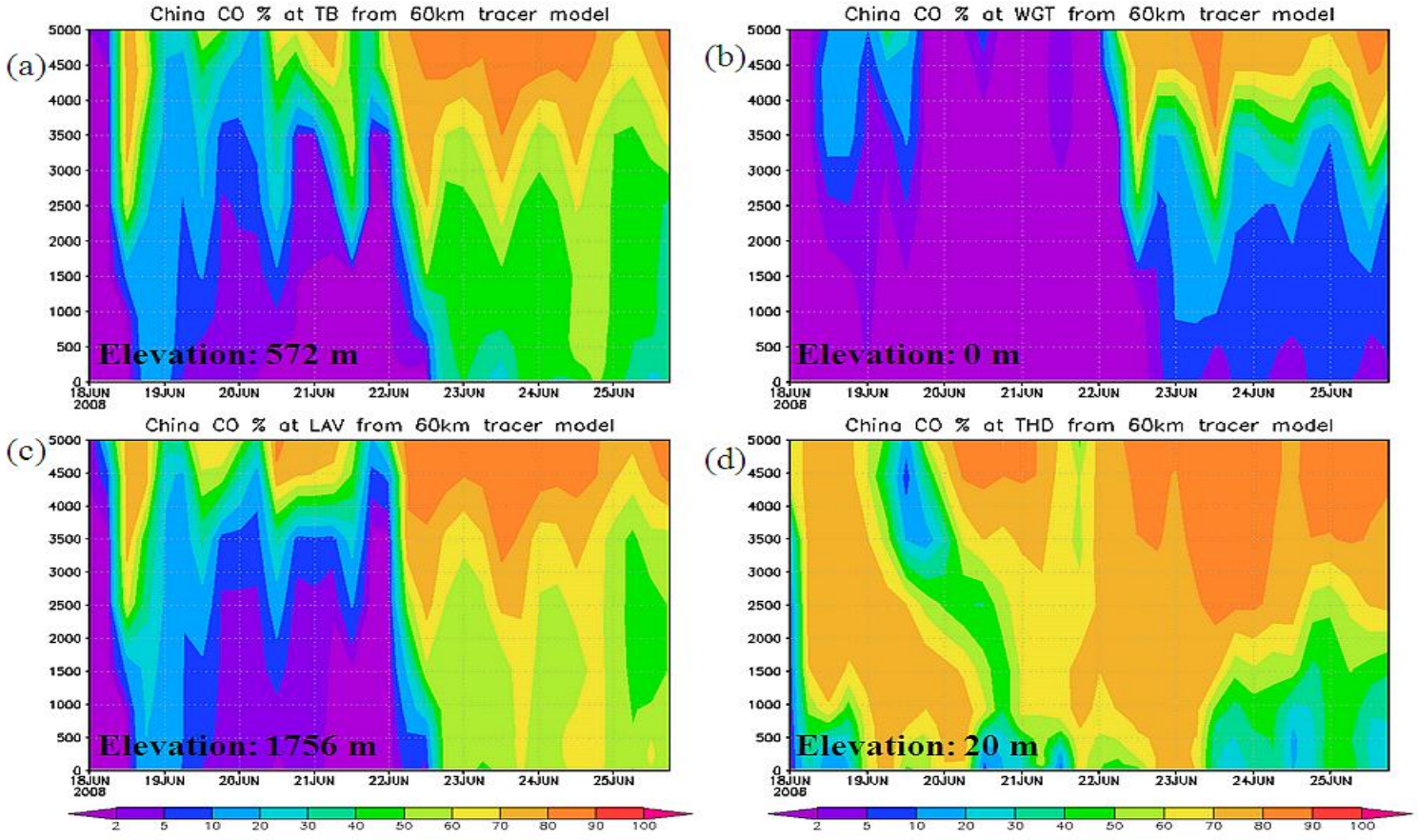

Figure 2.6 Time-height (AGL, m) curtain plots of China CO contributions across four sites. (a) TB; (b) WGT; (c) LAV; (d) THD

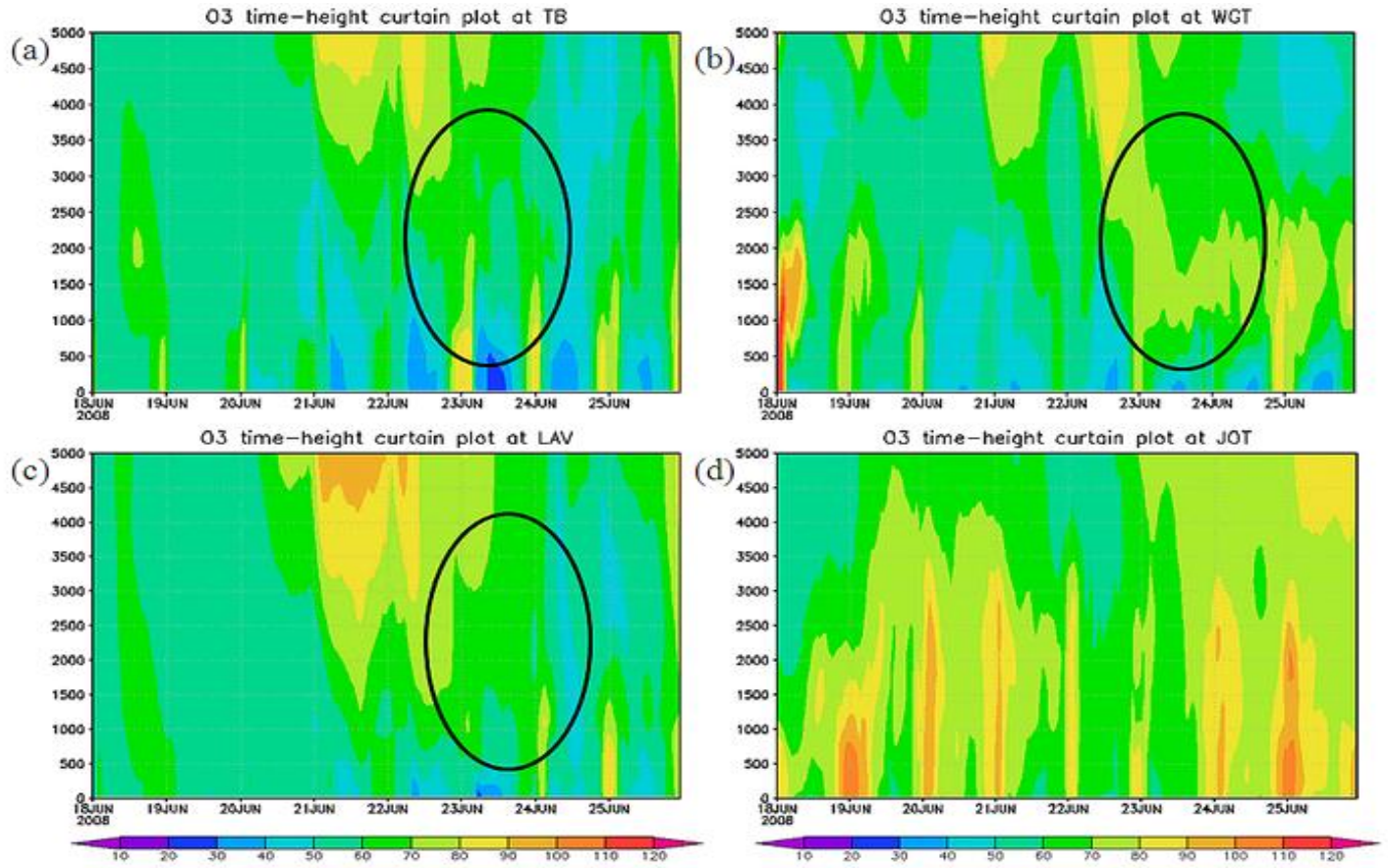

Figure 2.7 O_3 time-height (AGL, m) curtain plots from the 12 km base case across four sites. (a) TB; (b) WGT; (c) LAV; (d) JOT

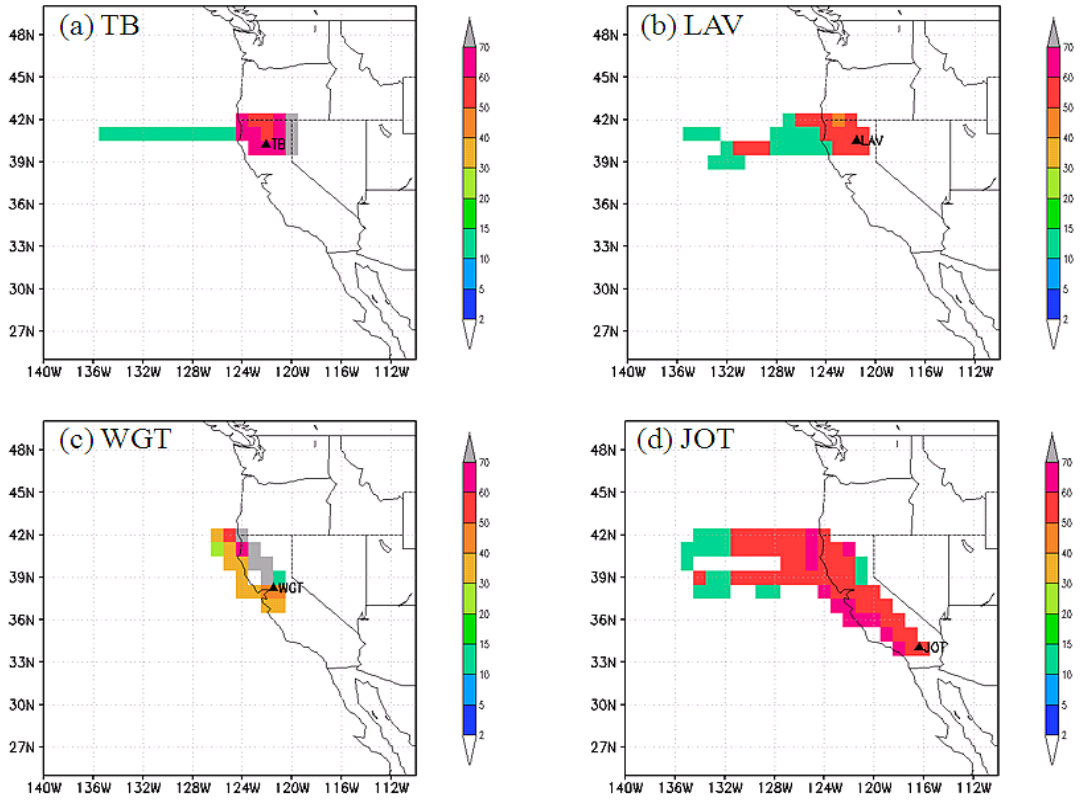

Figure 2.8 Reconstructed O_3 concentrations along three-day back trajectories based on 12 km meteorology fields originating at four sites on June 23. (a) TB; (b) LAV; (c) WGT; (d) JOT

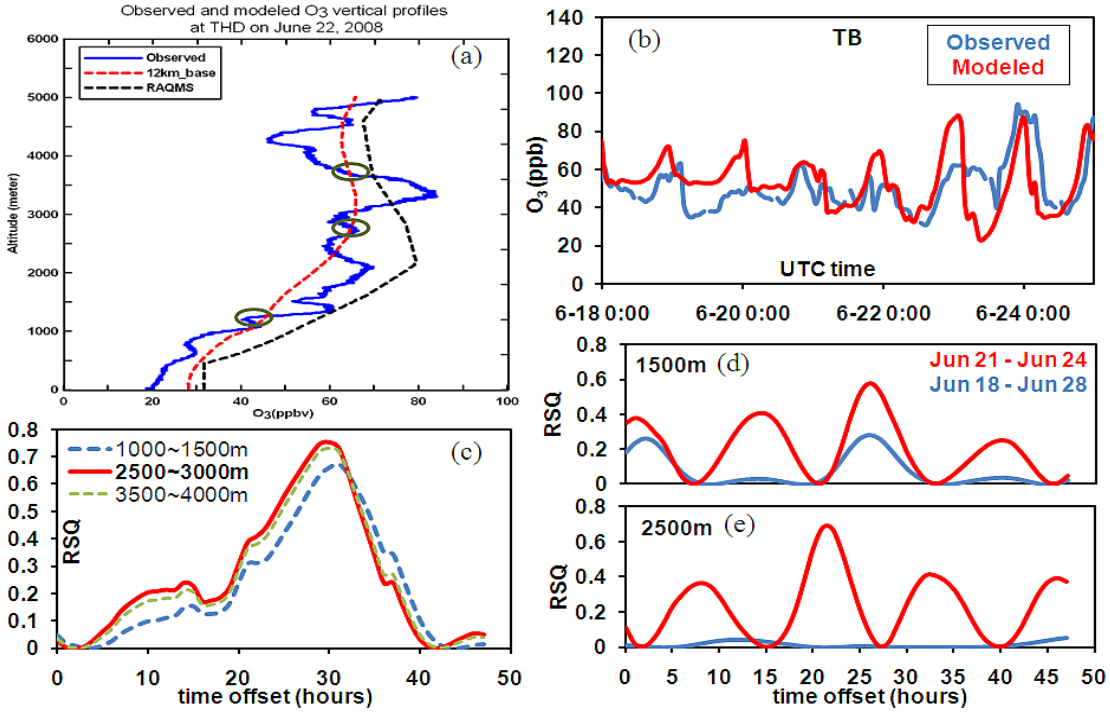

Figure 2.9 The coastal-inland transport pattern. (a,b) Observed and 12 km-modeled O_3 profiles at THD (coastal) and TB (inland); (c) Time-lag correlation analysis based on observations (d-e) Time-lag correlation analysis based on model simulations

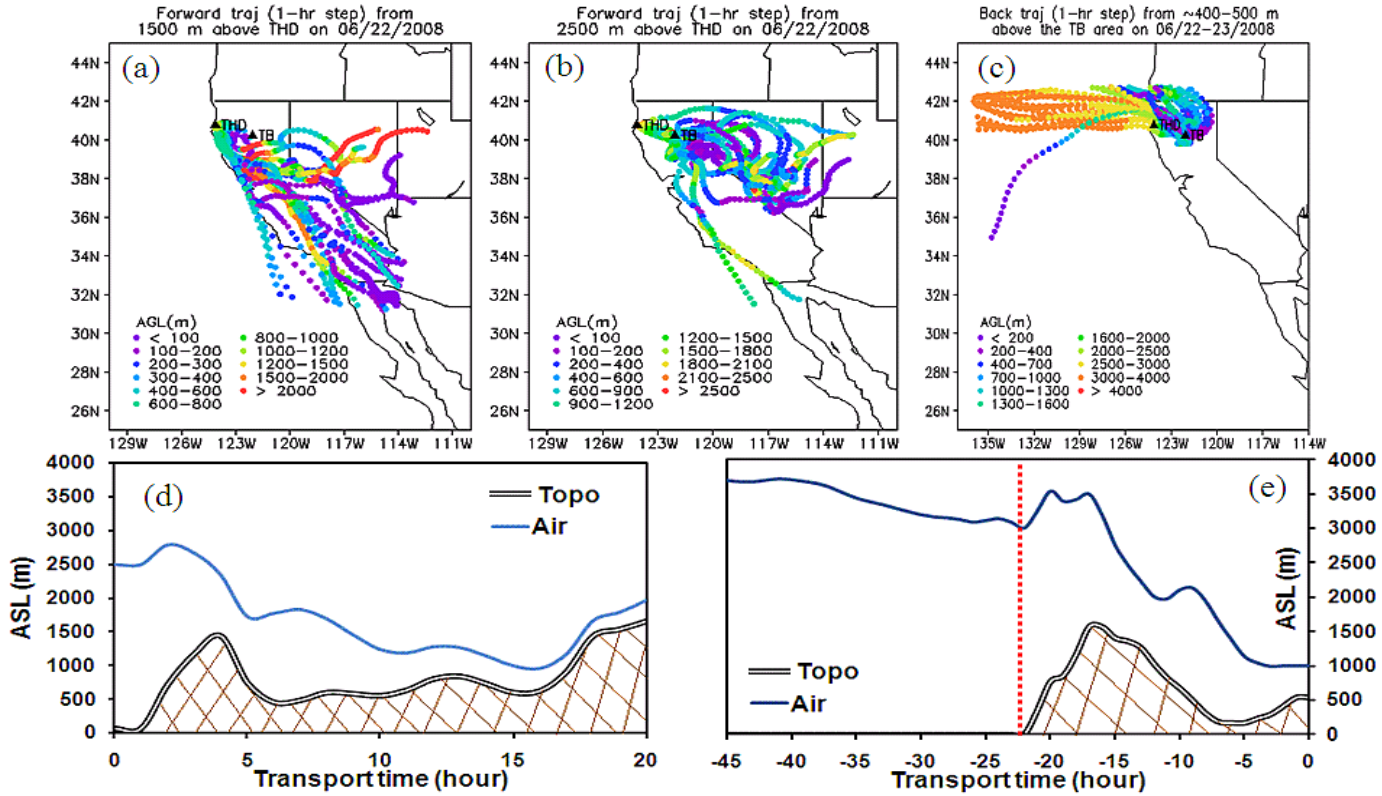

Figure 2.10 Trajectories during the specific period. Forward trajectories originating on 06/22 from (a) 1500 m (b) 2500 m above THD;(c) Back trajectories originating from 400-500 m above TB area; Transport height as a function of time along with topography along the (d) forward trajectory originating at 2500 m above THD, June 22 01UTC (e) back trajectory originating from 400-500 m above TB area, 06/23 00 UTC

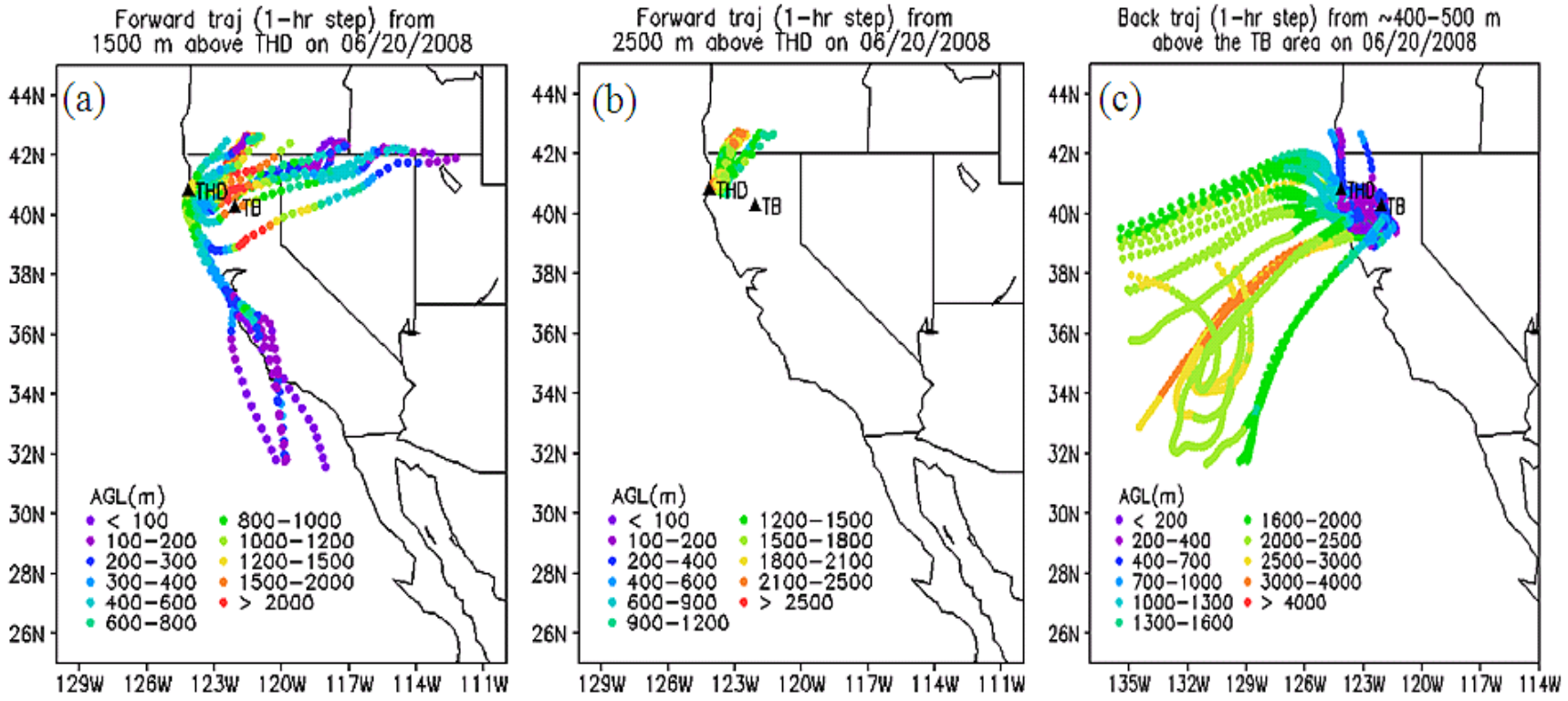

Figure 2.11 Trajectories out of the June 21-24 period. Forward trajectories originating on 06/20 from (a) 1500 m (b) 2500 m above THD; (c) Back trajectories originating from 400-500 m above TB area

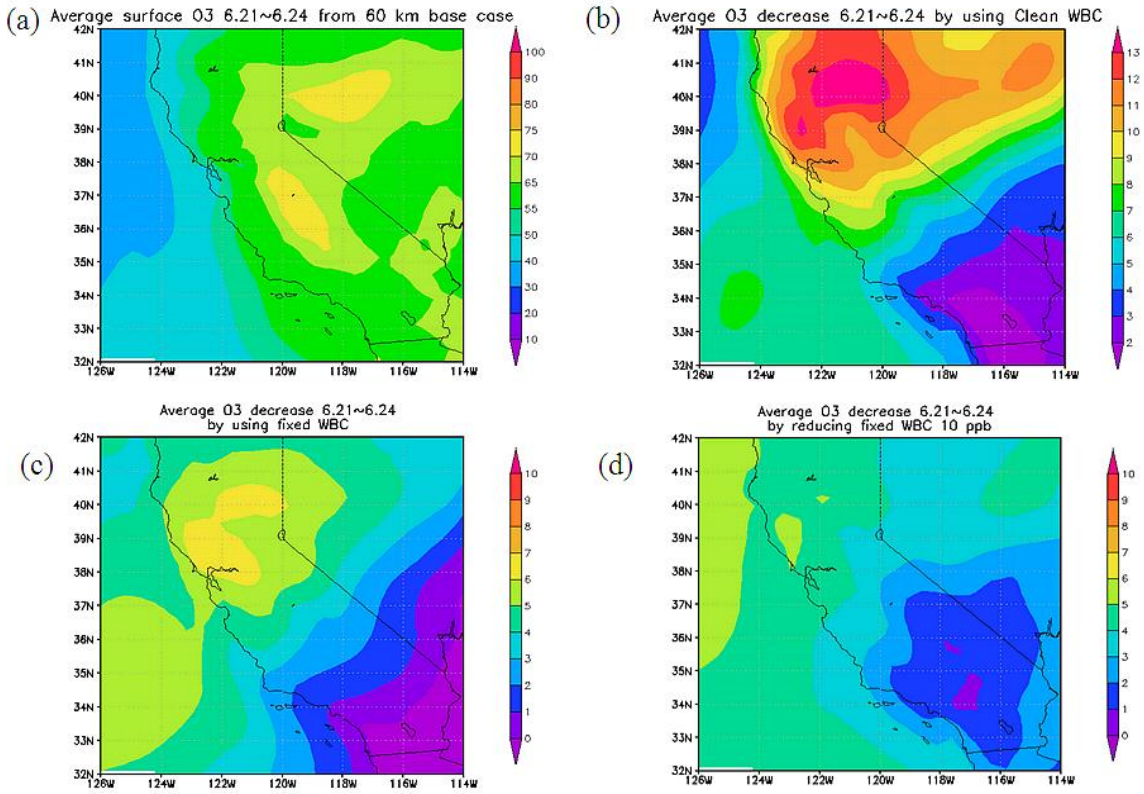

Figure 2.12 Two-dimensional plots of LBC sensitivity study in 60 km grids (a) Average surface O_3 from the base case; Average surface O_3 decrease relative to the base case during June 21 – 24 by using (b) Clean WBC (c) Fixed BC; (d) O_3 reduction relative to the Fixed BC case by using Reduced WBC

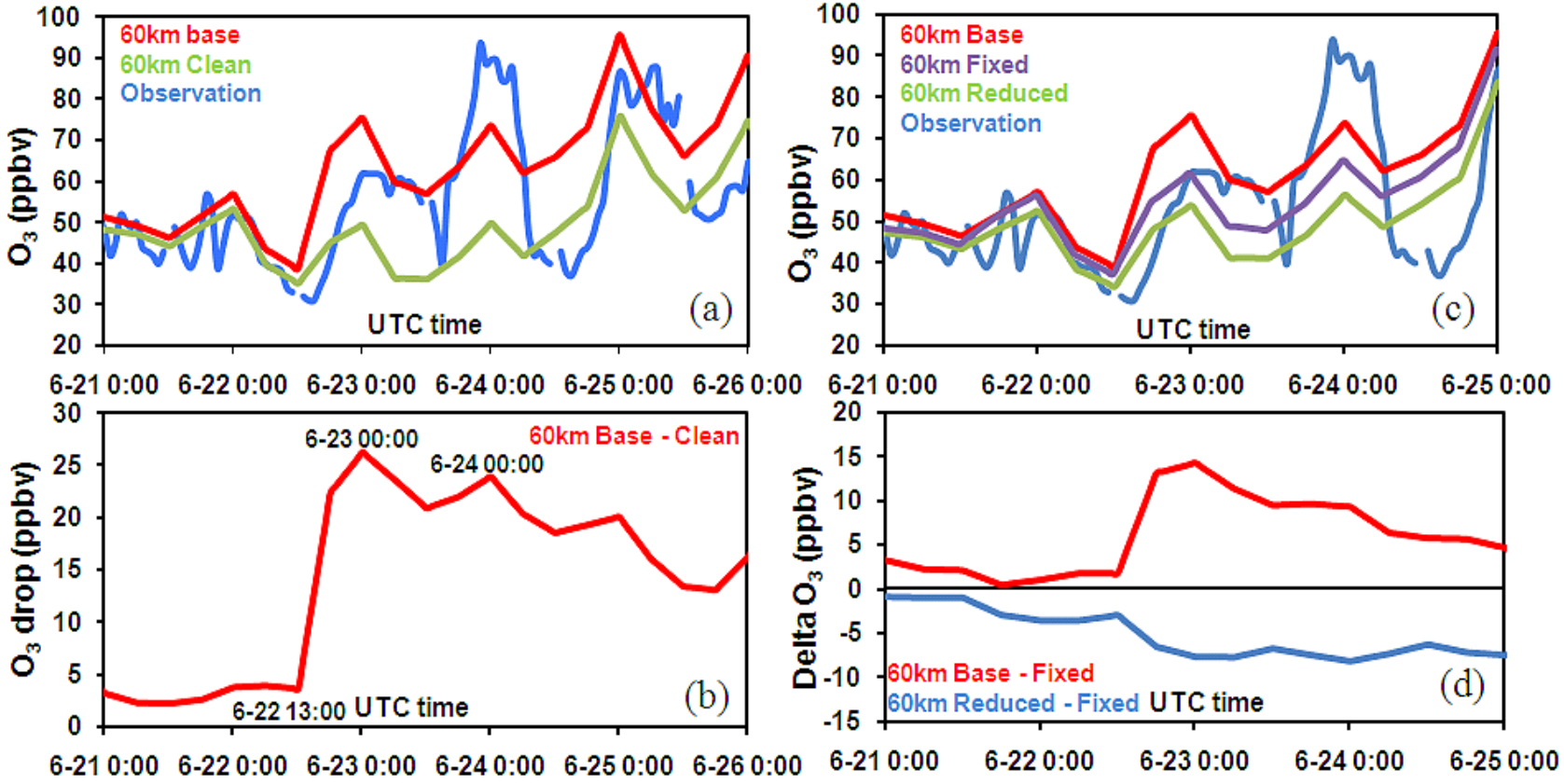

Figure 2.13 Time series plots of LBC sensitivity study in 60 km grids. (a) Time series plots of O_3 from STEM 60 km simulations and observations at TB; (b) The O_3 drop in the Clean WBC case relative to the base case at TB; (c) Time series plots of O_3 from STEM 60 km simulations and observations at TB; (d) Delta O_3 between Base case and Fixed BC case, Reduced WBC case and Fixed BC case

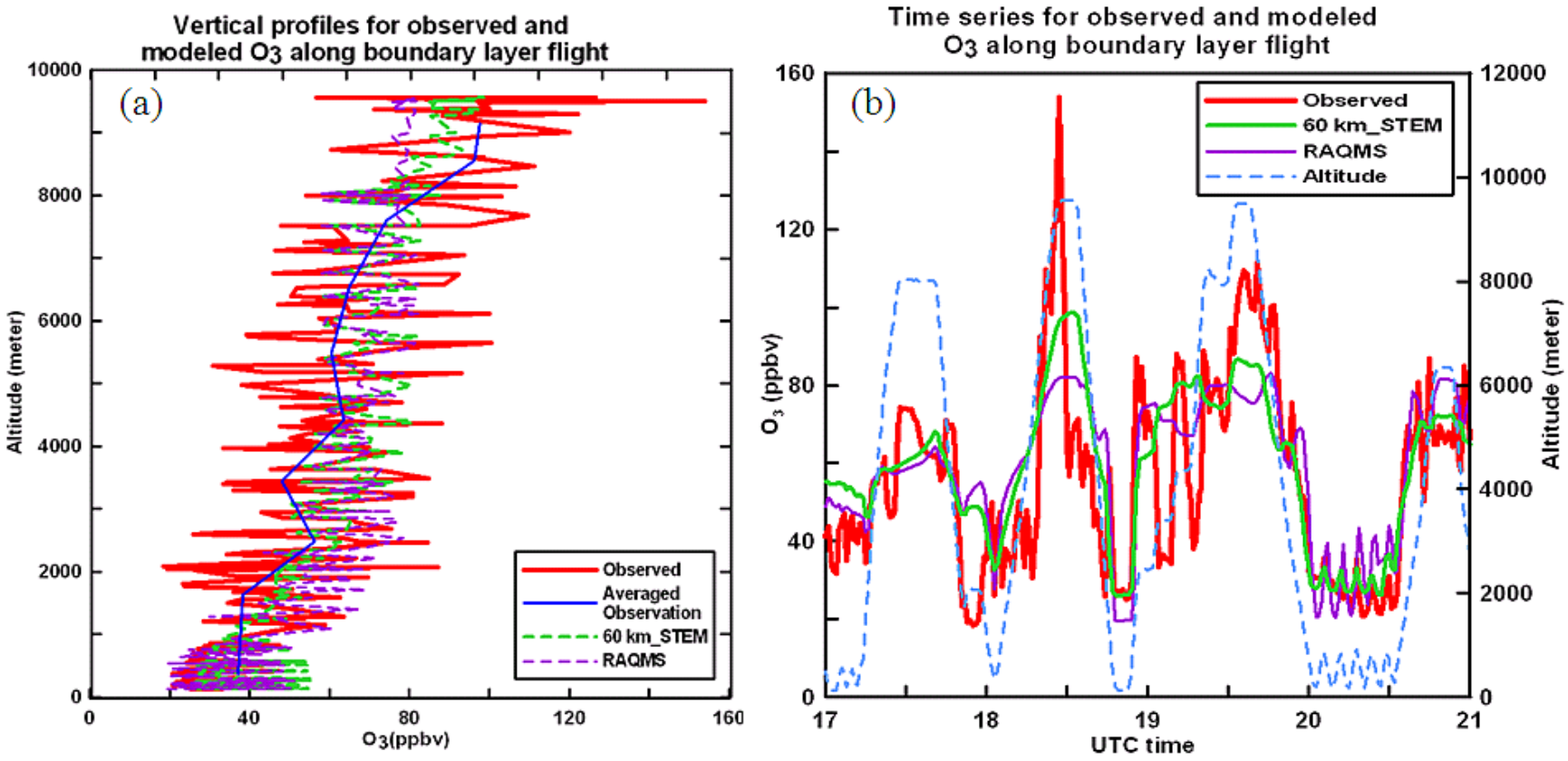

Figure 2.14 Assessment of LBCs: RAQMS and 60 km STEM base results were used as LBCs for 60 km and 12 km STEM base cases, respectively. (a) Observed and Modeled O_3 vertical profiles and (b) Time series plots along oceanic flight path.

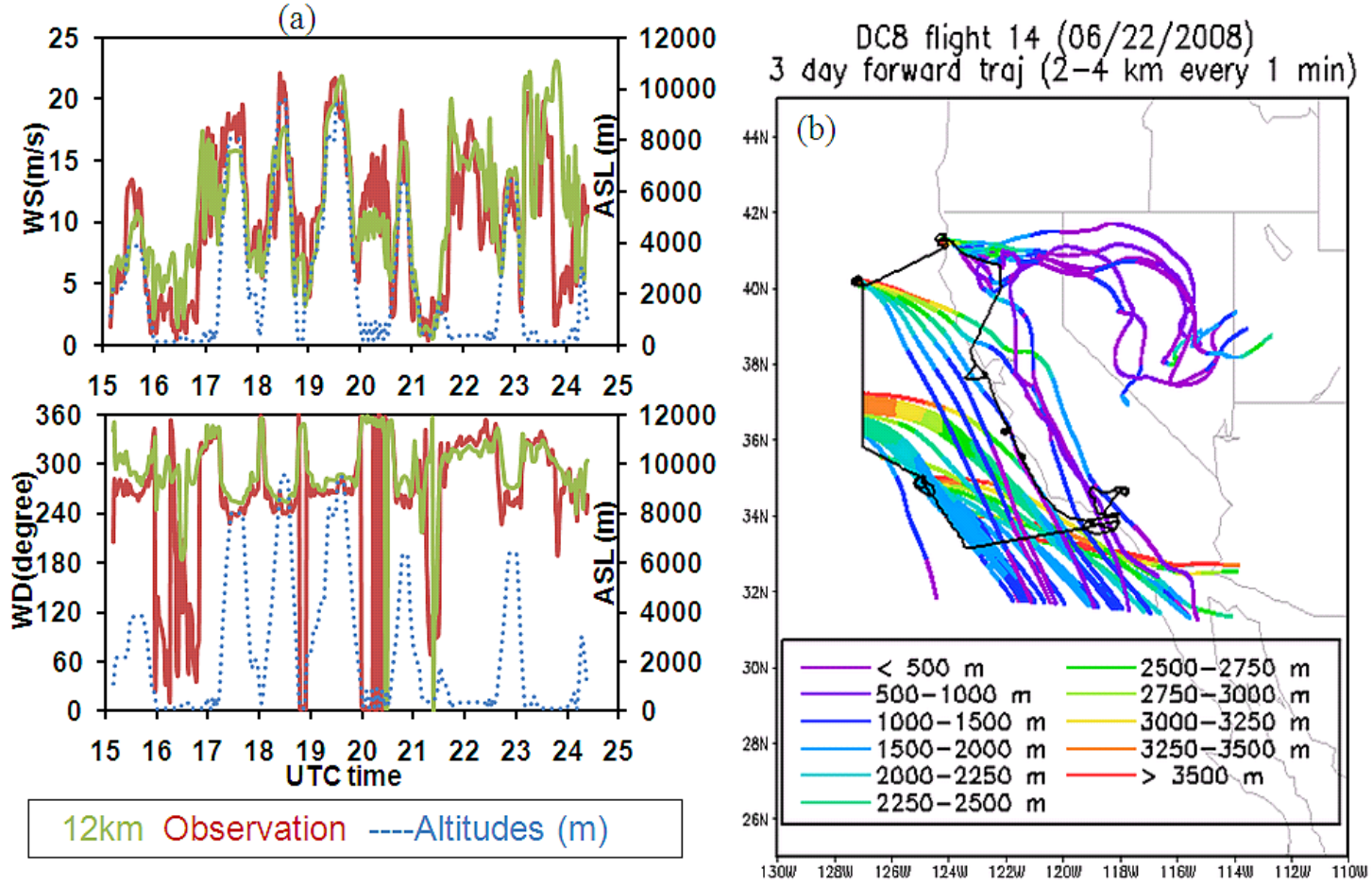

Figure 2.15 Wind fields along the June 22 DC-8 flight path, and the downwind areas (a) Observed and 12 km WRF modeled wind fields; (b) Forward trajectories originating at 2 - 4 km of oceanic part of the same flight

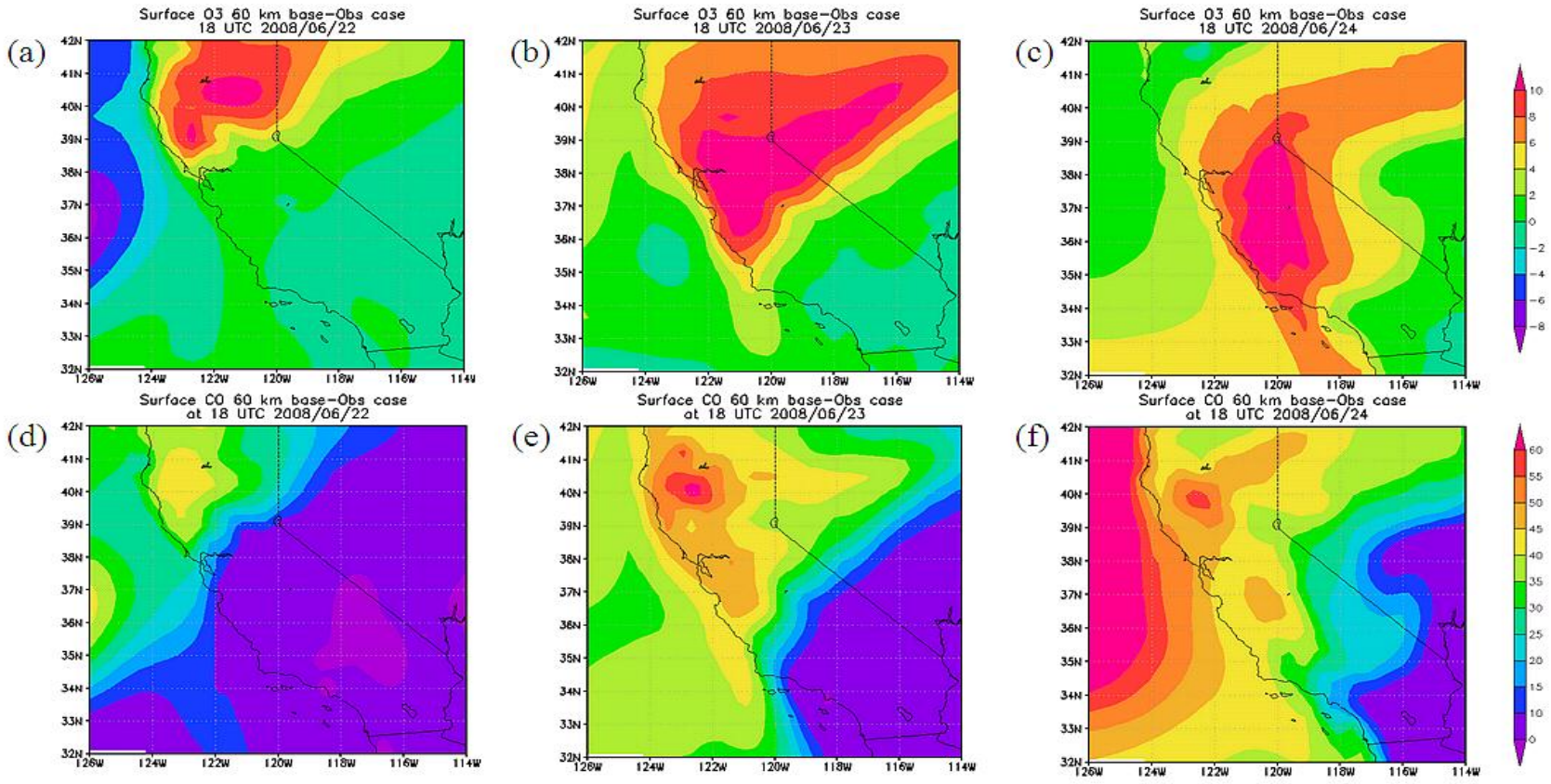

Figure 2.16 Impacts of using observational-based LBC on predicted California surface O_3 and CO at 18 UTC on three days of June, 2008 in 60 km grids. (a-c) O_3; (d-f) CO; (a;d) 22; (b;e) 23; (c;f) 24

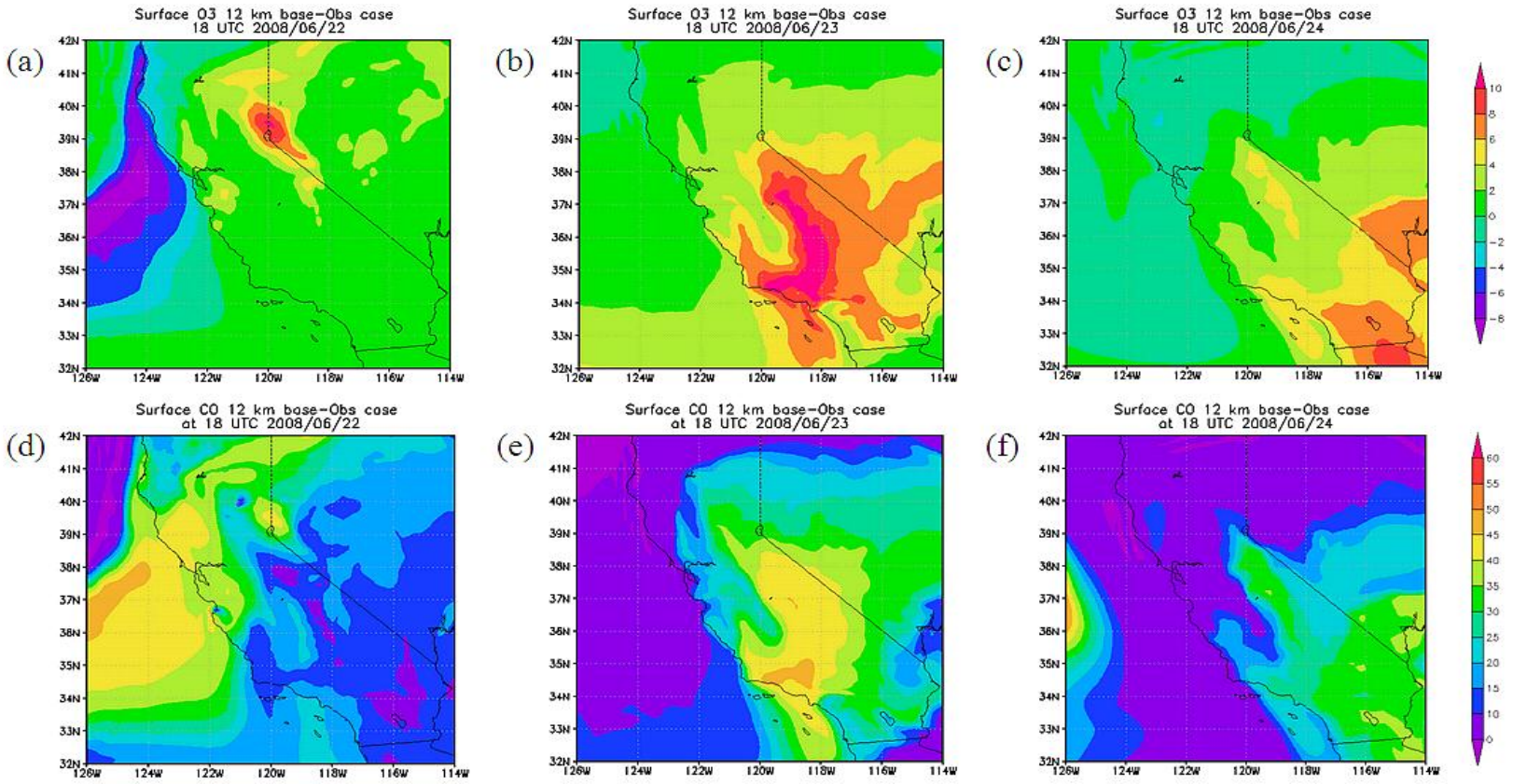

Figure 2.17 Impacts of using observational-based LBC on predicted California surface O_3 and CO at 18 UTC on three days of June, 2008 in 12 km grids. (a-c) O_3; (d-f) CO; (a;d) 22; (b;e) 23; (c;f) 24

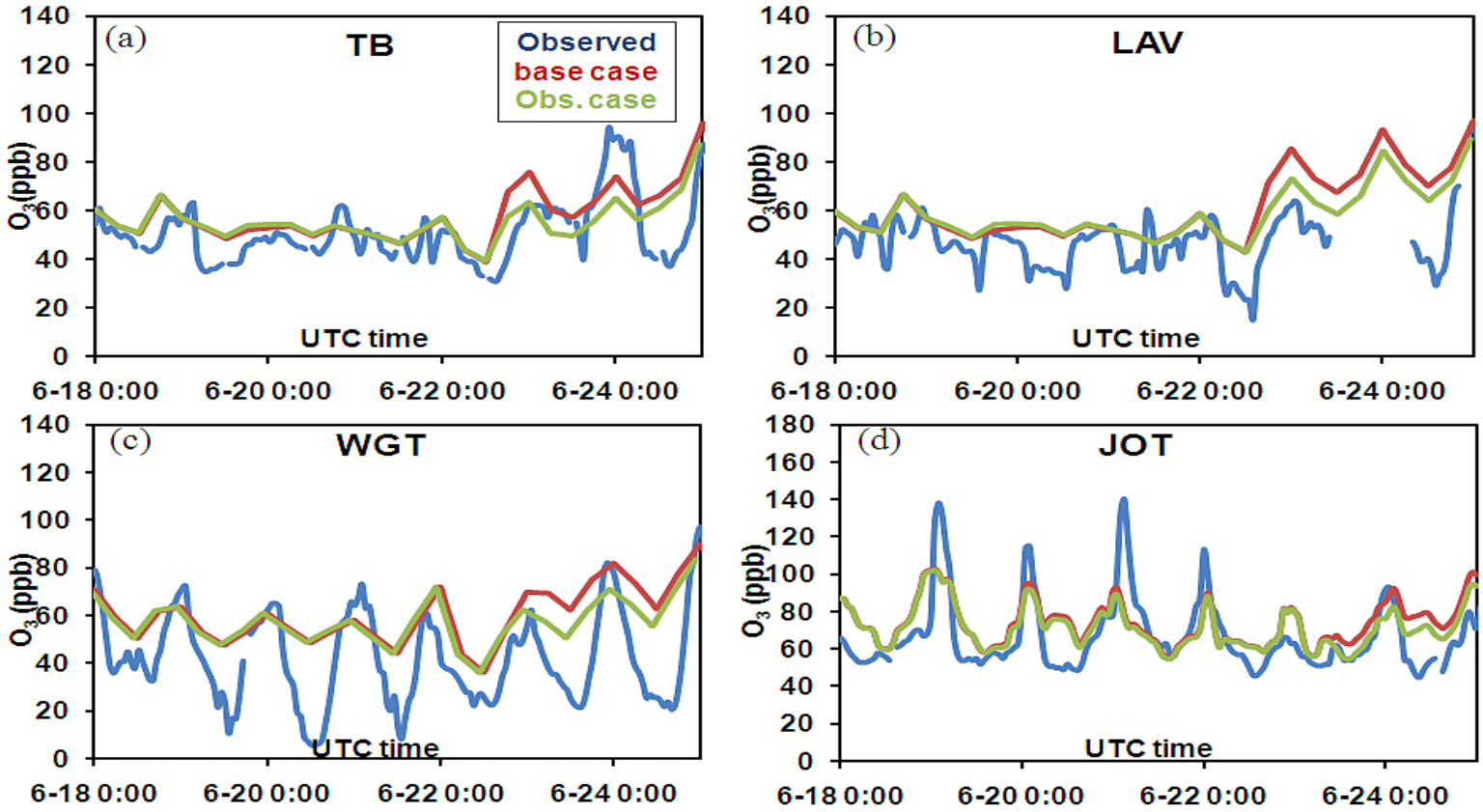

Figure 2.18 Observed O_3 time series in comparison with STEM simulations at four sites during the flight week. (a) 60 km TB; (b) 60 km LAV; (c) 60 km WGT; (d) 12 km JOT

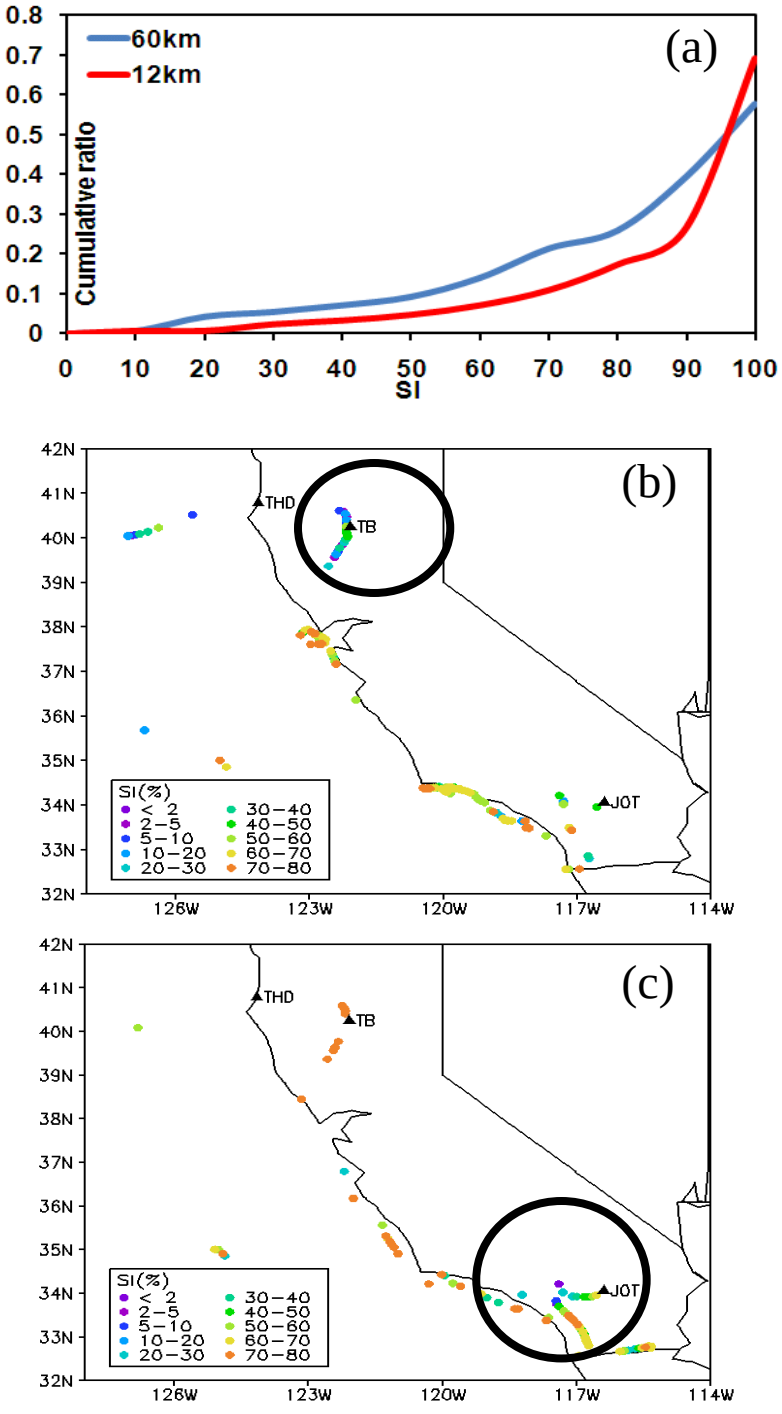

Figure 2.19 Impacts of using observational-based LBC on predicted O_3 along the June 22 and June 24 DC-8 flight tracks below 1km. (a) Cumulative ratios for 60 km and 12 km cases; Data points below 80% SI in (b) 60 km and (c) 12 km cases

CHAPTER 3

EFFECTS OF EMISSIONS AND TRANSPORT ON SULFUR DISTRIBUTIONS OVER CALIFORNIA

3.1 Introduction

Sulfur dioxide (SO_2) is a highly reactive gas harmful to human respiratory system. It can be emitted from anthropogenic and natural sources, or can be oxidized from other chemicals such as hydrogen sulfide (H_2S) by hydroxyl radical (OH). The ultimate fate of all sulfur in the atmosphere is to be oxidized to the sulfate (SO_4) by a variety of oxidants such as OH and hydrogen peroxide (H_2O_2) in gas and/or liquid phases. Sulfate aerosols play an important role in the climate system for both direct and indirect effects (IPCC report, 2007). They can be transported to places at long distance, and adversely affect human health and visibility. The largest sources of SO_2 emissions in the U. S. are from fossil fuel combustion at power plants (66%) and other industrial facilities (29%) (U. S. EPA, http://www.epa.gov/air/sulfurdioxide/). However, the major SO_2 emission sources over California vary from place to place, and the emission inventories (EI) have been developed through time. Around the coastal areas such as San Francisco (SF) and Los Angeles (LA) counties, the shipping emissions are estimated to have increased by over 20 %, an account for 96.7% and 59.8% of total SO_x emissions in 2005 summer. The contribution of SO_x emissions from shipping in 2010 summer are expected to reach 98.5% and 60.8% over SF and LA counties, respectively, reported by California Air Resource Board (CARB, http://www.arb.ca.gov/app/emsinv/t25cat/cat_top25.php).

Modeling and experimental studies on the effects of shipping emissions on regional air quality have been conducted since 1997 (Corbett et al., 1997) over different regions, and they concluded that the control of shipping emissions can reduce air pollution in important ways. For example, Vutukuru et al. (2008) and Ault et al. (2009) focused their studies on the emissions from LA – Long Beach area, where one third of

the cargo containers to the U. S. arrive (BST associates, 2007). The former study concludes that the SO_2 emissions from shipping cause a rise in on-shore SO_2 concentrations by 2 – 4 ppb in 2002 and 8 – 10 ppb by 2020, and the latter study finds that SO_4-NO_3 in fine aerosols from shipping emissions, port traffic and industry emissions, can be transported to downwind areas of the south coast such as San Diego in regional transport events during August – October, 2006. The amount of SO_4-NO_3 in fine aerosols can be 2 – 4 times higher during the event period than non-event periods.

In addition to the shipping emissions, SO_2 emitted from terrestrial industrial processes and area sources contribute to the SO_x concentrations over southern California. A previous field experiment, the Intercontinental Transport and Chemical Transformation of Anthropogenic Pollution (ITCT), conducted by NOAA in 2002 concluded that the estimated emissions from area sources over the south coast air basin were ~15 times lower than observation-derived emissions (CalNex science plan, 2008). The presently documented SO_x emissions by CARB in Central Valley are much lower than the coastal areas, and are mostly from industrial sources.

Currently, the quantitative understanding of temporal and spatial distribution of SO_x over extended areas of California (not only the south coast air basin) remains limited. Continuous SO_2 surface measurements are available at a few surface sites covering limited areas, mostly located over coastal urban areas, and they are low in instrument sensitivity. A number of Interagency Monitoring of Protected Visual Environments (IMPROVE) sites and Clean Air Status and Trends Network (CASTNET) sites provide weekly or twice-a-week SO_4 (or fine SO_4) distributions over California and therefore these observations are low in temporal resolutions. Satellite observations only show early afternoon SO_2 profiles, with no vertical structures, and the sensitivity is highly dependent on various factors such as retrieval methods and weather conditions. The existing EIs are based on different data sources and assumptions, and differ spatially

and temporally. Modeling study comparisons with various three-dimensional observational datasets are important methods to validate these inventories.

Long-range transport of secondary pollutants is usually believed to be weaker during summertime than springtime. However, in Chapter 2, strong Asian air-masses have been observed entering California during the ARCTAS-CARB period from around June 22 and the elevated O_3 background in the eastern Pacific strongly affected some regions over California.

The majority of northern Mexico people live in the U.S.-Mexico border region, where the population and industrial development are expected to increase significantly in the near future. The composition of the atmosphere over the California-Mexico border region is affected by cross-border transport of emissions in both directions, especially around two of the sister city pairs (Tijuana-San Diego and Mexicali-Calexico) that have the most severe air pollution problems (Molina, 2010). The Canada and Mexico emissions caused an average of 3 – 4 ppb O_3 enhancement in a coarse grid global modeling study for a 2001 summertime case, and the enhancement can be as high as 18 ppb under certain meteorological conditions in southwest of the U. S. (Wang et al., 2009). Therefore, it is useful to understand the concentration of transported SO_4 in both Asia and Mexico inflows and their effects on California sulfur budget.

This study has multiple objectives. We compare spatial and temporal variations in three SO_x EIs that were developed at different years and use them as emission inputs into the STEM regional-scale modeling system, including a tracer model and full-chemistry simulations at two horizontal resolutions. We compare the flight sulfur observations by different measurement teams, and the modeled SO_x results with various observational datasets (flight, ground, satellite) during the ARCTAS-CARB field experiment, in order to evaluate the EIs and identify potential missing sources. We also analyze the properties of the Asian and Mexico air-masses and their effects on California sulfur distributions.

Finally, we assess the impacts of maritime sulfur emissions on regional air quality over California, especially along the coast.

3.2 Observational data

ARCTAS-CARB campaign had multiple scientific objectives, including improving the state emission inventories, characterizing off-shore shipping emissions, and quantifying the import of pollution from Mexico and Asia (Jacob et al., 2009). Two SO_2 measurement teams (CIT and GIT) and another two SO_4 measurement teams (UNH and CU – Boulder) were on board for all the flights. The CIT and GIT both used chemical ionization mass spectroscopy (CIMS), and UNH and CU-Boulder used Soluble Acidic Gases and Aerosol (SAGA) and Aerosol Mass Spectrometry (AMS), respectively. In addition to the airborne measurements, continuous hourly SO_2 measurements were made at a number of CARB surface sites (http://www.arb.ca.gov/qaweb/siteinfo.php). At sixteen IMPROVE sites over California, daily-averaged fine SO_4 (diameter 0 – 2.5μm) mass was reported on June 20 and June 23 (http://views.cira.colostate.edu/web/DataWizard/). At six CASTNET surface sites over California, SO_4 was measured as a weekly average during this flight week. Daily SO_2 columns by Ozone Measurement Instrument (OMI) on board of Aura satellite below the boundary layer (PBL) at 0.125 º×0.125 ºresolution are available during this period (http://mirador.gsfc.nasa.gov/). The NASA Aura satellite passed California everyday during the flight week at around 21:00 UTC (14:00 LT). The retrieval assumed a 1 km PBL height and was screened for clouds, viewing angle, solar zenith angle, and line number.

3.3 Results and discussions

3.3.1 Emission inventory comparisons

In this study, three different EIs were applied for full-chemistry model simulations. To identify the differences between these inventories, three regions with the highest SO_2 emissions from shipping and /or industry in California were selected for comparison: South Coast Basin (SC); San Francisco Bay (SF); and Central Valley (CV) – Fresno. Their domains are shown in line boxes together in Figure 3.1, and the latitude/longitude ranges that they cover are 33N – 34.5N, 121W – 117W; 37N – 39N, 123W – 121W; 36N – 37N, 119W – 121W, respectively. Figure 3.2, 3.3, 3.4 compare the average surface SO_2 emissions during June 18 – June 24 over these three regions, on weekdays, Saturday (June 21) and Sunday (June 22).

In the SC area, shipping emissions were included in both CARB and DS' EIs, and DS' EI appears uniform over the ocean because of its coarse spatial resolution. The maximum average SO_2 emissions by DS are shifted southeast and are between ~5×10^{10} – 1×10^{11} molecules/cm^2/s compared to 5×10^{11} – 1×10^{12} molecules/cm^2/s in CARB EI on weekdays. The NEI 2001 does not include shipping emissions and the terrestrial SO_2 emissions are generally much lower than the other two, with the maximum average weekday emissions between 5×10^{9} – 1×10^{10} molecules/cm^2/s. In the CARB EI, the Saturday shipping emissions dropped by less than 10%, while the terrestrial emissions rose by up to 20 %, and the Sunday emissions are similar as the Saturday's. In NEI 2001, Saturday emissions dropped by 15 – 20 % relative to weekdays, and the Sunday emissions dropped by 8–12 % relative to Saturday over most terrestrial areas.

In the SF area, weekday onshore emissions from NEI 2001 and CARB EI are similar while NEI 2001 emissions are more than 10 times lower over the suburban areas in the north of the domain. DS' EI shows less spatial gradient - lower at the east and south bay areas than in the NEI 2001, but higher over the rest of the areas. Similar as in

SC, the CARB Saturday emissions dropped 5% in shipping emissions and terrestrial emissions rose up to 20 % mostly. The Sunday emissions were slightly decreased or remained the same relative to Saturday emissions. The NEI 2001 Saturday emissions decreased by < ~5% over most regions compared to weekdays, and so do the Sunday emissions relative to the Saturday's.

At Fresno and surrounding areas in CV, both NEI 2001 and CARB EI on weekdays show strong gradients around the city and the CARB emissions indicate the major sources emission strengths are between $5\times10^{10} - 1\times10^{11}$ molecules/cm^2/s, in contrast to the maximum average emission rate of $2\times10^{10} - 5\times10^{10}$ molecules/cm^2/s from NEI 2001. The emissions over city regions in CARB EI rise by 10 – 20 % compared to the weekdays and the Sunday emissions remain almost the same as the Saturdays. The NEI 2001 Saturday emissions dropped by ~5% relative to weekdays over the whole domain and the Sunday emissions dropped 2–5 % relative to Saturday emissions over most areas. From the DS' EI, no distinguishable gradient over the city is shown and the maximum emissions are much lower.

Figure 3.5 compared the weekday SO_4 emissions between CARB EI and NEI 2001 over the three regions (DS' EI does not include SO_4 emissions). Again, NEI 2001 shows less strong gradients over SC and SF areas, with the highest emission rates at ~4×10^9 and 8×10^9 molecules/cm^2/s, in contrast to CARB EI ~2×10^{10} and 1×10^{10} molecules/cm^2/s. NEI and misses the important sources over Fresno area located at 120W-119.5W, as well as terrestrial sources over SC and SF. Figure 3.6 shows the weekday/weekend variations in both EIs. In CARB 2005, emissions from shipping, port and major industry decreases on Saturdays, similar as the Sunday emissions (not shown). However, terrestrial sources can emitted up to 1.5 times of SO_4 than on weekdays. In NEI 2001, Saturday emissions decrease from weekdays', and the Sunday emissions dropped from Saturdays' over all three regions. The most significant drop occurred over the port areas.

At these three regions, several surface monitoring stations (six in SC, nine in SF, one in CV- Fresno and one in CV– North Height) are set up by CARB to measure hourly SO_2 concentrations. Their latitude/longitude locations are listed in Table 3.1. The amount of emissions, diurnal circles and daily variations over these three regions are different in the three EIs we used. The emission time-series for these regions are shown in Figure 3.7, along with the emissions for CV – North Height. The 24-hour average emission rates during the experiment week for three regions from each EI are also summarized in Table 3.2. The diurnal patterns in DS' EI at all regions are similar, with double peaks each day before and after 00 UTC. The CARB EI peaks before 00 UTC for all regions and shows the strongest diurnal cycles over Fresno and the weakest over the SF area. The NEI 2001 shows peaks at around 00 UTC, which are sharp over SC and North Height. The magnitudes in CARB EI are much higher than the other two except at the North Height site. Its average emissions over SF and CV-Fresno are close, and are higher than over SC. NEI 2001 estimates the lowest SO_2 emissions over SC and North Height. Its emissions over SF are close to the amount in DS' EI, which estimates the lowest SO_2 emissions over the Fresno area.

3.3.2 Model results validation

3.3.2.1 Comparison with surface observations

The predicted 24-hour surface average total sulfur levels in ppb during the experiment week from the three cases are shown in Figure 3.8 together with the corresponding SO_2 contribution to total sulfur. High sulfur level can be seen over the SC, SF, CV areas as well as around the California – Nevada border and the west California – Mexico border in all cases, due to the fresh emissions (SO_2 % > 60 %). The simulated sulfur levels at these areas from the 60 km base case are generally lower than the other two cases, especially over the SC area. Due to the lack of the shipping emissions in the NEI 2001, the sulfur levels over the ocean are low in the 60 km case, except the near-

shore areas of the central coast. The sulfur distribution over the ocean from the DS case indicates the coarse shipping emissions and meteorology fields. In contrast, the 12 km base case shows more detailed local features over land and the gradients along ship tracks.

SO_2 temporal variations are influenced by both emission patterns and regional meteorology conditions. Figure 3.9 shows the surface wind flows at multiple times (3, 9, 15, 21 UTC) on June 20, 2008 over California based on the 12 km WRF calculations, to illustrate the typical diurnal variations in wind fields during the week. At this resolution, the model is able to capture the sea – land breeze and mountain – valley flows over the coastal and CV areas.

In order to understand the SO_2 temporal variations at surface sites over these three regions, we averaged the modeled and observed time series for the same sites (as in section 3.1) over these three regions, as shown in Figure 3.10. The maximum (Max.), minimum (Min.) and 24 – hour mean values from observation and model simulations are also summarized in Table 3.3. The 60 km base case predicted SO_2 more than 10 times lower than the observed over SC and more than five times lower over the SF area in general. The 60 km DS case and the 12 km base case produce higher Max., Min. and mean SO_2 values, which are closer to the observations. In SC, the modeled SO_2 peaks shifted earlier each day during the week. In SF, the SO_2 peaks were captured well, but on June 22 – June 23, both of them over-predicted SO_2. The observed SO_2 at the two CV surface sites vary regarding daily variations and magnitudes. The peak SO_2 at Fresno ranged from 10 – 60 ppb, whereas SO_2 at North Height was always below 3 ppb. At Fresno, SO_2 was generally higher before June 22, during which time SO_2 was at its lowest weekly level at North Height. None of the cases predicted more than 2 ppb of SO_2 at Fresno, and showed a shift in peak time. The 12 km base case showed the largest values, while the 60 km base case predicted the lowest. The 60 km base case is also

biased low at the North Height site and the 60 km DS case captured the magnitude and the diurnal trend best during the episode of June 22 – June 24 in these three cases.

We looked at the six surface sites within the SC region separately and plotted the modeled and observed time series in Figure 3.11. The SO_2 at the North Long Beach site was overall ~3 times higher than at the Costa Mesa site to its south, reflecting the high emissions associated with the heavy industry processes and from terrestrial and maritime traffic. The 60 km base case predicted more than 10 times lower SO_2 than observations at both sites. The 12 km base case shows the best results in general. For the other four sites, which are located near highways, the 60 km DS case shows similar SO_2 temporal variation as 10 times of the 60 km base case. At three sites out of the four, SO_2 was under-predicted; while at the Los Angeles north Main Street site, the model results captured the general SO_2 structure, and 12 km base case showed some peaks with wrong timing.

The SO_4 mass was measured and analyzed once a week at six California CASTNET sites. Their locations are shown in Figure 3.12b. Modeled and observed weekly SO_4 are plotted together in Figure 3.12a. Central and southern California inland sites observed higher SO_4 (> 1.1 $\mu g/m^3$) than the north California site (LAV, ~0.6 $\mu g/m^3$). All model cases under-predicted SO_4 for this week on average, and the 60 km base case showed the highest bias. At LAV, results from the three model simulations are almost identical. At the PIN, YOS and SEK sites, the 60 km DS case predicted higher SO_4 than the 12 km base case. At the other two sites to the south, the 12 km base case provided the best results in SO_4.

Fine SO_4 (diameter 0 – 2.5 μm) mass was measured on June 20 and June 23 during the flight week for sixteen IMPROVE sites over California. The observations were compared with results from all model cases in Figure 3.13. The average SO_4 mass and standard deviation for all sites on the two days are summarized in Table 3.4. The 60

km base case predicted the lowest fine SO_4 in general. 60 km DS case and 12 km base case improved the predictions but are still biased low.

The IMPROVE sites at San Gabriel, Point Reyes National Seashore and Fresno are located in the SC, SF and CV domains that we focus on in this paper. They show strong daily variations between June 20 and June 23. On June 20, SO_4 at Fresno was ~2 $\mu g/m^3$, which was the highest among all sixteen sites. At both of the other two sites <1 $\mu g/m^3$ of SO_4 was observed. On June 23, SO_4 at Fresno dropped by ~50 %, and at the other two sites SO_4 was measured higher than 1.2 $\mu g/m^3$.

3.3.2.2 Comparison with flight observations

Figure 3.14 shows the observed total sulfur along all four DC-8 flights (below 5 km ASL), together with the SO_2 % for the three regions of interest. The observed total sulfur is calculated by the following method: We added SO_2 and SO_4 measured by different teams (four combinations in total) and averaged them; And the SO_2 % is based on the averaged SO_2 concentrations measured by two teams. Fresh SO_2 and high sulfur were observed at the port areas such as around the Long Beach and the north SF Bay, as well as Fresno areas. These are represented in the EIs. High sulfur was also observed inland of SF (in black circle) with high SO_2 %, and these sources are missed in CARB EI.

The modeled total sulfur concentrations are compared with observations along all four DC-8 flights (below 5 km ASL), and are shown as vertical profiles in Figure 3.15 for three regions. The vertical structure differs over the three regions. Over SC, multiple layers are indicated, that sulfur is elevated from the surface to ~3–4 km. Over SF, sulfur is enhanced below ~1.5 km. At Fresno, there is large sulfur enhancement at the surface, as well as slightly elevated level at ~4 km. The observed average surface sulfur over SC and SF are close (both ~1.4 – 1.5 ppb), and higher surface sulfur (~3.5 ppb) was observed over Fresno with a large standard deviation. Slight aloft can be seen at mid-troposphere around SC and Fresno. The predictions show the lowest sulfur (and the highest biases) at

all locations in the 60 km base case. The highest sulfur is calculated in the 60 km DS case, which also captured the mid-troposphere structure. In this case, the sulfur was over-predicted over SC, while under-predicted over SF and Fresno below ~1.5 km. The 12 km base case under-predicted sulfur over all the regions but improved the 60 km base predictions to different extent by regions. The 12 km simulations well captured the vertical structures over the SC regions.

The comparisons of observed and modeled SO_2 and SO_4 along all DC-8 flight paths over the three regions are also shown as vertical profiles in Figure 3.16a-c. The R-squares between modeled and observed SO_x, as well as the linear regressions between the two observational datasets for SO_2 and SO_4 are listed in Table 3.5, and the best correlations are in bold. The ratios of observed and modeled SO_2 and SO_4 below 500 m are calculated and tabulated in Table 3.6. In the SC area, GIT SO_2 is lower than CIT SO_2 below 1 km and higher at 1 – 3 km. The two sets of measured SO_4 follow the same trend below 2 km but CU Boulder SO_4 is ~20% lower than UNH SO_4. Only the CU Boulder team observed aloft SO_4 at 2 – 4 km. The 60 km base case predicted the lowest SO_2 and SO_4, which also had the lowest correlations with the observations. The 60 km DS case was biased high in SO_2 at low in SO_4 at all altitudes, but showed the best correlations with observations. Its predicted SO_2 and SO_4 vertical structures are close to the GIT and UNH's observations, respectively. The 12 km base case SO_2 generally followed the CIT SO_2, but was ~30 % biased low at the surface. Its SO_4 captured the vertical structure of UNH SO_4, but was more than 50% under-predicted at most altitudes.

In the SF area, the SO_2 data measured by CIT and SO_4 measured by UNH are fewer than the other two teams. CIT and GIT SO_2 differed significantly at the surface whereas the UNH and CU Boulder SO_4 are similar below 1 km. The 60 km base case again predicted the lowest SO_2 and SO_4 at most altitudes and had the lowest correlation with the observations. The 12 km base case had the highest correlation with the CIT SO_2. 60 km DS case correlated GIT SO_2 best, but was ~30 % biased low at the surface, and

over-predicted SO_2 above 1 km. Both the 12 km base case and the 60 km DS case predicted low SO_4, and missed the features at 2 – 3 km showing SO_4 aloft. 60 km DS case SO_4 predicted higher SO_4 than the 12 km base case below 5 km and was better correlated with Boulder SO_4.

Over the Fresno area in CV, CIT SO_2 measurements were missing and SO_2 observations by GIT were much higher than all model results below 1 km. SO_4 below 1 km was observed high by both UNH and Boulder teams, while only the CU Boulder team observed elevated value extending to ~4 km. The 60 km DS case predicted the highest SO_2 and SO_4 below 4 km. The 60 km and 12 km base cases predicted similar vertical structures below 3 km and both of them showed high correlations with observations.

The partitioning between SO_2 and SO_4 are highly affected by OH. The R-square values between observed and modeled OH along all DC-8 flight paths over the three regions are also listed in Table 3.7. The 12 km base case improved OH predictions over SC and Fresno, and the 60 km DS case performed best for OH over the SF.

3.3.2.3 Comparison with OMI columns

The SO_2 PBL columns provided by OMI were averaged for the flight week in order to reduce noise in daily profiles, and are shown in Figure 3.17a in the units of molecule/m^2. We divided the columns by a factor of 10 (Figure 3.17b) in order to compare with the modeled PBL SO_2 columns. The model columns (Figure 3.17c) based on the 12 km base simulations show distinctly high SO_2 concentrations over SC, SF, and CV at 21:00 UTC, as do the OMI PBL columns. The other areas are of the similar magnitude of 1/10 of the OMI columns. Hot spots observed along the state borders are shown in Nevada in the modeled columns, possibly due to the uncertainty in meteorology fields. The missing hot spots in the model at the northern coast were also seen in the average SO_2 PBL columns over a long period (June 1 – July 31, not shown). They can be due to missing emission sources in northern California.

3.3.3 Long-range and regional SO_4 transport events

3.3.3.1 Asian inflows and Mexico effects

Long-range transport of pollutants from Asia is usually believed to be weaker and less frequent during summertime relative to springtime. During the ARCTAS-CARB experiment week, the June 22 flight aimed at characterizing the upwind boundary conditions necessary to model inland O_3 and aerosols (Jacob et al., 2009). On this day, the DC-8 took off from Palmdale, CA, flew over the Pacific Ocean to THD, and then circled back to Palmdale along the coast (Figure 3.1). At the outbound part of this flight (approximating UTC 17 – 21 UTC), strong Asian inflows were encountered, indicated from the VOC age (ranging from 200 – 400 hours) shown in Figure 3.18a, together with five – day back trajectories based on the 60 km WRF meteorology fields in Figure 3.18e. Vertical profiles and time series of observed and modeled SO_2 and SO_4 are shown in Figure 3.18 for this flight. Strongly elevated SO_4 (only by the Boulder team) were observed at 6 – 8 km ASL, majorly at flight leg 2 and partially at leg 3 (leg 1 SO_4 missing by both Boulder and UNH teams). These air-masses containing high SO_4 were also high in China CO % based on the tracer model calculations (not shown) as shown at 6 – 8 km (Figure 3.18a). Three – day forward trajectories originating from > 6 km ASL flight heights based on the 12 km WRF meteorology fields are shown in Figure 3.18f. The air-masses at these heights generally traveled above 3 km AGL over California and may finally descend down to other downwind states.

At flight leg 3 (THD), the DC-8 also observed slightly lofted SO_4 at 1 – 4 km (Figure 3.18a, h). In a previous study, we conclude that elevated O_3 background at 2 – 4 km on the same flight day in eastern Pacific can be transported into northern central valley, directly affecting several surface sites there and indirectly affecting southern California sites (Figure 3.18g). Similarly, the 0.1 – 0.4 μg/std m^3 of under-prediction in SO_4 by tracer and 60 km base case (being used as 60 km and 12 km base boundary

conditions) at these altitudes contributes to the negative biases to sulfur amount over downwind areas in central valley (Figure 3.18h).

SO_2 peaks (< 0.6 ppb) were also observed (by CIT team, GIT data was missing for the whole flight) at 6 – 8 km ASL at flight legs 1 and 2. These were the residuals in Asian plumes that were not reacted into SO_4 through long-range transport, as indicated by similar peaks for a number of observed species and the tracer calculations (not shown). Being used as boundary conditions, the RAQMS and the 60 km base case missed the SO_2 peaks at both legs 1 and 2, but same as SO_4, air-masses containing the high SO_2 did not affect California.

To study the pollution transport from Mexico, the meteorological conditions (wind fields) at California – Mexico border at 19 UTC (noon, LT) on four flight days are shown in Figure 3.19. Westerly or northwesterly winds dominated at the border during June 18 – June 22 at daytime. The situation on June 24 was different at the area east of -115W (the Mexicali-Calexico region) , as shown in Figure 3.19d, when southerly winds flowed north into California, entering Nevada, and circled back to California. They were finally merged with the westerly winds from the South Coast Basin. Another flow passing across the border to this region originated from the south coast. It entered Mexico and shifted southwest before joining the flows into California. The Tijuana-San Diego area shows relatively stagnant winds because of the mixture of flows. Figure 3.9 a, b further present similar nighttime wind features inland but different from daytime at the coastal areas. Northwesterly winds meet land breeze and shifted southerly. These different wind fields resulted in pollutant interactions through both directions at the Tijuana-San Diego area.

Part of the June 24 DC-8 flight took samples at lower altitudes (below 2 km) parallel to the California – Mexico border, at approximately 18 – 19 UTC. The observed and modeled wind fields and SO_x time series are shown in Figure 3.20. The yellow circle highlights high-observed SO_2 (~3 ppb) and SO_4 (~2 μg/std m^3) concentrations at 18.517

and 18.533 UTC, respectively, over the Mexicali-Calexico area as shown in the blue circle in Figure 3.19d. The elevations over there are below sea level, and the wind directions differed from the surrounding areas, with flows coming from Mexico with higher wind speed (Figure 3.20 a, b). Therefore, the model predictions of wind fields and SO_x at this area directly affected modeled SO_x levels over the southeast California. We compared simulated WRF wind fields and SO_x over this region with flight observation and show them in Figure 3.20. Figure 3.20a, b show that the 60 km WRF simulation failed to capture the wind complexity there, while the 12 km meteorology improved the predictions. The 60 km base case did not predict the SO_4 peak, while the 12 km base case shows a slightly shifted peak. The 60 km DS case captured the right SO_4 magnitude at the peak location, but over-predicted the surrounding areas (Figure 3.20c). Regarding SO_2, the 60 km base case missed the peak, whereas the 12 km under-predicted it by ~10 times. As the DC-8 headed west to the coast, the SO_2 levels remained below 0.5 ppb, while SO_4 was observed high when the flight reached the San Diego-Tijuana area. At this location, the absolute wind speed is low due to the offset by flows from multiple directions (Figure 3.19d) at the flight period, and is also under the influence of Mexico inflows during nighttime (Figure 3.9 a, b). Therefore, the area is affected together local sulfur emissions as well as the transport of maritime emissions from both SC and Mexico. The under-prediction of SO_4 in the 60 km and 12 km base case can be due to low local emissions, partitioning issue (SO_2 over-predicted, Figure 3.20d) and/or the transport of under-predicted SOx. The DS case over-predicted SO_2 over the whole border areas but captured the SO_4 trend best mainly because of a large amount of emissions in DS' EI.

3.3.3.2 Local contributions

To better understand the source of air masses along the flight paths over the SC, SF and CV – Fresno regions, we made three day back-trajectories originating along the four DC-8 flight paths that covered these regions and show the ones starting below 1 km

in Figure 3.21. The June 18, 22, and 24 flights sampled over the SC area, and the June 20 flights flew over both the SF and CV – Fresno areas. We also summarize the VOC age and CO contributions from China and North America based on the tracer calculations in Table 3.7. On those flight days, air-masses below 1 km over SC are mostly from the central valley at > 800 – 1000 m or/and have come from the north via winds parallel the coastline below 500 m. On June 22, westerly winds in the eastern Pacific at altitudes above 2 km carry the air-masses to SC. Most of the air-masses had China CO % less than 0.5 % and North America CO % > 99 %, except the air-masses on June 24 during UTC 23 – 24 (during flight). These had Chine CO % at ~40 %, because these air-masses were transported through areas influenced by strong Asian inflows on June 22. The averaged SO_2 and SO_4 concentrations in sampled air ranged from 0.55 – 1.07 ppb and 1.8 – 2.92 μg/std m^3, respectively for these three days. The air samples that the DC-8 collected on June 20 over SF and CV - Fresno areas are shown to mostly be from > 2000 m above the eastern Pacific and partially through San Francisco Bay, as well as from Oregon at < 500 m. Around Fresno, similar amount of SO_4 and higher SO_2 levels were observed compared to the SC area. Whereas around SF, SO_4 was more than two times lower than those observed in SC and Fresno samples.

In order to identify the air-mass sources that caused the sulfur aloft in the mid-troposphere (Figure 3.16), we analyzed the three day back-trajectories originating along four DC-8 flight paths separately at 2 – 4 km ASL by regions (Figure 3.22). During flights on June 18 and 24 over SC, the air was lifted and moved from CV. In contrast, during the other two flights, air masses over SF, CV and SC were from southwest of the domain, and they descended from 3500 – 5500 m.

3.3.3.3 Shipping effects on air quality at coastal and downwind areas

As discussed in section 3.3.3.1 and 3.3.3.2, during the week of experiment, North America had the largest impact on SO_x distribution over the three regions we analyzed. It is important to understand the contributions of the local sources. Over coastal areas such as SC and SF, the sulfur concentrations are contributed by both terrestrial (highway, port heavy transportations, industry) and maritime emissions (mainly shipping).

To further understand the contribution from terrestrial and maritime emissions to sulfur concentrations over these regions separately, we conducted one model simulation with only the terrestrial emissions for all chemical species. This sensitivity case was done in the 12 km grid using CARB EI, which estimates 2.26 Tg of SO_2 and 0.27 Tg of SO_4 were emitted from area, point and biogenic sources over California during June 18 – June 24 in total. 41.38 % of the SO_2 and15.59 % of the SO_4 were contributed from maritime emissions. The 24-hour averaged surface SO_4 and SO_2, and the contributions from maritime sulfur emissions during the flight week are shown in Figure 3.23 and 3.24, for SC and SF areas, respectively.

For both regions, SO_2 concentrations are directly affected by both terrestrial and maritime emissions. As expected, the terrestrial emissions led to the high SO_2 concentrations over land and on shore, and the maritime emissions caused high SO_2 levels over the ocean and on shore (SO_2 > 70 %). Figure 3.11 shows the change of SO_2 at six SC sites through the flight week. SO_2 concentrations at all six sites were impacted by maritime SO_2 emissions. The change varied through time and from site to site, but stays below 2 ppb.

As for the secondary pollutant SO_4, the spatial distribution is highly influenced by reaction rate and wind fields. As Figure 3.19 shows, the south coast is heavily under the impact of northwest winds during the daytime. Consequently, the maritime emissions generally contributed 30 – 50 % of SO_4 along the coast and further affected the extended

areas on land by 20 – 30 %. This effect extends as far as San Diego and the California – Mexico border area, contributing up to 40 % SO_2 and SO_4 around San Diego – Tijuana and 10 %–30 % of SO_2 and SO_4 over Calexico-Mexicali (not shown). The wind directions in the SF area were similarly from the northwest, but were almost parallel to the coastal line (Figure 3.9). Therefore, the SO_4 formed from maritime emissions only affected limited areas along the coast of south bay, and account for up to 20 % of SO_4. The SO_4 formed from terrestrial emissions were blown east and eventually into the central valley.

Figure 3.11 shows the change of the vertical distributions of SO_2 and SO_4 in response to cutting off maritime emissions at three regions vertically along DC-8 flight paths. During the flight period, no change of SO_2 or SO_4 at SF and CV-Fresno areas was shown in the vertical profiles due to the smaller number of data points and the limited areas that the flight covered. In the SC area, SO_2 and SO_4 were reduced up to ~2000 m. The maximum reduction happened at the surface, by 50 % and 40 % for SO_2 and SO_4, respectively. The changes are determined by flight path and flight time.

In order to better understand the regional SO_x quantities, as well as the amounts contributed from maritime emissions over extensive areas (that the flight did not pass through), we averaged 12 km model-calculated surface SO_2 and SO_4 during the flight times (approximately 16 – 24 UTC, which was also the period that SO_x peaked) for SC (June 18, 22, 24) and SF area (June 20), respectively, and multiplied by the corresponding scaling factor highlighted in Table 3.6, based on the model – flight observation comparisons. They are shown in Figure 3.25 and 3.26 for SC and SF areas, respectively. The absolute SO_2 and SO_4 amounts from the sensitivity case were processed in the same method and also shown.

In the SC area, maritime emissions led to the increases of SO_2 as high as 8 ppb over the port area, ~1 – 2 ppb near shore and 0.3 – 0.7 ppb over land, and a rise of SO_4 between 3 – 4 $\mu g/m^3$ in maximum around Long Beach and 1 – 2 $\mu g/m^3$ over land. The

terrestrial emissions contributed 3 – 5 ppb of SO_2 near the port, 1 – 2 ppb over land east and northeast to the port; 2 – 4 μg/m^3 of SO_4 over extensive areas of SC were contributed from terrestrial emissions.

In the SF area, the maritime emissions caused the rise of SO_2 along the coast, by up to 2 – 3 ppb. The effects of shipping on SO_4 levels were below 1 μg/m^3 in contrast to the SC area. The highest SO_2 (2 – 5 ppb) and SO_4 (~ 1.5 μg/m^3) over south and east bay were due to terrestrial emissions.

3.4 Conclusions

In this study, we compared three EIs and evaluated the model performance using them. The EIs vary temporally and spatially over California. NEI 2001 lacks the shipping emissions, and has the lowest emission levels overall. DS' EI and CARB EI improved the magnitudes of simulated SO_x, closer to the observations, especially over SC and SF areas. However, there remain uncertainties of spatial and temporal variations in them and the resolutions of the DS' EI need to be improved. Fresno and extended CV areas have not been paid enough attention, and all three EIs still have much space for improvement.

The transport of SO_x was also analyzed in this paper. Asian inflows were shown strong on June 22, slightly (SO_4 < 0.8 μg/m^3) affecting CA through mid-altitude. Highly elevated SO_4 and SO_2 in these long-range transported air-masses above 6 km passed CA; Mexico border SO_x concentrations were high over two sister city pairs. On a particular day of June 24, limited areas at southeast of California were affected by Mexico inflows due to the southerly winds around Mexicali-Calexico, differing from the dominated westerly wind fields. Coastal San Diego-Tijuana area was affected by winds through opposite directions during daytime and nighttime. The high concentrations of SO_x over three regions near the surface were mostly contributed by local emissions. The SO_x aloft over these regions at mid-troposphere can be contributed by both local and foreign sources, dependent on varied meteorological conditions.

We also analyzed the effects of maritime and terrestrial emissions on SO_x distributions over coastal California. The maritime emissions directly contribute to the high SO_2 over the ocean and on-shore. SO_4 along the downwind areas of the fresh emissions increased due to the maritime emissions. Terrestrial emissions also contributed more than 50 % SO_x concentrations over both SC and SF areas. We also quantified the absolute contributions from shipping and terrestrial SO_x emissions during flight period by multiplying modeled SO_x concentrations with scaling factors over SC and SF.

It is suggested that continuous and high sensitivity of SO_x measurements (including comparison between measurement teams) should be conducted over the coastal areas as well as extensive areas in CV and over the Nevada – California and Mexico – California borders in order to better understand the spatial and temporal SO_x variations for EI improvement and pollution control. The continued emission control regulations from shipping and port activities are necessary.

Table 3.1 CARB surface sites monitoring hourly SO_2

Site Name	County	Basin	Latitude	Longitude
SF				
Pittsburg-10th Street	Contra Costa	San Francisco Bay	38.02917	-121.8969
Martinez-Jones Street	Contra Costa	San Francisco Bay	38.01278	-122.1344
Crockett-Kendall Avenue	Contra Costa	San Francisco Bay	38.055	-122.2331
Concord	Contra Costa	San Francisco Bay	37.93611	-122.0264
Richmond-7th Street	Contra Costa	San Francisco Bay	37.94806	-122.365
Bethel Island Road	Contra Costa	San Francisco Bay	38.00667	-121.6414
San Pablo-Rumrill	Contra Costa	San Francisco Bay	37.96	-122.3564
San Francisco-Arkansas Street	San Francisco	San Francisco Bay	37.76611	-122.3992
Berkeley-6th & Camelia	Alameda	San Francisco Bay	37.87778	-122.3014
SC				
Burbank	Los Angeles	South Coast	34.17583	-118.3169
North Long Beach (Long Beach)	Los Angeles	South Coast	33.82361	-118.1886
Los Angeles-North Main Street	Los Angeles	South Coast	34.06639	-118.2267
Costa Mesa-Mesa Verde Drive	Orange	South Coast	33.67389	-117.9258
Rubidoux - Mission Blvd	Riverside	South Coast	34.00056	-117.4153
Fontana-Arrow Highway	San Bernardino	South Coast	34.10028	-117.4919
CV				

Table 3.1 Continued

Fresno - First Street	Fresno	San Joaquin Valley	36.78194	-119.7731
North Highlands-Blackfoot Way	Sacramento	Sacramento Valley	38.71222	-121.3811

Source: http://www.arb.ca.gov/qaweb/sitelist_create.php

Table 3.2 Summary of the 24 – hour average emissions (in molecules/cm^2/s) from surface sites in three cases, highest and lowest amounts are in bold and italic respectively

Area / EI	SC	SF	CV-Fresno	CV-North Height
CARB 2005	**6.01×10^{10}**	**1.05×10^{11}**	**8.60×10^{10}**	3.75×10^{9}
NEI 2001	*5.09×10^{9}*	*3.69E+10*	2.03×10^{10}	*1.56×10^{8}*
DS 2009	3.78×10^{10}	4.05E+10	*6.32×10^{9}*	**8.96×10^{9}**

Table 3.3 Observed and modeled SO_2 at surface sites over multiple regions

	SC (ppb)				SF (ppb)			
	Obs	12 km	60 km	60 km DS	Obs	12 km	60 km	60 km DS
Mean	1.97	1.46	0.077	1.86	1.58	1.57	0.28	2.4
Max.	4	3.2	0.12	2.98	4.11	3.24	0.64	3.5
Min.	1	0.56	0.05	1.04	0	0.59	0.13	1.52
	CV - Fresno (ppb)				CV - North Height (ppb)			
	Obs/10	12 km	60 km	60 km DS	Obs	12 km	60 km	60 km DS
Mean	1.725	0.79	0.22	0.51	0.58	0.18	0.04	0.57
Max.	6	1.79	0.41	0.15	3	0.05	0.01	0.17
Min.	0	0.22	0.11	1.16	0	1	0.11	1.21

Table 3.4 Observed and modeled fine SO_4 ($\mu g/m^3$)
at sixteen IMPROVE sites over California

	20080623				20080620			
	Obs	12 km	60 km	60 km DS	Obs	12 km	60 km	60 km DS
Mean	1.10	0.47	0.30	**0.62**	0.86	**0.40**	0.14	0.33
Standard Deviation	0.34	0.11	0.15	**0.17**	0.40	0.15	0.03	**0.16**

Table 3.5 R^2 between modeled and observed SO_x and OH along all flight tracks over three regions, highest correlations are in bold.

	SC			SF			CV-Fresno		
	12 km Base	60 km Base	60 km DS	12 km Base	60 km Base	60 km DS	12 km Base	60 km Base	60 km DS
CIT SO_2	0.13	0.08	**0.18**	**0.30**	0.24	0.25	NA	NA	NA
GIT SO_2	0.18	0.04	**0.3**	0.03	0.007	**0.20**	0.62	**0.63**	0.26
Regression for two obs datasets	GIT=CIT×0.7272+0.1476 R^2=0.7943			NA			NA		
UNH SO_4	0.16	0.001	**0.22**	**0.06**	0.002	0.01	0.58	**0.73**	0.64
CU Boulder SO_4	0.23	0.02	**0.26**	0.07	0.26	**0.23**	**0.3**	0.06	0.03
Regression for two obs datasets	Boulder=UNH×0.8014+ 0.0948, R^2=0.4625			Boulder=UNH×0.4883+ 0.6257, R^2=0.1384			Boulder=UNH×0.5602+ 1.3867 R^2=0.1478		
OH	**0.22**	0.17	0.09	0.02	0.002	**0.23**	**0.77**	0.08	0.31

Table 3.6 Ratios of Observed/modeled SO_x at < 500 m, based on vertical profiles figures, bold numbers were used to scale shipping emission figures in section 3.3.3

	SC			SF			CV-Fresno		
	12 km Base	60 km Base	60 km DS	**12 km Base**	60 km Base	60 km DS	12 km Base	60 km Base	60 km DS
SO_2	**1.47**	22.04	0.58	**1.72**	4.57	0.87	10.60	31.97	7.82
SO_4	**2.66**	9.31	1.51	**2.12**	3.53	1.37	5.27	8.96	3.32

Table 3.7 Air masses properties below 1 km AGL along four flight paths, summarized by regions

	UNH SO_4 (µg/std m^3)	**Boulder SO_4 (µg/std m^3)**	**CIT SO_2 (ppb)**	**GIT SO_2 (ppb)**	**VOC age (hour)**	**China CO%**	**North America CO%**
06/18 SC	2.31	1.80	0.99	0.85	11.26	0.01	99.94
06/20 SF	0.91	0.99	/	1.18	5.58	0.2	99.75
06/20 CV (Fresno)	2.24	2.18	/	2.60	13.85	0.11	99.85
06/22 SC	2.92	2.23	1.07	/	10.73	0.2	99.74
06/24 SC	2.46	2.30	/	0.55	15.78	16.61 ~40 % 23 – 24 UTC	78.42, ~40 % 23 – 24 UTC

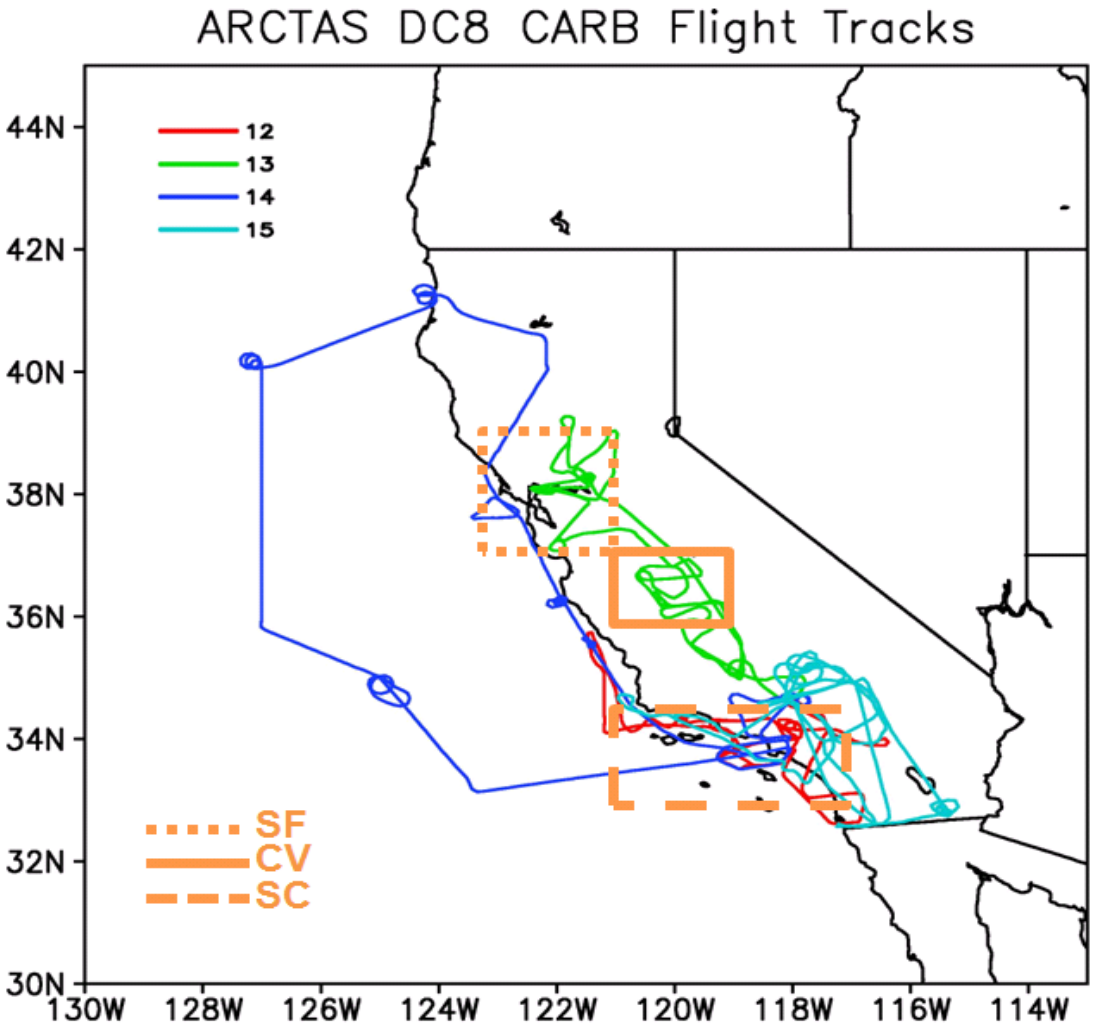

Figure 3.1 DC-8 flight 12-15 (June 18, 20, 22, 24, 2008) paths during the ARCTAS-CARB period. The domains of SC, SF and CV were defined in the boxes.

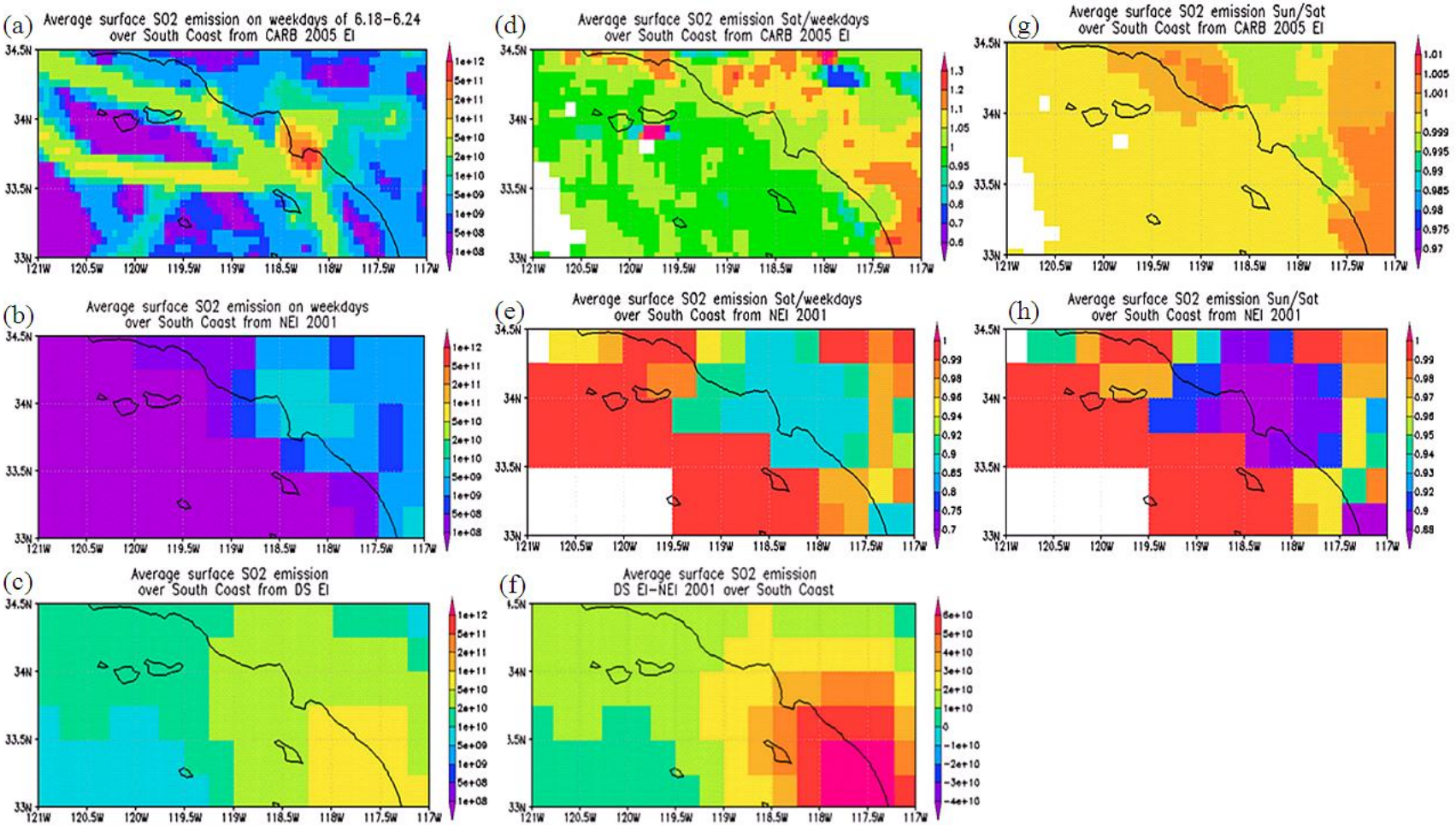

Figure 3.2 The average surface SO_2 emissions during 06/18-24 over the SC area during weekdays, Saturday (June 21) and Sunday (June 22), for three EIs. (a;d;g) CARB EI; (b;e;h) NEI 2001; (c) DS' EI; (d) difference between NEI and DS' EI

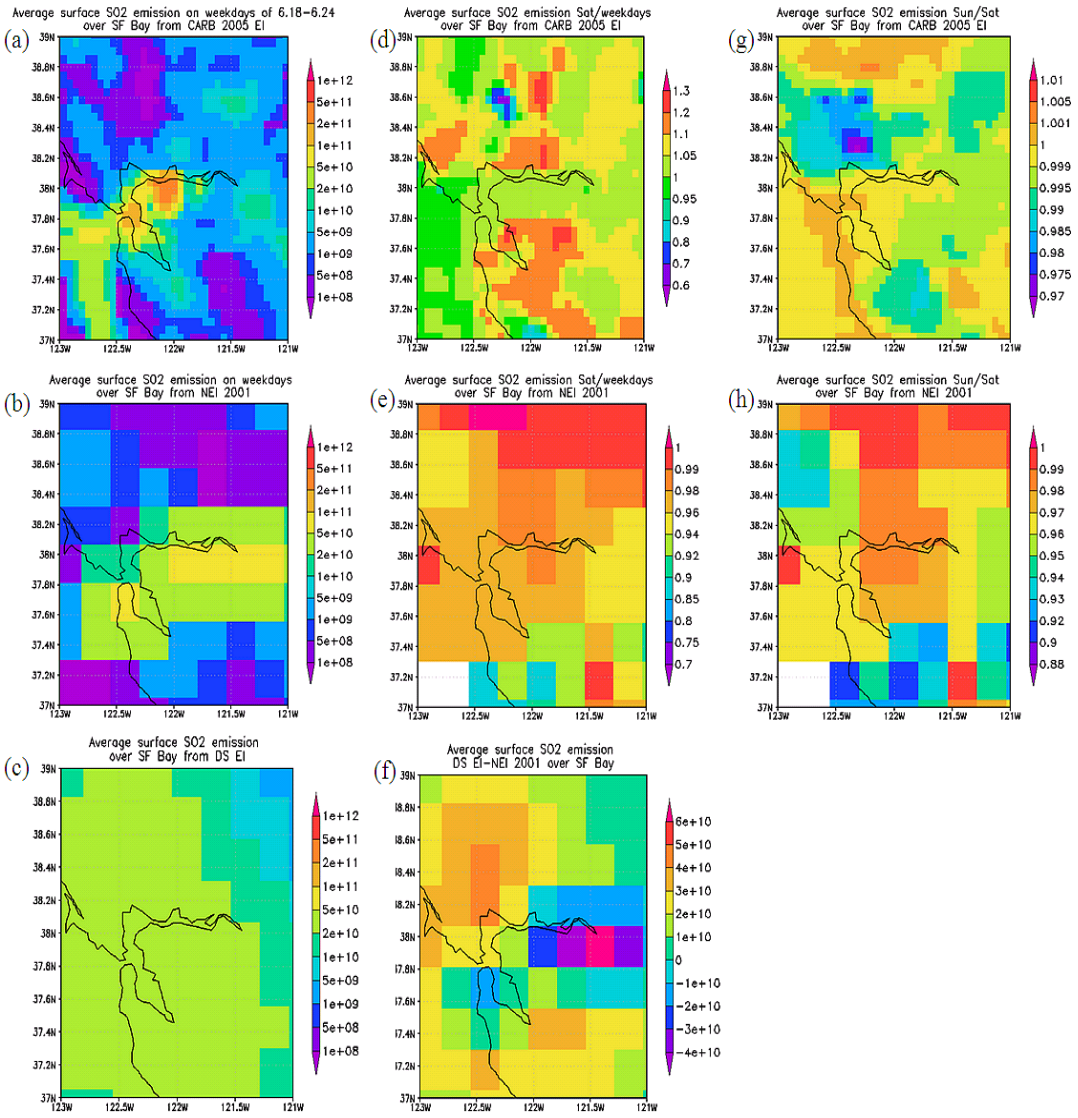

Figure 3.3 The average surface SO_2 emissions during 06/18-24 over the SF area during weekdays, Saturday (June 21) and Sunday (June 22), for three EIs. (a;d;g) CARB EI; (b;e;h) NEI 2001; (c) DS' EI; (d) difference between NEI and DS' EI

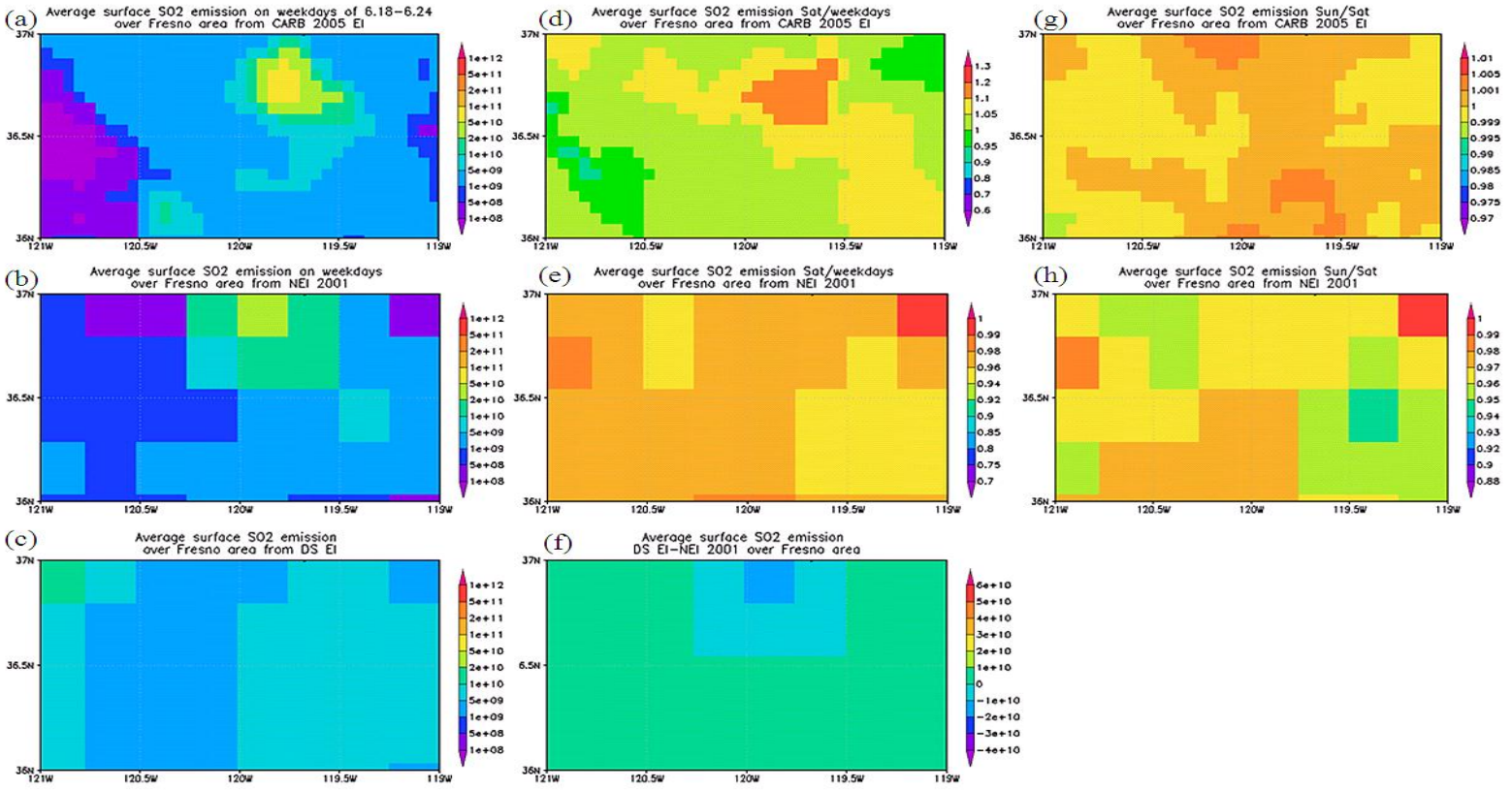

Figure 3.4 The average surface SO_2 emissions during 06/18-24 over the Fresno area during weekdays, Saturday (June 21) and Sunday (June 22), for three EIs. (a;d;g) CARB EI; (b;e;h) NEI 2001; (c) DS' EI; (d) difference between NEI and DS' EI

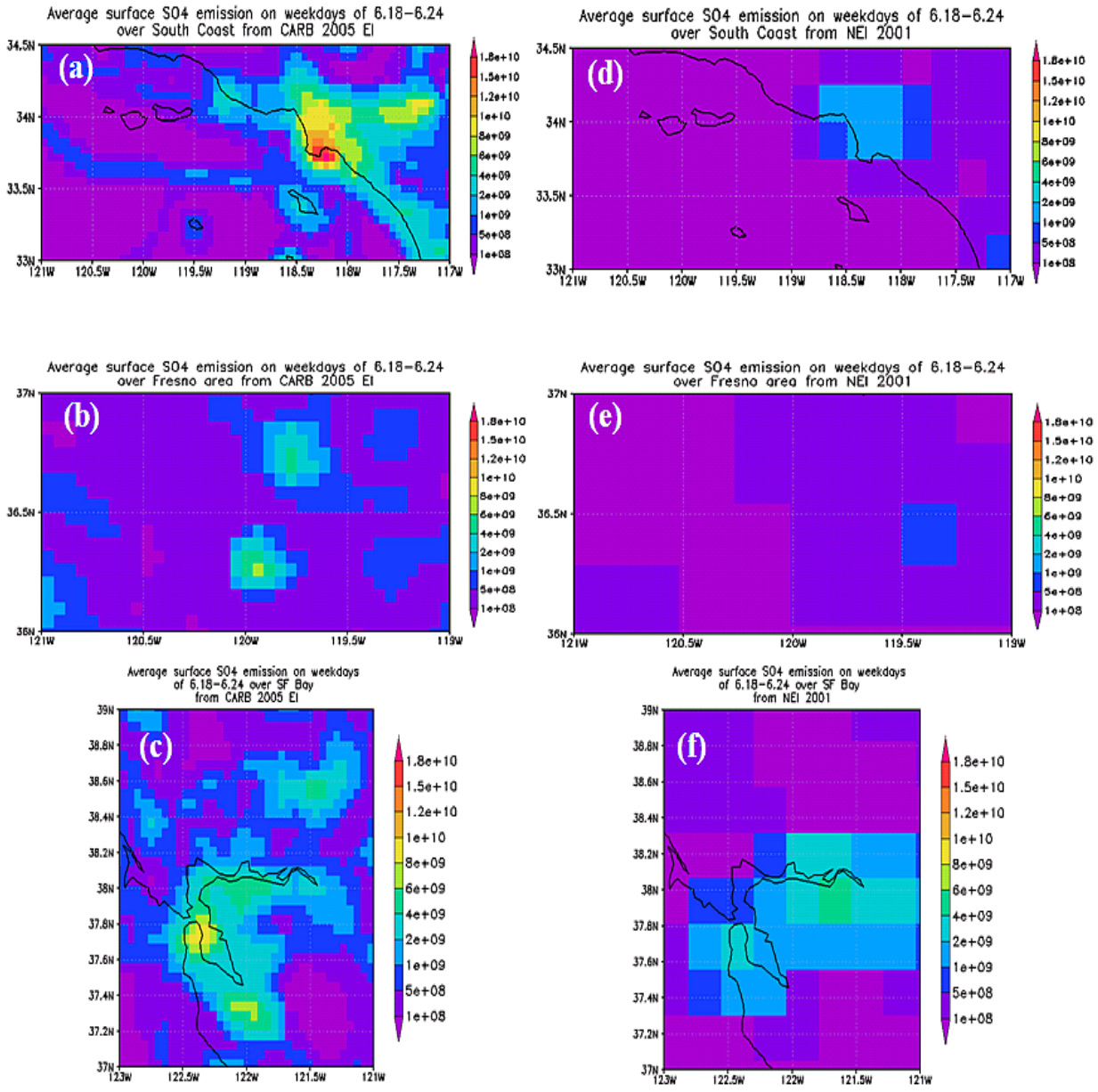

Figure 3.5 The average surface weekday SO_4 emissions during 06/18-24 from two EIs over three regions. (a-c) CARB EI; (d-f) NEI 2001; (a;d) SC, (b;e) CV-Fresno; (c;f) SF

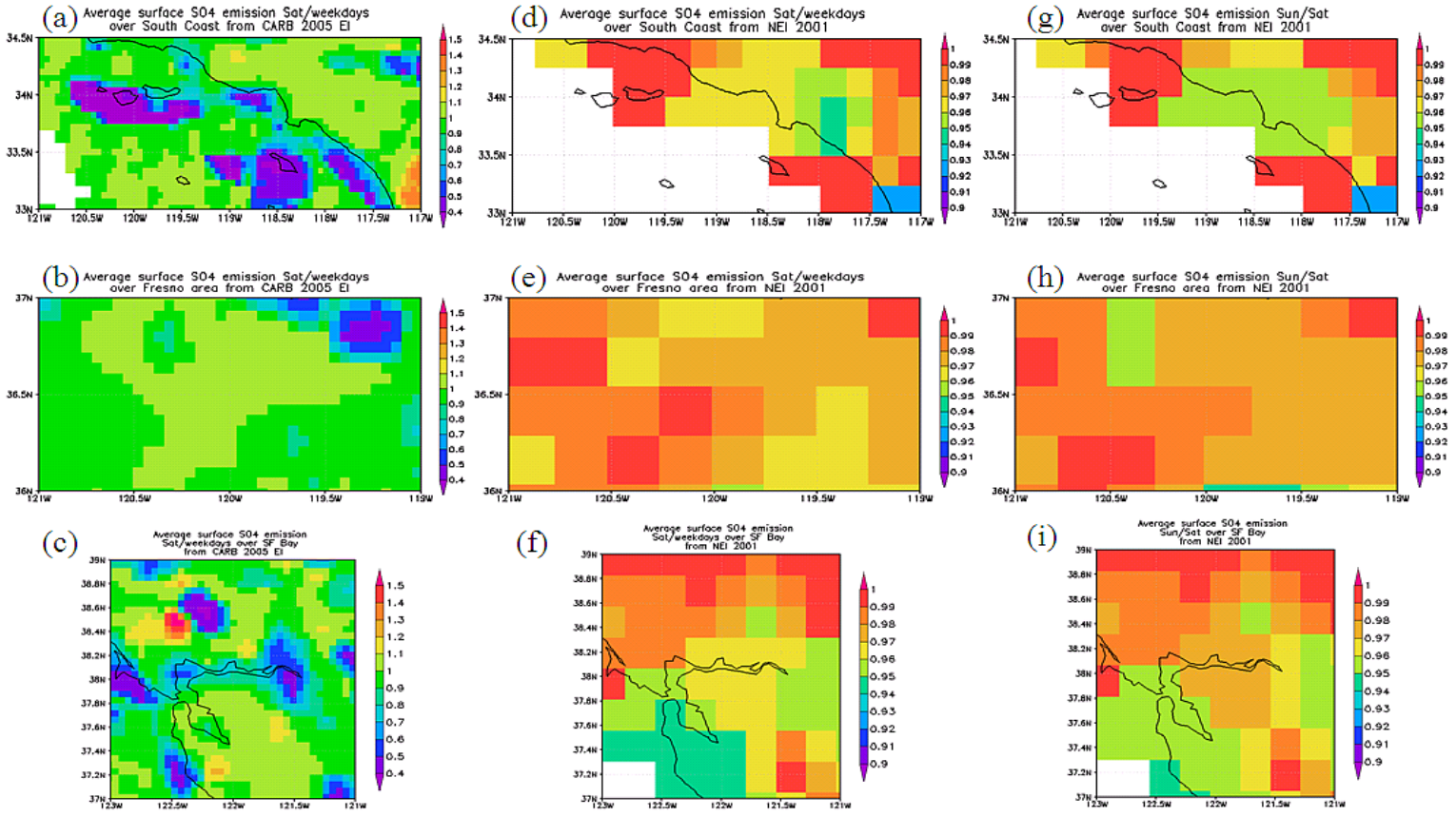

Figure 3.6 The weekday-weekend variations of average surface SO_4 emissions over three regions, during June 18–24. (a-c) CARB EI, Saturday/weekday; (d-e) NEI 2001, Saturday/weekday; (g-i) NEI 2001, Sunday/Saturday; (a;d;g) SC; (b;e;h) CV-Fresno; (c;f;i) SF

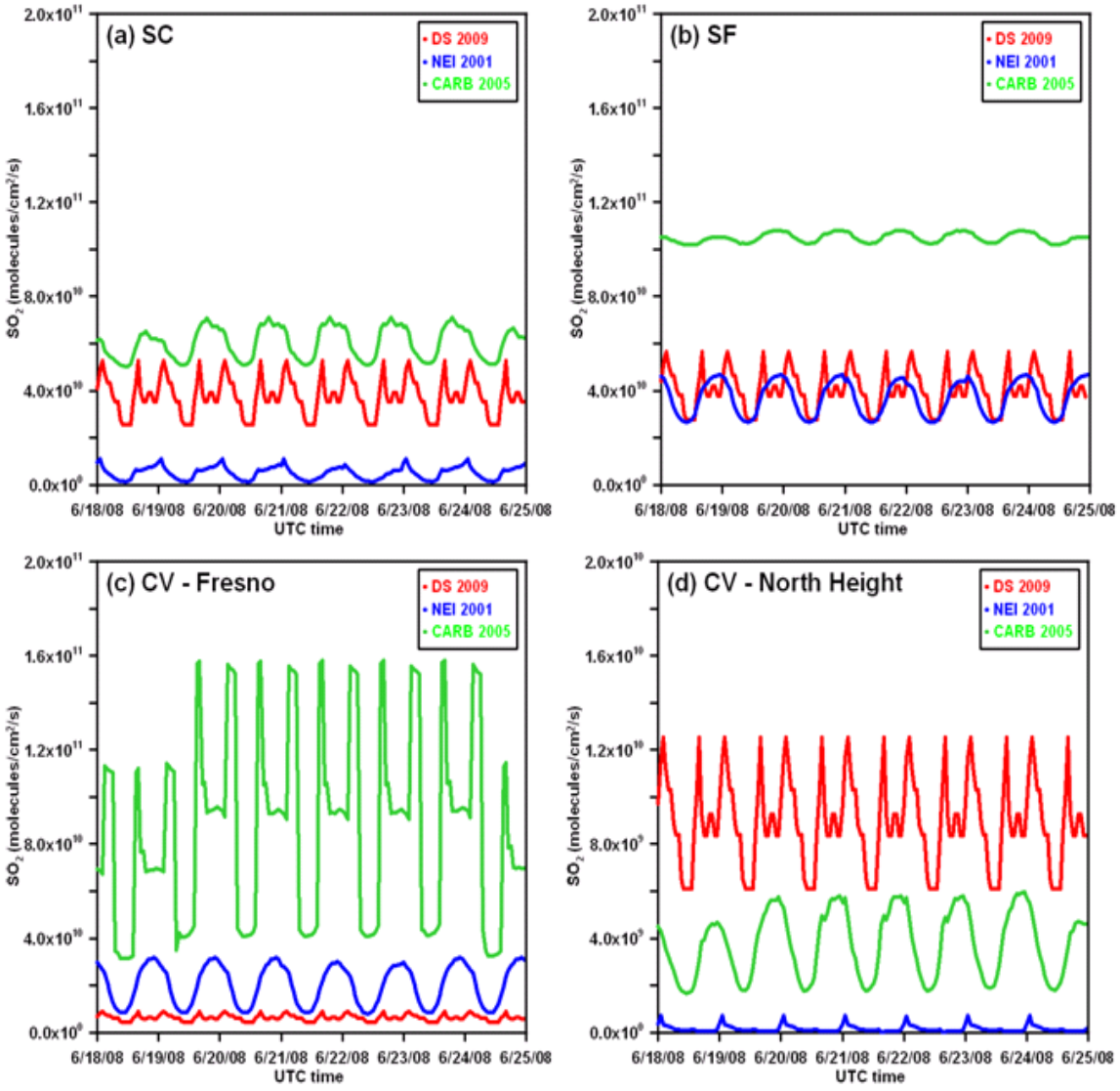

Figure 3.7 Time series of surface SO_2 emissions from the three emission inventories during 06/18-24 over multiple regions. (a) SC; (b) SF; (c) CV-Fresno; (d) CV-North Height

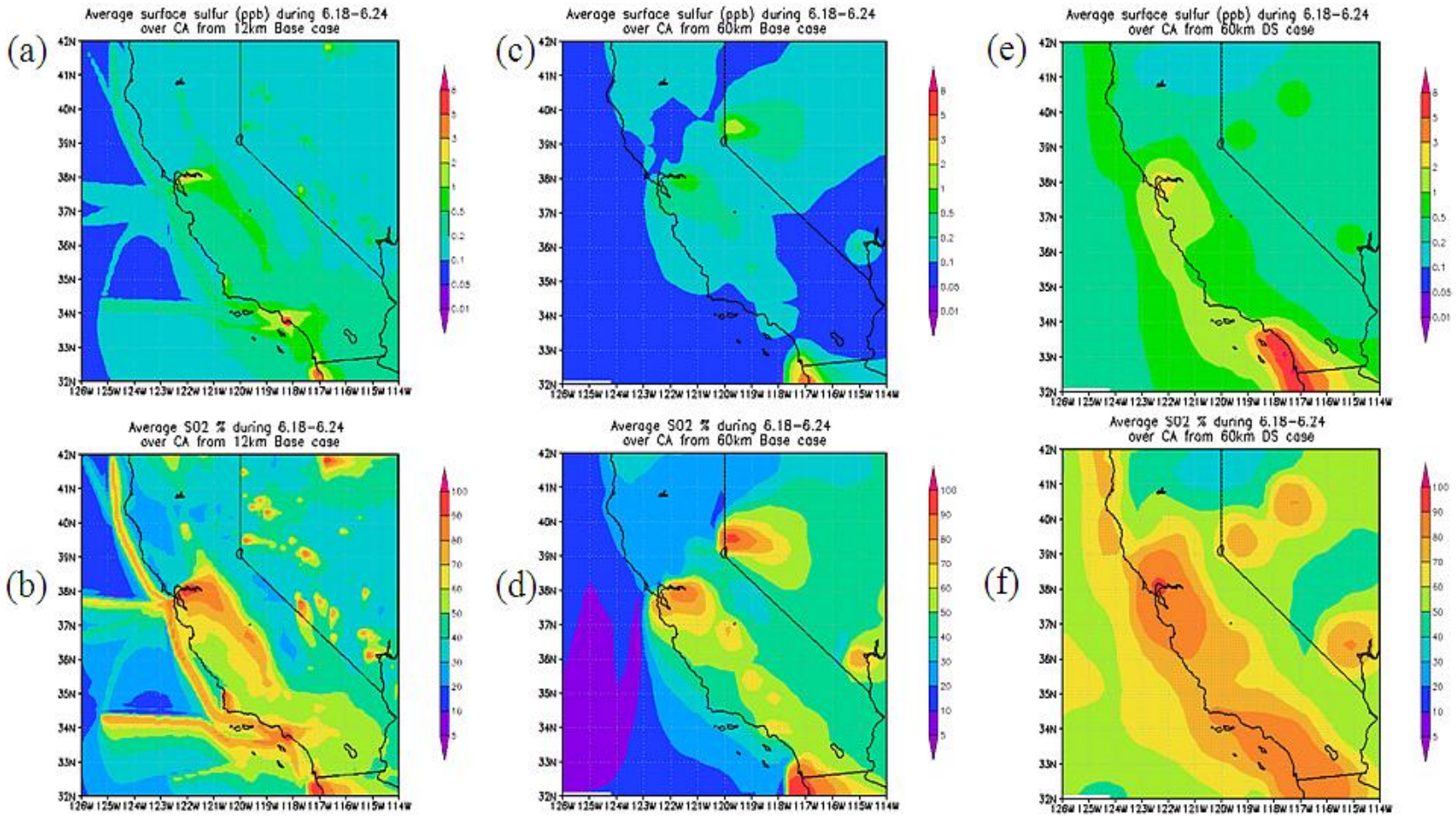

Figure 3.8 The 24-hr average surface SO_x distributions during 06/18-24 from three model simulations. (a;b) 12 km base (c;d) 60 km base (e;f) 60 km DS; (a;c;e) total sulfur (ppb); (b;d;f) SO_2%

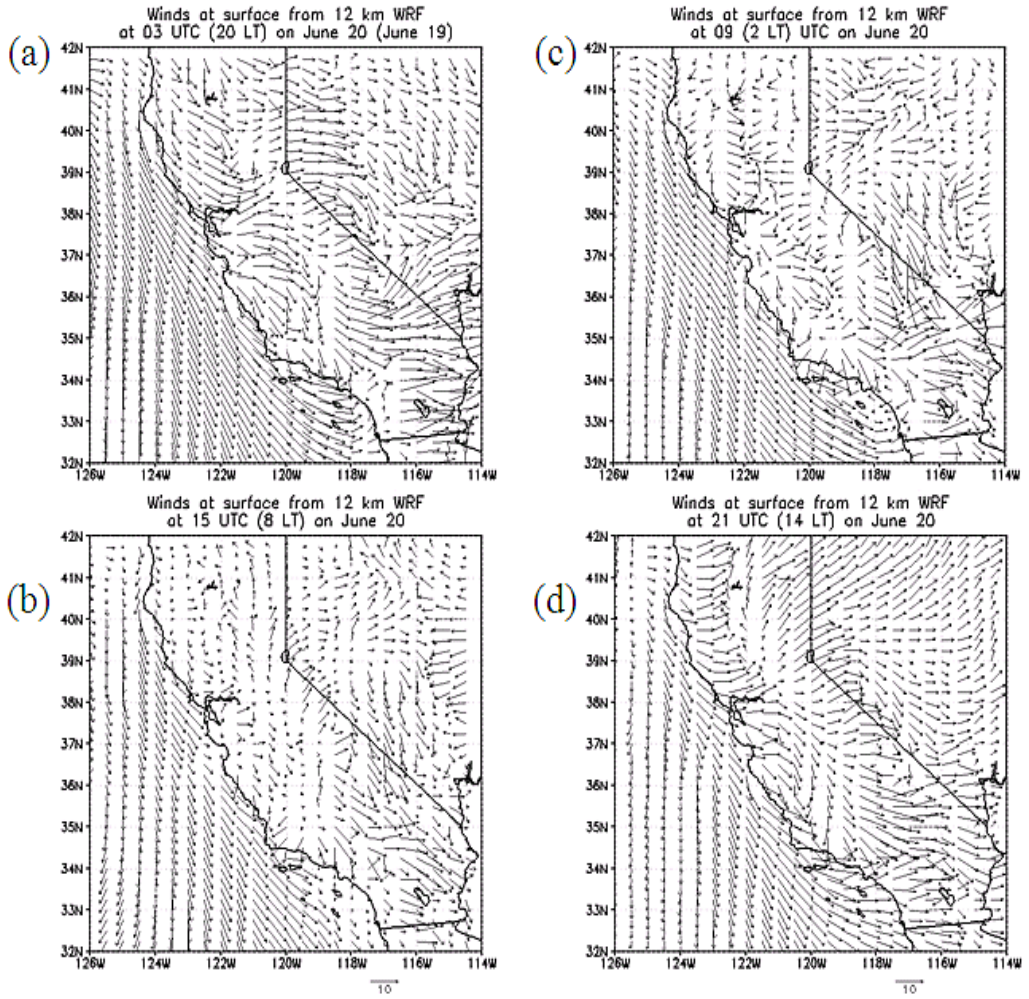

Figure 3.9 12 km WRF wind fields at surface, at multiple times on 06/20. (a) 03 UTC; (b) 09 UTC; (c) 15 UTC; (d) 21UTC

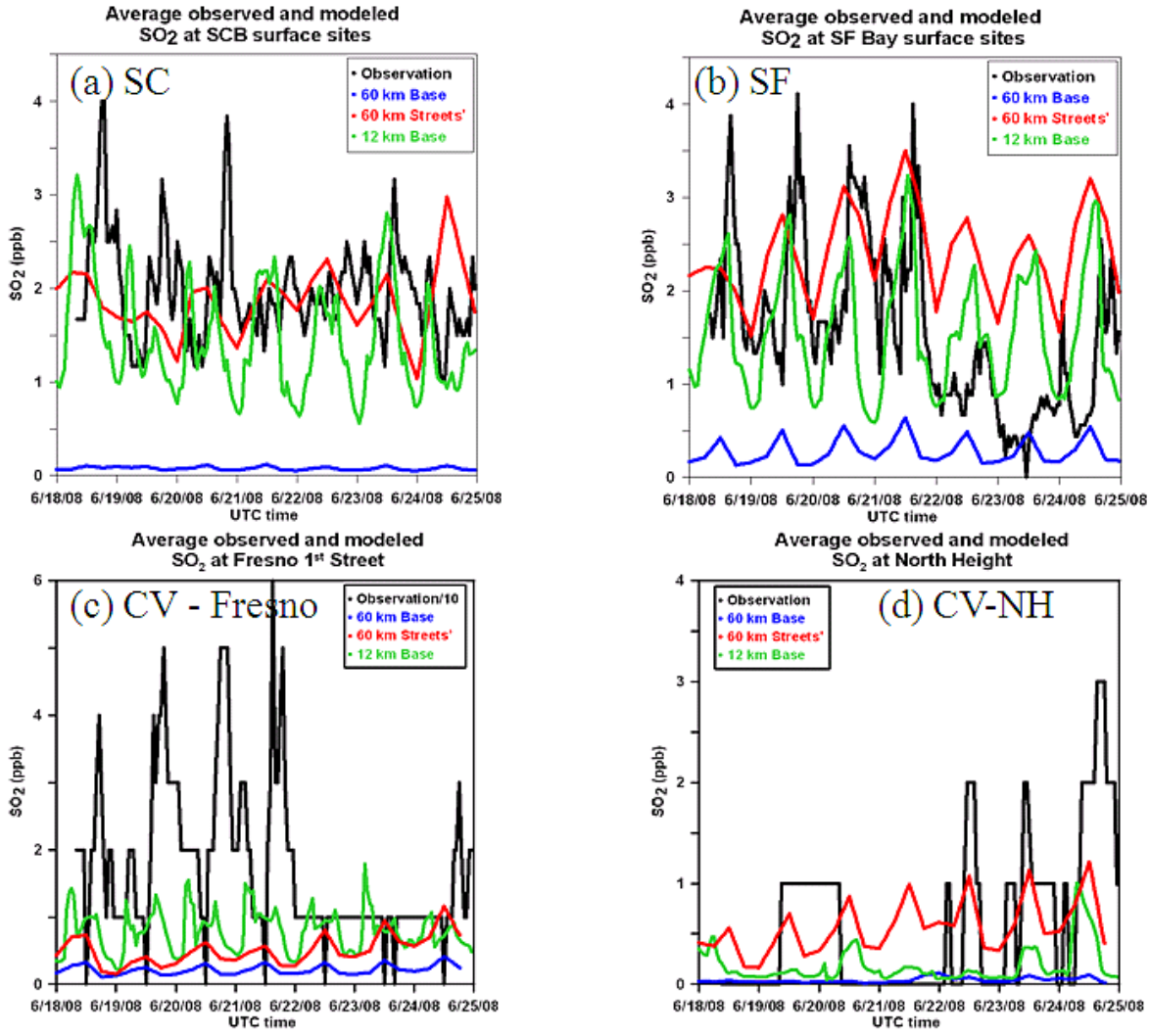

Figure 3.10 Time series plots for observed and modeled SO_2 and SO_4 over four surface regions. Data at multiple sites over SC and SF areas are averaged. (a) SC (6 sites); (b) SF (9 sites); (c) CV-Fresno; (d) CV-North Height

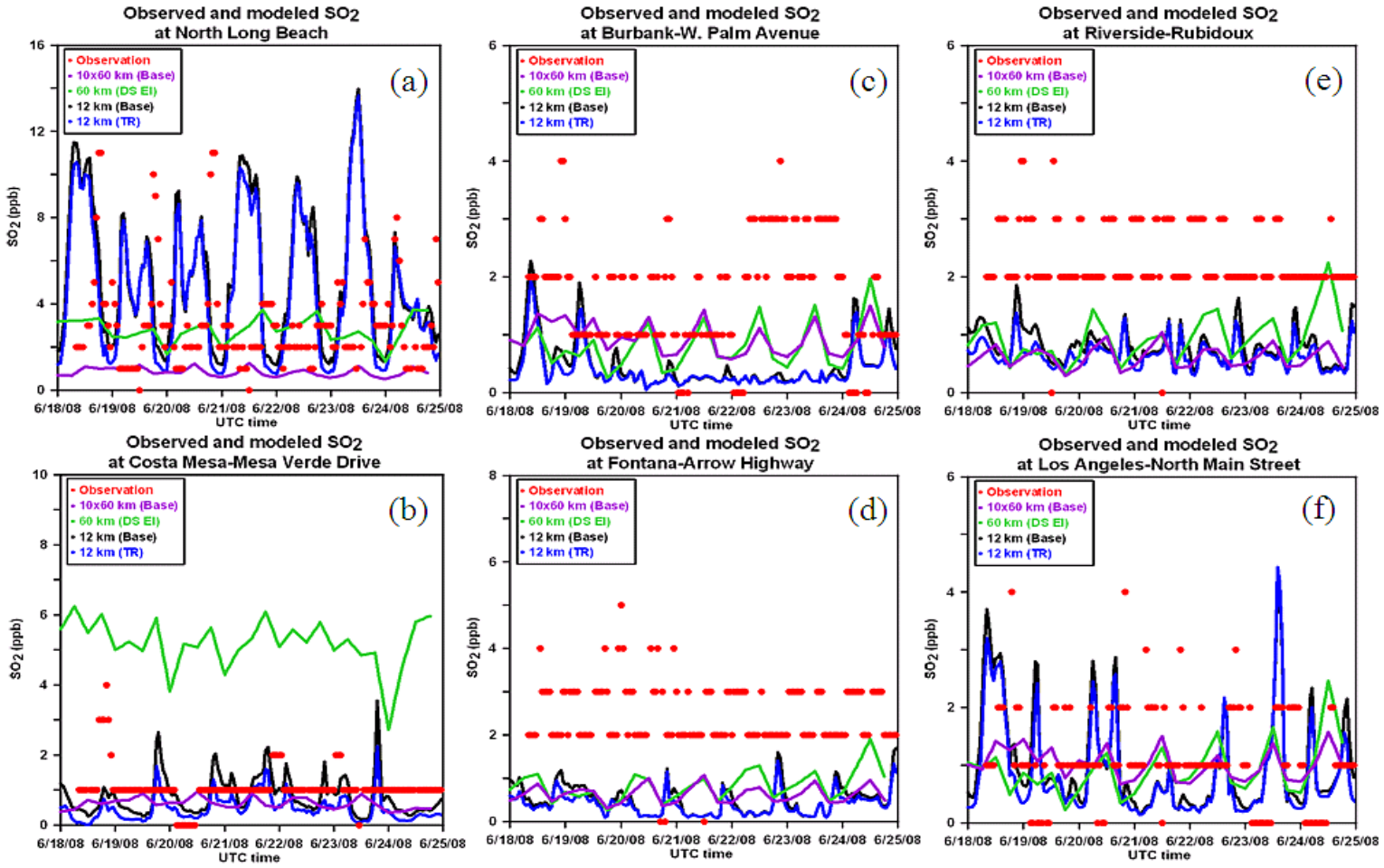

Figure 3.11 Time series plots for observed and modeled surface SO_2 at SC individual sites. (a, b) two sites in industrial and its downwind areas; (c – f) four sites close to highway areas.

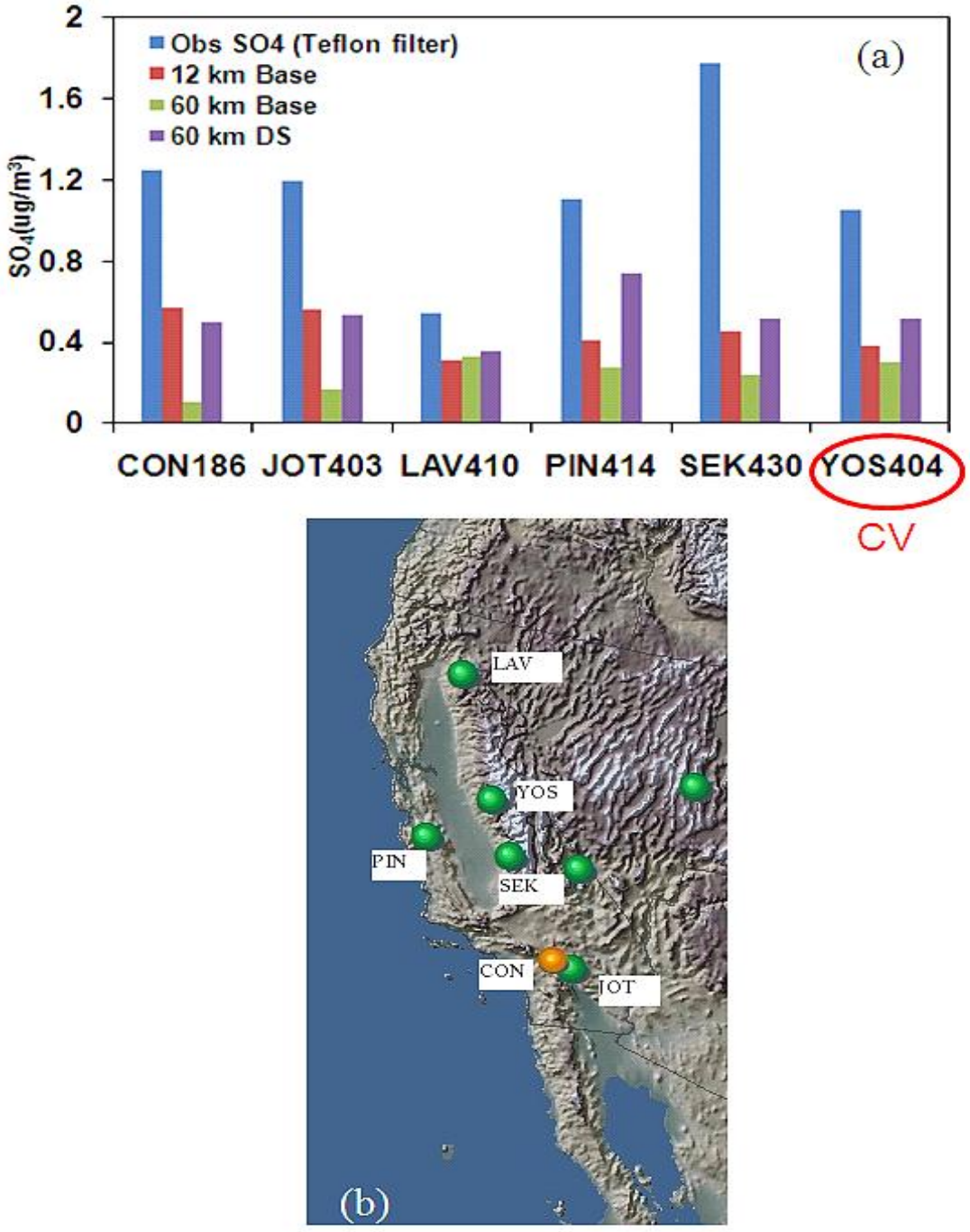

Figure 3.12 Weekly-averaged (June 18 – June 24) SO_4 at six California CASTNET sites. (a) Comparison of observations and model simulations; (b) California CASTNET sites locations

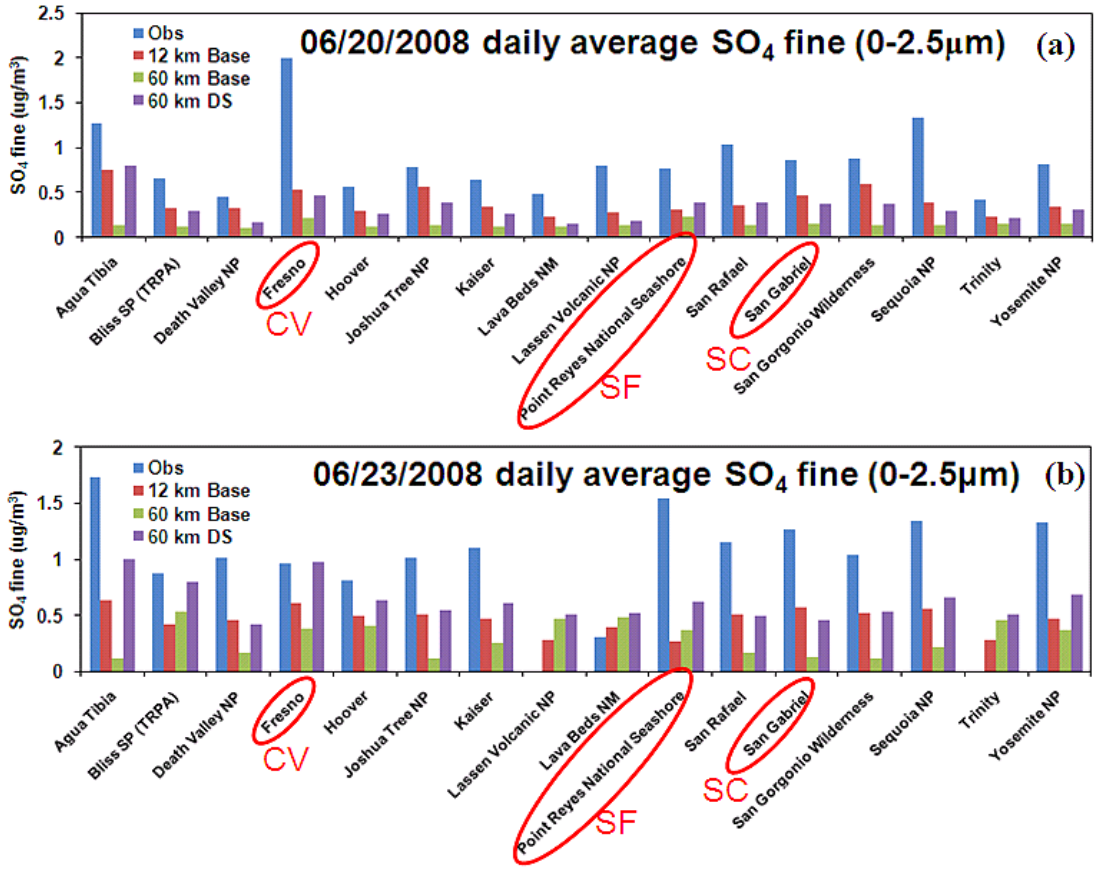

Figure 3.13 Daily-averaged fine SO_4 (0 – 2.5 µm) at sixteen California IMPROVE sites from observations and model simulations. (a) June 20; (b) June 23

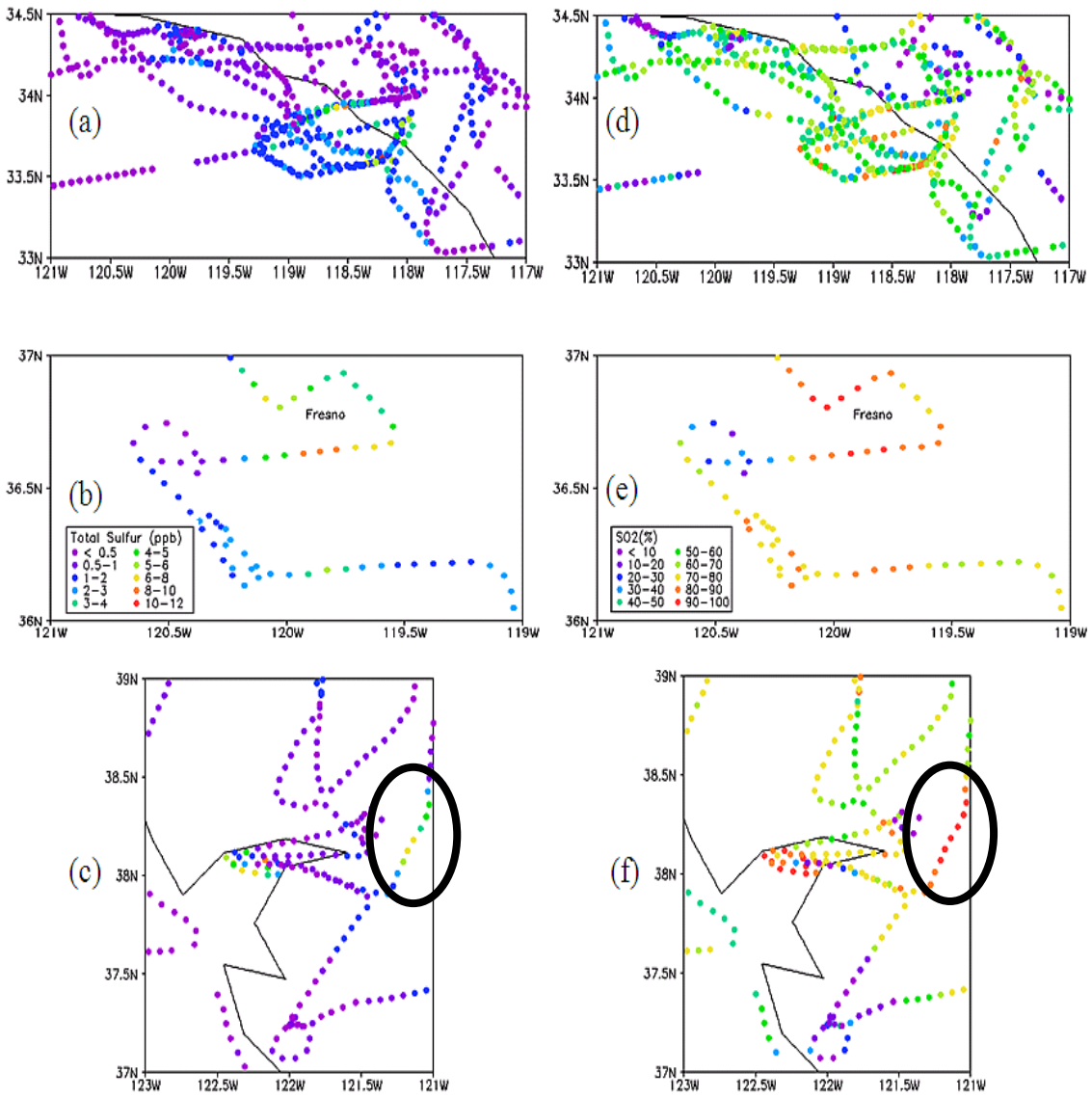

Figure 3.14 Observed SO_x distributions along all DC-8 flight paths (below 5 km ASL), over three regions. (a-c) total sulfur; (d-f) SO_2 %; (a;d) SC; (b;e) CV – Fresno; (c;f) SF

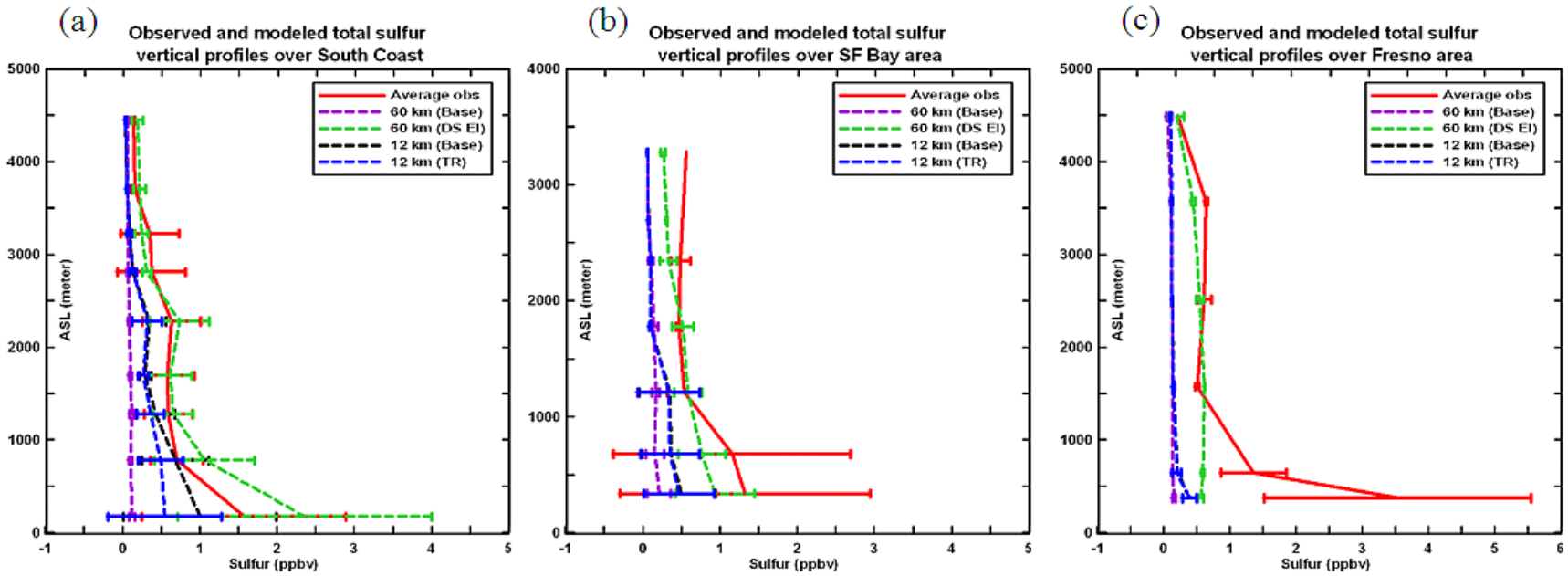

Figure 3.15 Vertical profiles of observed and modeled total sulfur along all DC-8 flight paths, over three regions. (a) SC (b) SF and (c) CV – Fresno

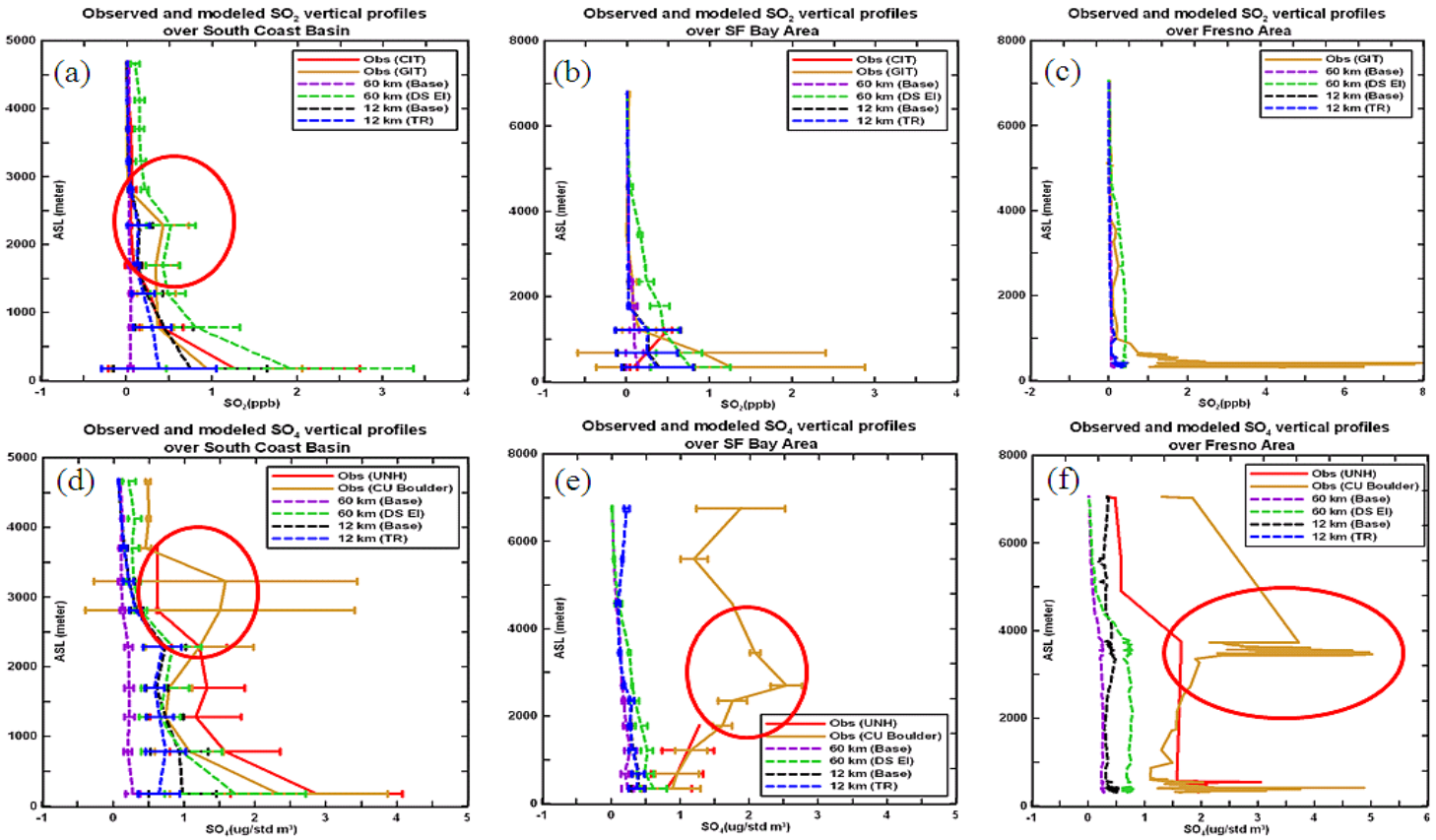

Figure 3.16 Vertical profiles for observed and modeled SO_x over three regions along all DC-8 flight paths. (a-c) SO_2; (d-f) SO_4; (a;d) SC; (b;e) SF; (c;f) CV – Fresno

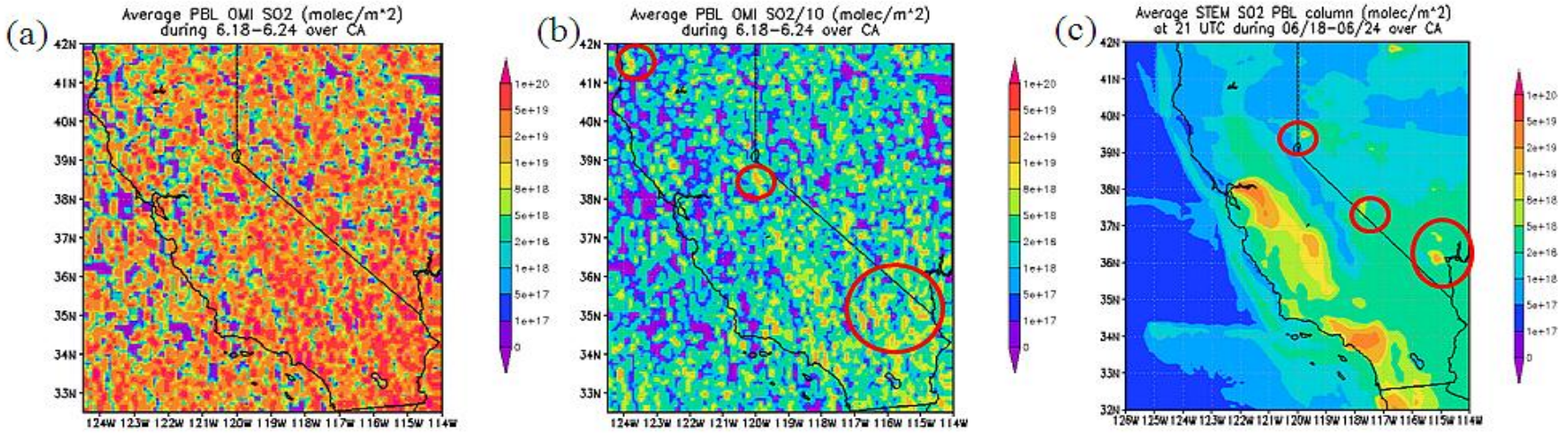

Figure 3.17 Weekly-averaged (June 18 – June 24) OMI and 12 km modeled PBL SO_2 column. (a) original OMI; (b)1/10 of original OMI; (c) modeled (profiles at 21 UTC each day during the week used for averaging)

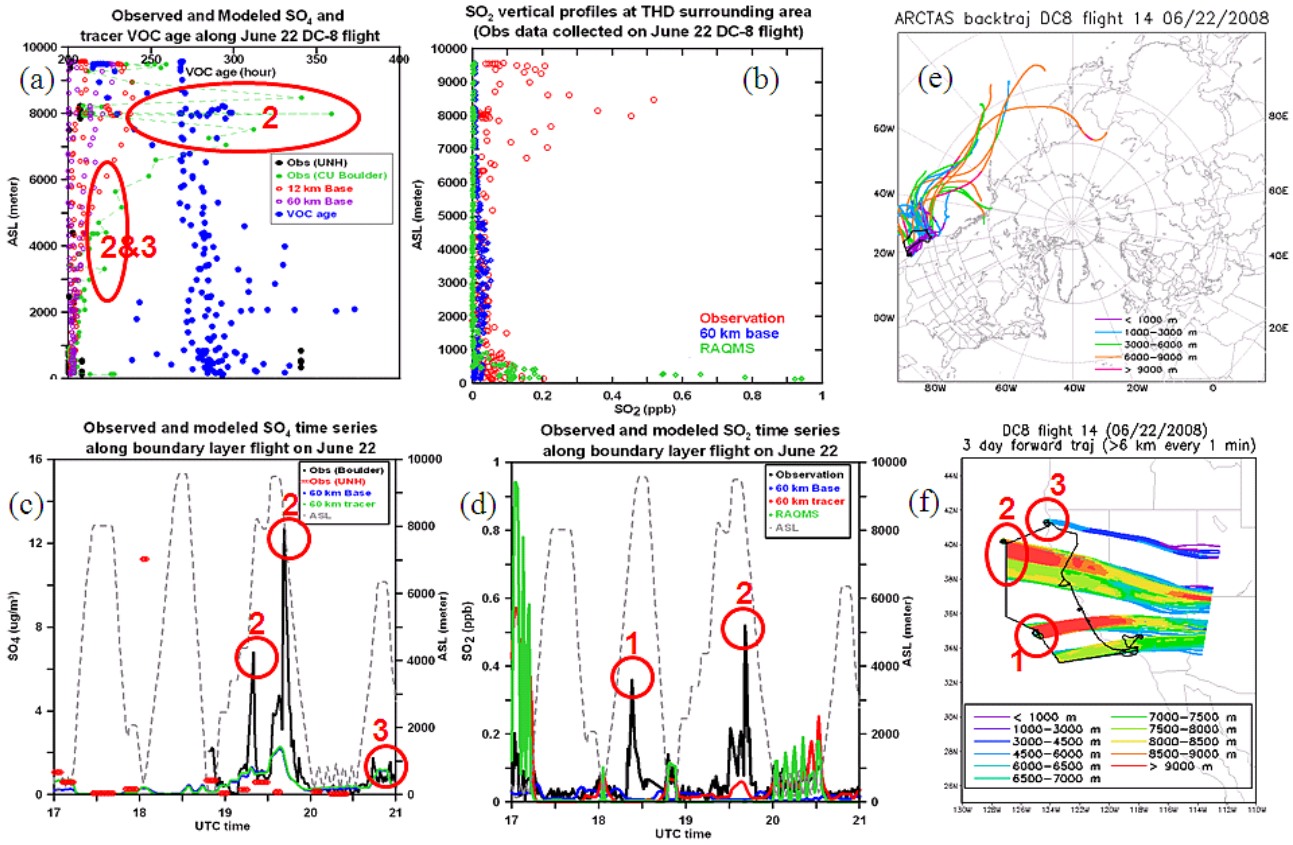

Figure 3.18 Effects of Asian SO_x on California air quality. Vertical profiles for (a) SO_4 (b) SO_2 and time series for (c) SO_4 (d) SO_2 along outbound of the 06/22 flight; (e) Back-trajectories and (f) Forward trajectories (ASL > 6 km) along this flight path

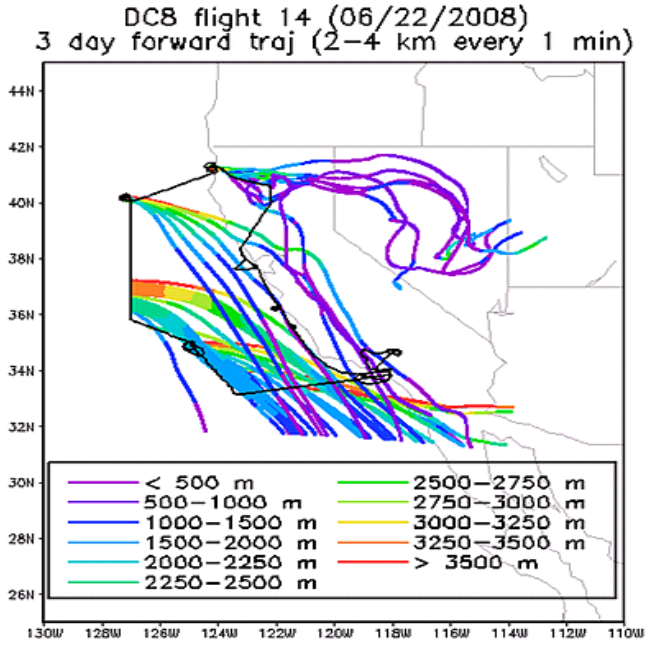

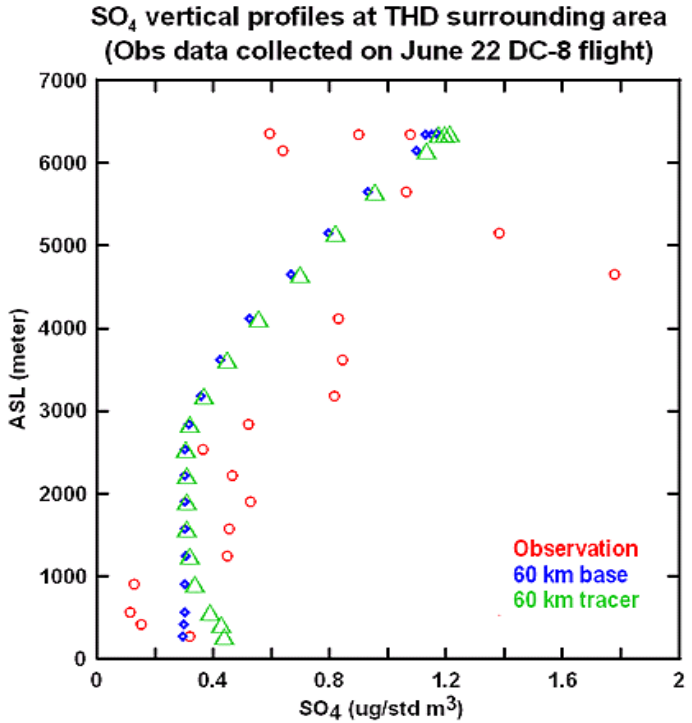

(g) Three-day forward trajectories (ASL between 2 – 4 km) along the June 22 flight path; (h) Vertical profiles for observed and modeled SO_4 at THD. This DC-8 flight circled at leg 3 (THD) at ~20.5 – 21 UTC

Figure 3.18 Continued

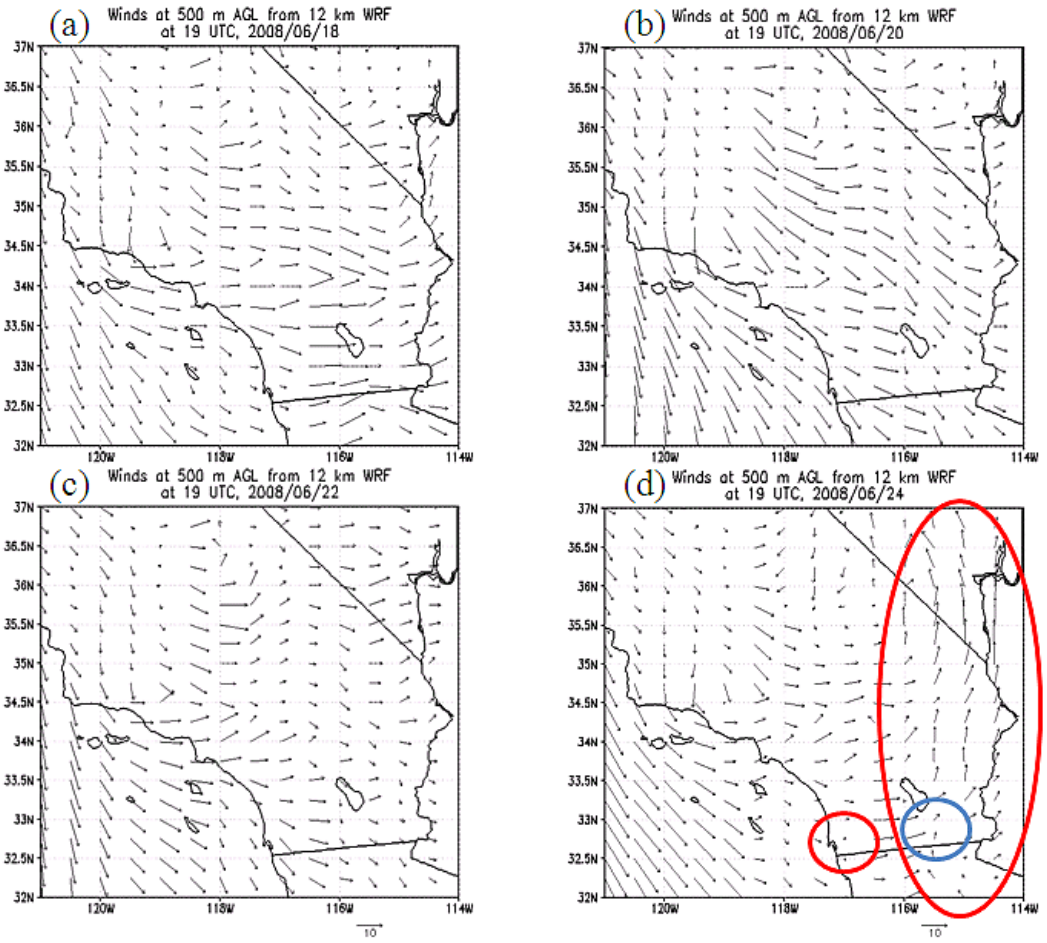

Figure 3.19 12 km WRF wind fields at ~500 m AGL, at 19 UTC (noon, LT), on four days of June. (a) June 18, (b) 20, (c) 22 (d) 24

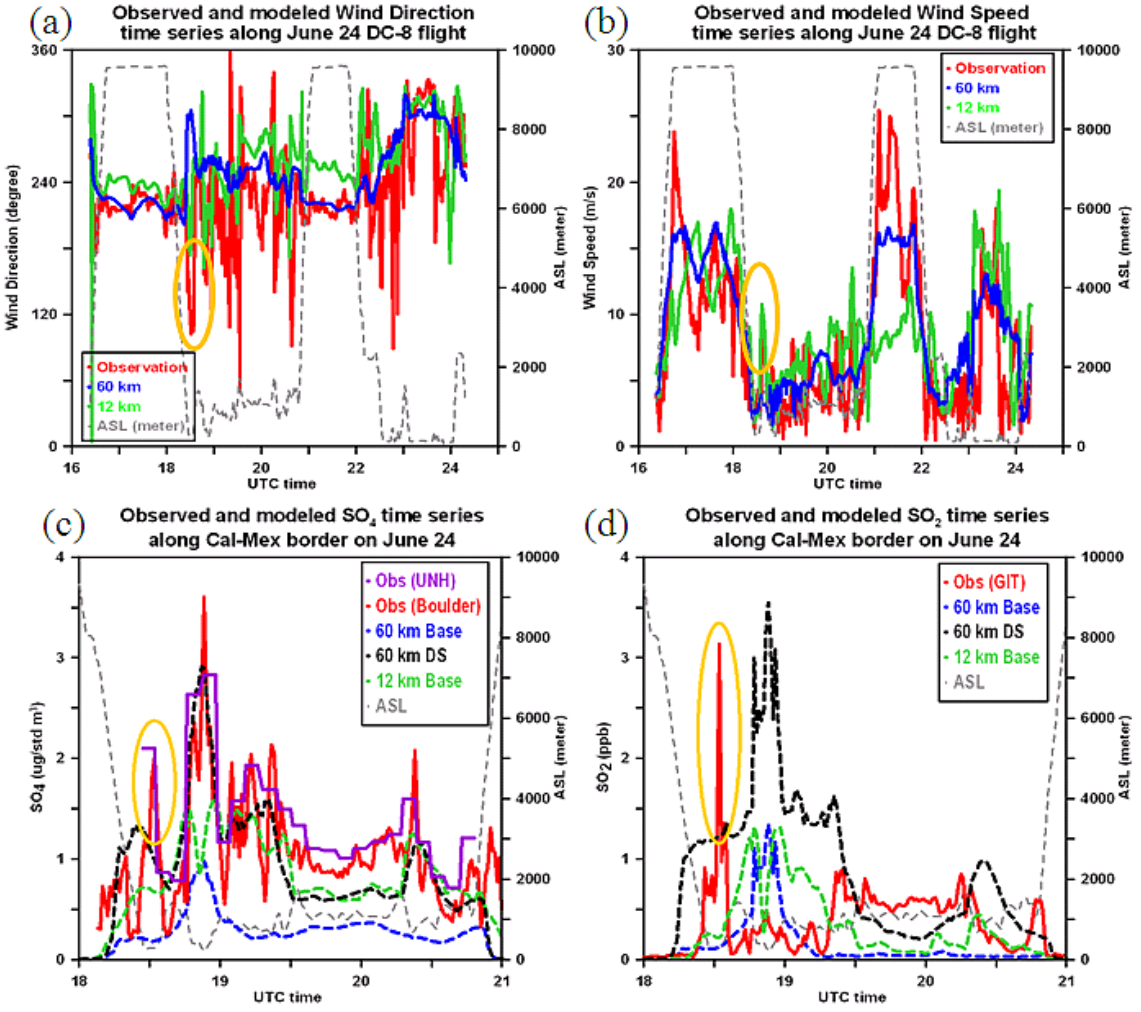

Figure 3.20 Time series for DC-8 observed and modeled wind fields and SO_x over California – Mexico border on June 24. (a) wind direction (b) wind speed (c) SO_4 (d) SO_2

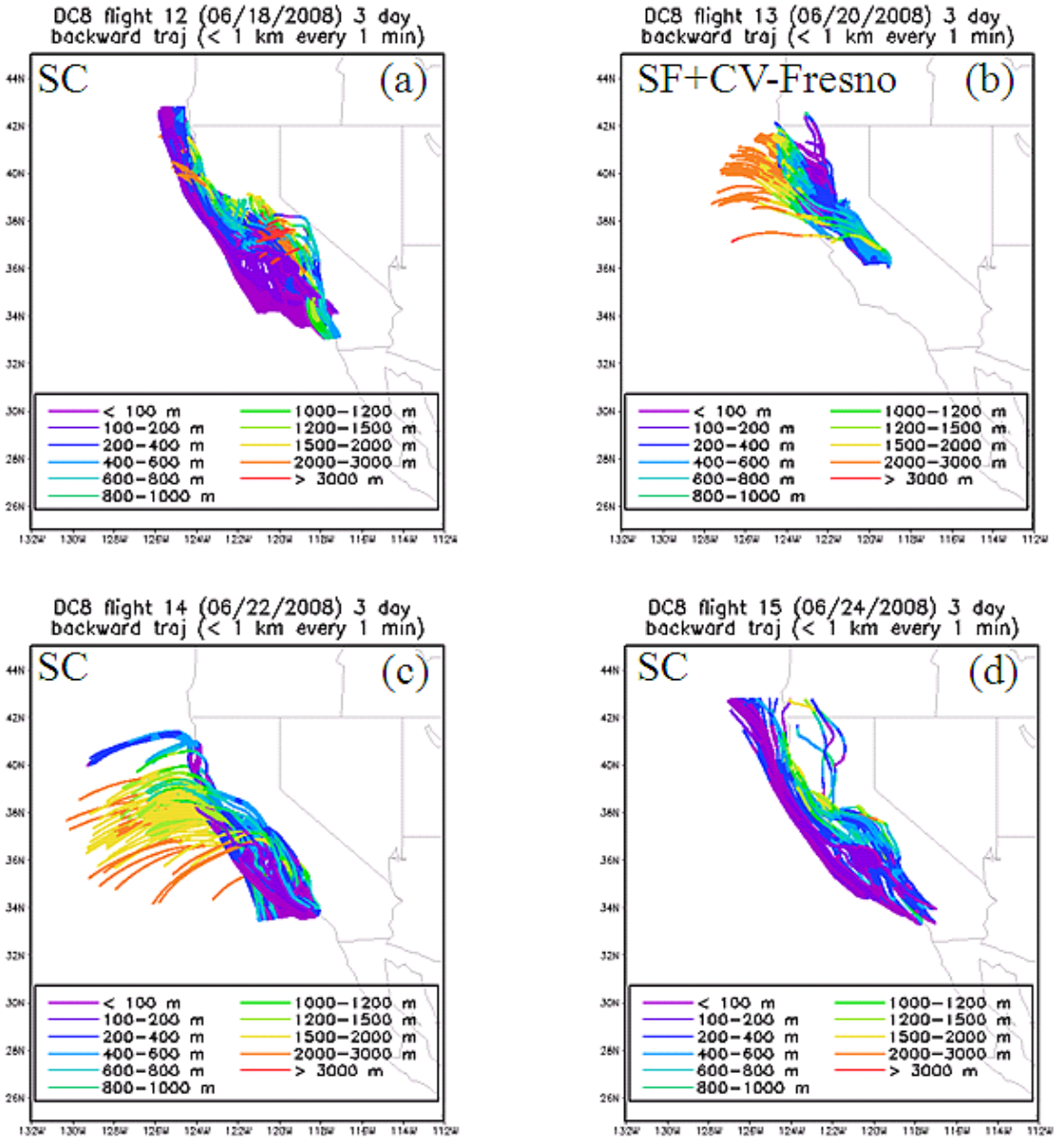

Figure 3.21 Back trajectories originating along flight paths, based on 12 km WRF meteorology fields, below 1 km AGL, shown by days and regions. (a) June 18, SC; (b) June 20, SF & Fresno; (c) June 22, SC; (d) June 24, SC

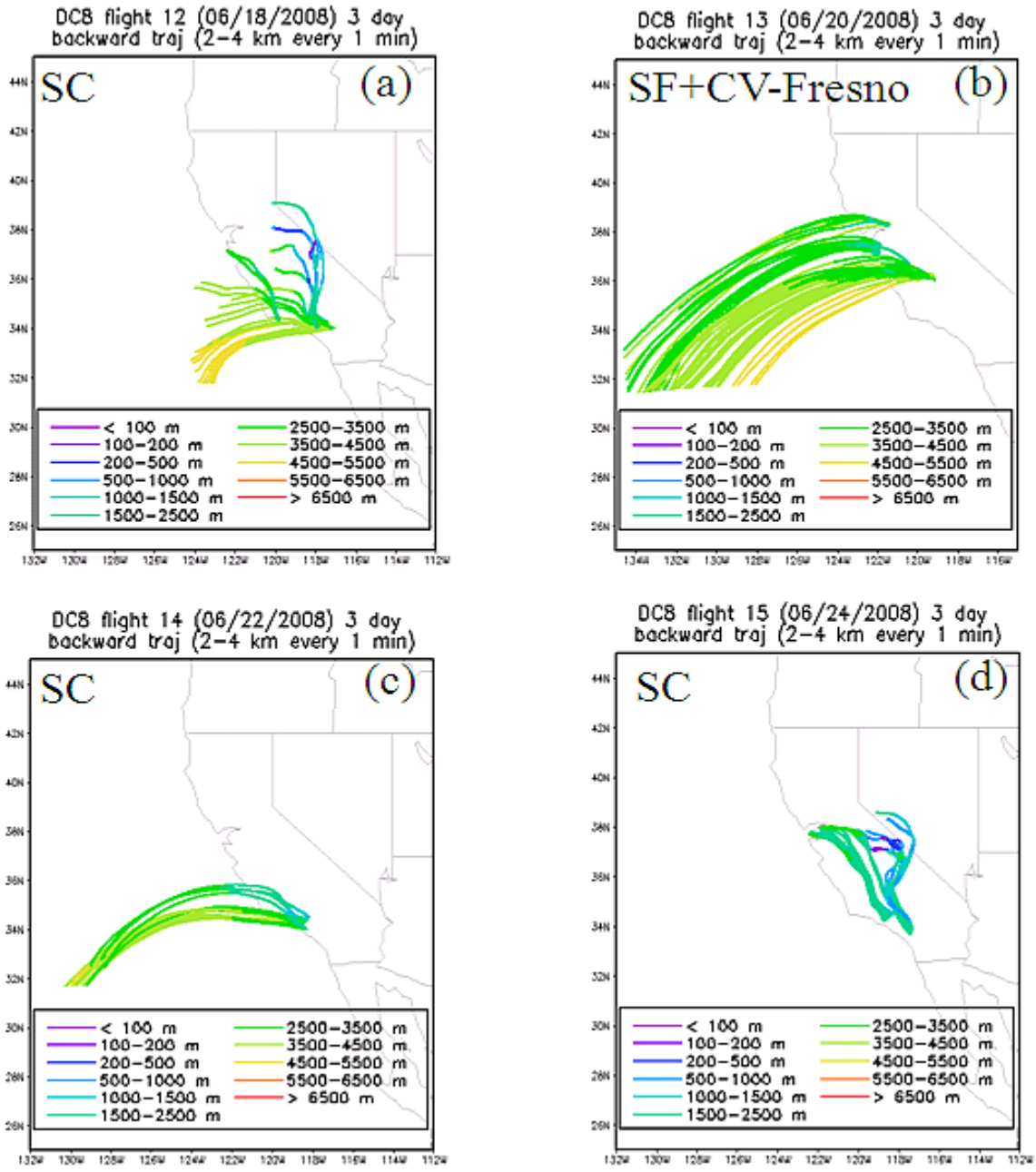

Figure 3.22 Back trajectories originating along flight paths, based on 12 km WRF meteorology fields, at 2 – 4 km ASL, shown by days and regions. (a) June 18, SC; (b) June 20, SF & Fresno; (c) June 22, SC; (d) June 24, SC

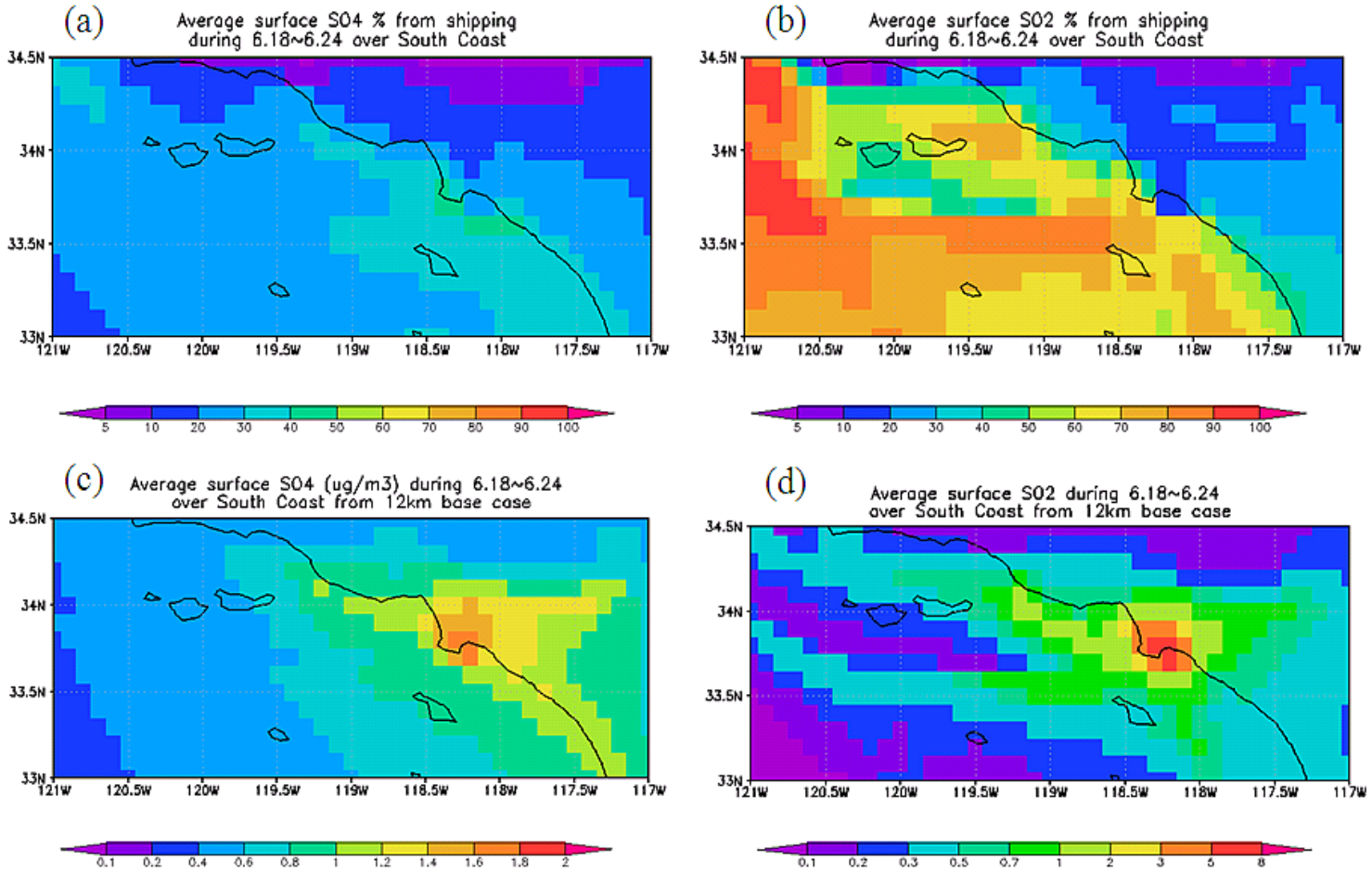

Figure 3.23 24-hr averaged contributions (%) of maritime and terrestrial SO_x emissions on SC surface air quality in 12 km grids, during 06/18-24. (a;c) SO_4; (b;d) SO_2; (a-b) maritime contribution; (c-d) terrestrial contribution

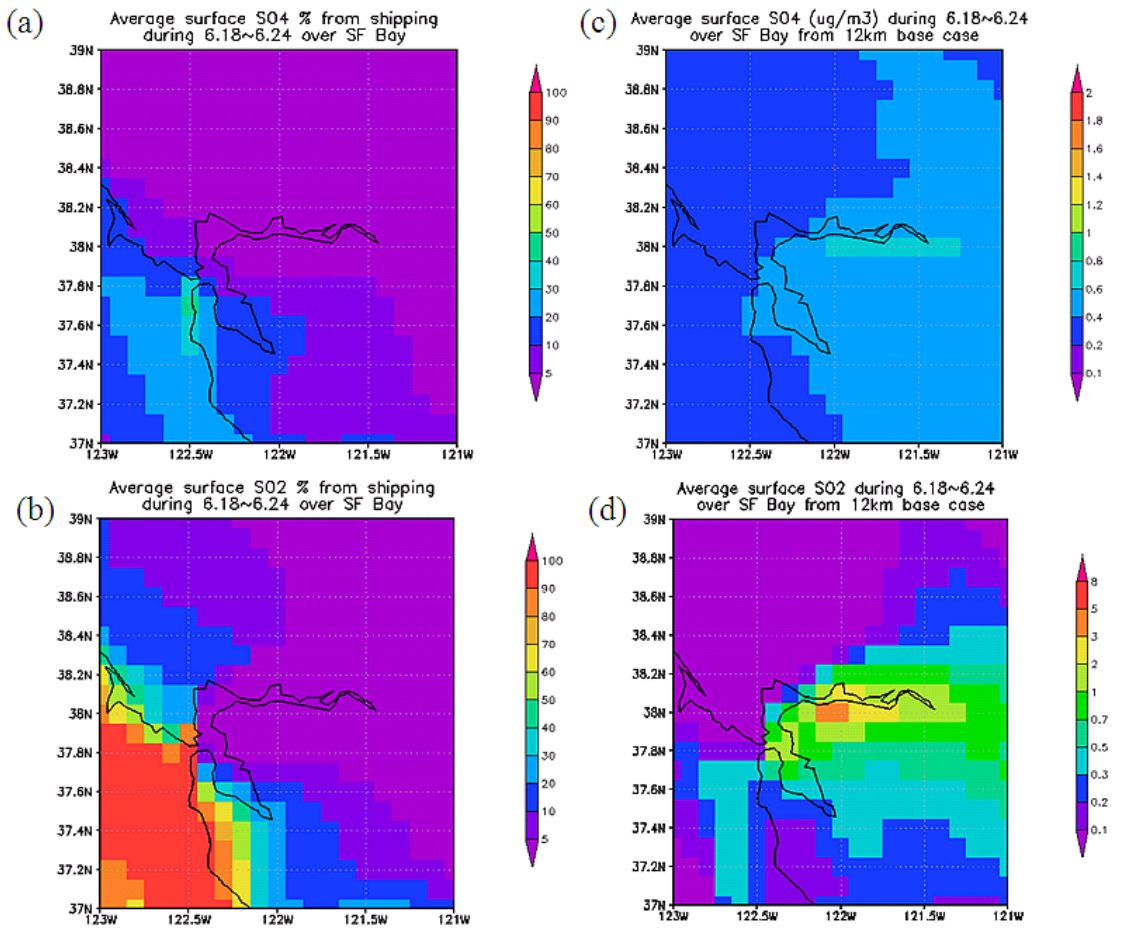

Figure 3.24 24-hr averaged contributions (%) of maritime and terrestrial SO_x emissions on SF surface air quality in 12 km grids, during 06/18-24. (a;c) SO_4; (b;d) SO_2; (a-b) maritime contribution; (c-d) terrestrial contribution

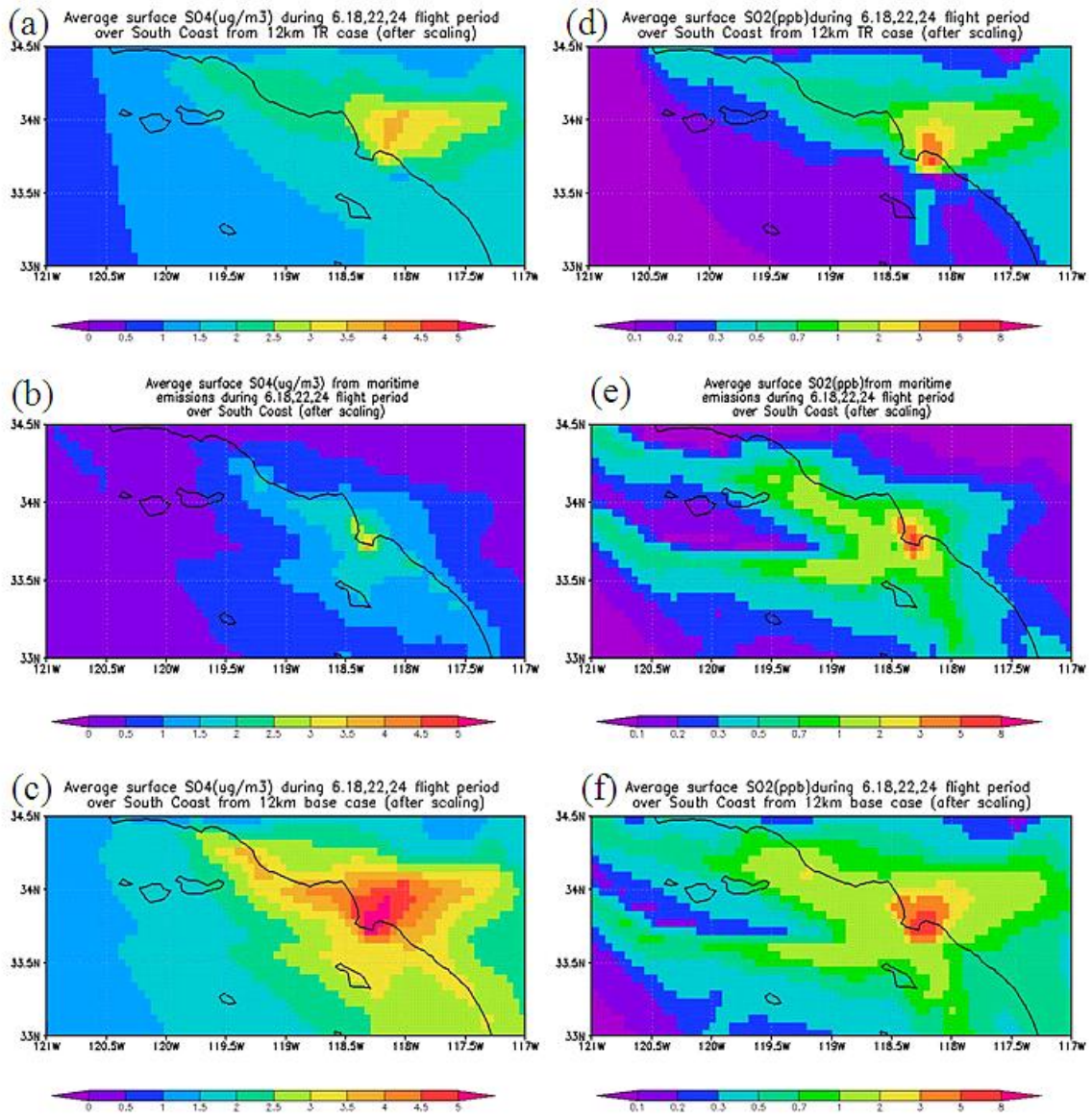

Figure 3.25 Contributions (after scaling) of maritime and terrestrial SO_x emissions on SC surface air quality in 12 km grids, during the 06/18, 22, 24 flight time 16 – 24 UTC. (a-c) SO_4 ($\mu g/m^3$); (d-f) SO_2 (ppb); (c;f) base case; (a;d) terrestrial; (b;e) maritime

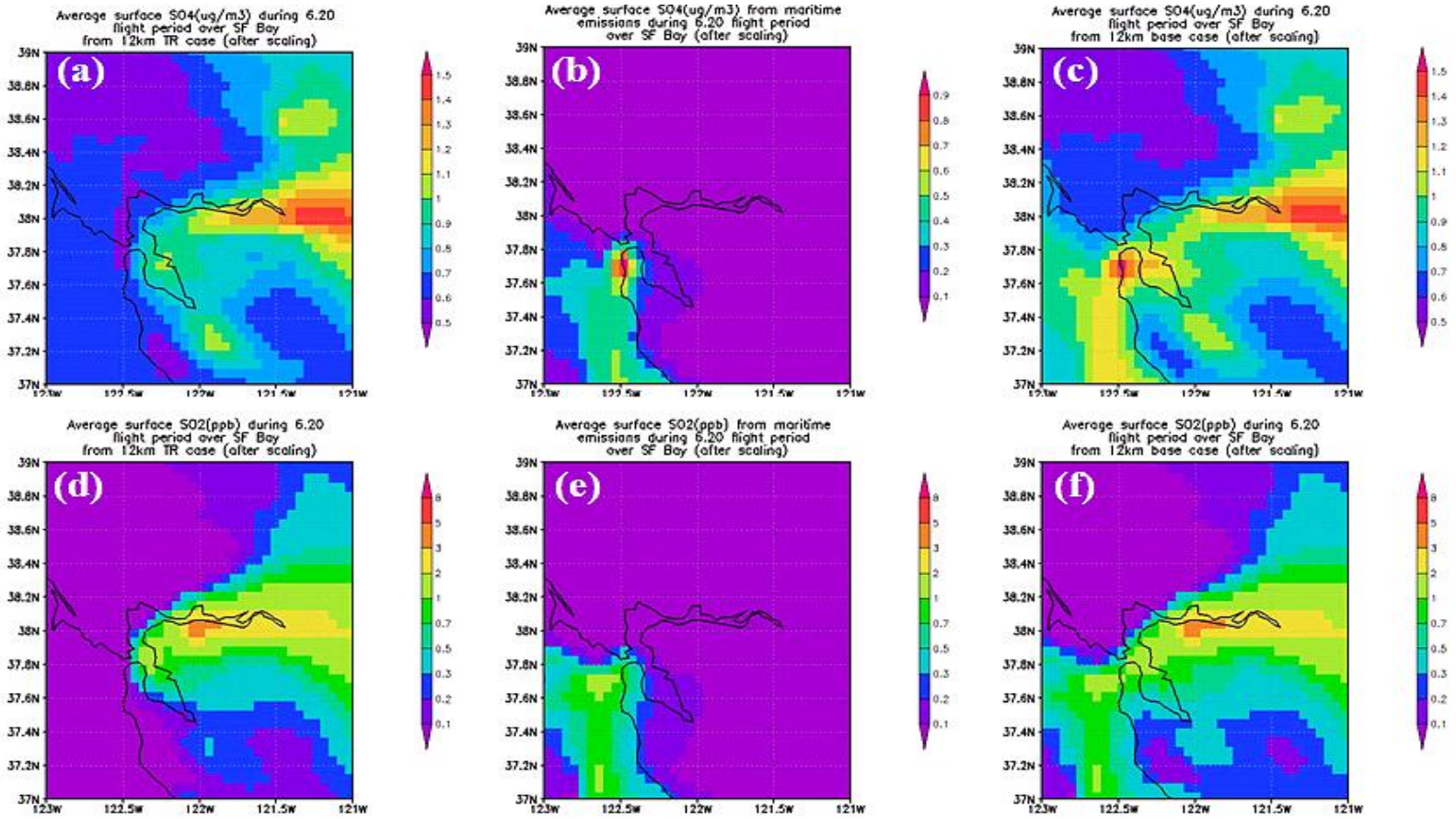

Figure 3.26 Contributions (after scaling) of maritime and terrestrial SO_x emissions on SF surface air quality in 12 km grids, during the 06/20 flight time 16 – 24 UTC. (a-c) SO_4 ($\mu g/m^3$); (d-f) SO_2 (ppb); (c;f) base case; (a;d) terrestrial; (b;e) maritime

CHAPTER 4

SUMMARY AND FUTURE WORK

4.1 Summary

California air quality is not only affected by the local emissions and processes (chemical reactions and in-state transport), but is also under the influence of the transported pollutants from out of the state (such as Asia and Mexico). All these transport and production processes are highly dependent on its spatially and temporally varied meteorology and complicated geography. In this study, multi-scale tracer and full-chemistry simulations with the STEM atmospheric chemistry model have been used to analyze the effects of transported and local production of pollutants on California air quality during the ARCTAS-CARB experiment conducted in June 2008.

In Chapter 1, we briefly introduced the California air quality and the research tool-STEM chemical transport model. In Chapter 2, we analyzed the impacts of transported background O_3 from the eastern Pacific on California air quality. Previous work has focused on the importance of long-range transport of O_3 to North America air quality in springtime. However during this summer experiment the long-range transport of O_3 is also shown to be important. Simulated and observed O_3 transport patterns from the coast to inland northern California were shown to vary based on meteorological conditions and the oceanic O_3 profiles, which are strongly episodically affected by Asian inflows. Analysis of the correlations of O_3 at various altitudes above the coastal site at Trinidad Head and at a downwind surface site in northern California, showed that under long-range transport events, high O_3 air-masses ($O_3 > 60$ ppb) at altitudes between about 2 and 4 km can be transported inland and can significantly influence surface O_3 20–30 hours later. These results showed

the importance of characterizing the vertical structure of the lateral boundary conditions (LBC) needed in air quality simulations. The importance of the LBC on O_3 prediction during this period was further studied through a series of sensitivity studies using different forms of LBC. It was shown that the use of the LBC downscaled from RAQMS global model that assimilated MLS and OMI data improves the model performance. We also showed that the predictions can be further improved through the use of LBCs based on NASA DC-8 airborne observations during the ARCTAS-CARB experiment. These results indicate the need to develop observational strategies to improve the representation of the vertical and temporal variations in the air over the eastern Pacific.

The transport of SO_x during the experiment week was also analyzed in Chapter 3. Asian inflows were shown strong on June 22, slightly ($SO_4 < 0.8$ μg/m^3) affecting CA through the mid-altitude. Highly elevated SO_4 and SO_2 in these long-range transported air-masses above 6 km passed CA. SO_x concentrations at the populous California-Mexico border were high, majorly around two sister city pairs. At the San Diego-Tijuana city pair, California and Mexico air crosses the border through opposite directions during day and night; round the Calexico-Mexicali city pair, air travels through various directions. On a particular day of June 24, limited areas at southeast CA were affected by Mexico inflows due to the southerly winds. The high concentrations of SO_x at surface of three regions (South Coast, San Francisco Bay and Central Valley-Fresno) were mostly contributed by local emissions. The SO_x aloft over these regions at mid-troposphere can have varied sources: upwind regions in state or outside of the North America, dependent on the meteorological conditions.

Another focus in Chapter 3 was the comparisons and validation of several SO_x emission inventories, mainly over three important regions in California: South Coast, San Francisco Bay and Central Valley. Modeled SO_x using three different SO_x

emission inventories (NEI 2001, CARB 2005, DS) were compared with various observational datasets (flight, ground and satellites), and all of them need to be further improved spatially and/or temporally. Overall, the terrestrial emissions over south coast and Fresno areas in the central valley were underestimated. It is also critical to add shipping (and other maritime) emissions into inventories because they highly influenced the SO_x distributions at coastal areas and the impacts over south coast and San Francisco areas were quantified. Extended areas such as San-Diego, coastal Mexico and California-Mexico border were also heavily affected by the south coast maritime emissions.

Finally, the input and model calculation resolutions are important for better capturing local features, diurnal cycles, and transport patterns, which can be reflected by both Chapter 2 and 3.

4.2 Future work

For the transport study, we combined the impacts of O_3 precursors on local O_3 levels. In future, the contribution of aerosols and individual O_3 precursors in long-range transported Asian air-masses can be analyzed in detail. The effects of Mexico inflows can be quantified by adding a Mexico tracer. The pollutant transport within the state can also be further studied by using the redistributed tracers.

For the emission study, this analysis only concentrated on the sulfur species. In future work, it is also important to evaluate the other primary chemical species (such as NO_x and CO) in the inventories and the influences of their biases on secondary pollutant distributions, for example, the compositions of secondary PMs, and the O_3 concentrations in connection with NO_x and VOC limitations. In addition, the impacts on primary and secondary pollutants distributions from other emission sectors such as biomass burning and biogenic sources can be quantified.

Finally, this analysis only analyzed a short period (~7 – 10 days). Multi-year comparisons and a longer duration of the experiment-modeling study are recommended, such as CalNex (http://www.esrl.noaa.gov/csd/calnex/) and SARP (http://www.nserc.und.edu/learning/SARP.html).

REFERENCES

Adhikary, B., Carmichael, G. R., Kulkarni, S., Wei, C., Tang, Y., D'Allura, A., Mena-Carrasco, M., Streets, D. G., Zhang, Q., Pierce, R. B., Al-Saadi, J. A., Emmons, L. K., Pfister, G. G., Avery, M. A., Barrick, J. D., Blake, D. R., Brune, W. H., Cohen, R. C., Dibb, J. E., Fried, A., Heikes, B. G., Huey, L. G., O'Sullivan, D. W., Sachse, G.W., Shetter, R. E., Singh, H. B., Campos, T. L., Cantrell, C. A., Flocke, F. M., Dunlea, E. J., Jimenez, J. L., Weinheimer, A. J., Crounse, J. D., Wennberg, P. O., Schauer, J. J., Stone, E. A., Jaffe, D. A., and Reidmiller, D. R.: A regional scale modeling analysis of aerosol and trace gas distributions over the eastern Pacific during the INTEX-B field campaign, Atmos. Chem. Phys., 10, 2091–2115, www.atmos-chem-phys.net/10/2091/2010/, 2010.

Akima, H.: A New Method of Interpolation and Smooth Curve Fitting Based on Local Procedures. J. ACM, 17:4, 589-602, 1970.

Ault, A. P., Moore, M. J., Furutani, H., Prather, K. A.: Impact of Emissions from the Los Angeles Port Region on San Diego Air Quality during Regional Transport Events. Environ. Sci. Technol., 43, 3500–3506, 2009.

BST Associates: Trade impacts study Prepared for Port of Los Angeles, Port of Long Beach and Almeda Corridor Transportation Authority. /http://www.portoflosangeles.org/DOC/REPORT_ACTA_Trade_Impact_Study.pdfS, 2007.

2010 CalNex Science and Implementation Plan, http://www.esrl.noaa.gov/csd/calnex/scienceplan.pdf, 2008

Carter, W. P. L.: Documentation of the SAPRC-99 chemical mechanism for VOC Reactivity Assessment, final report to California Air Resources Board, Contract No. 92-329 and 95-308, 2000.

Chen, F., and Dudhia, J.: Coupling an advanced land-surface/ hydrology model with the Penn State/ NCAR MM5 modeling system. Part I: Model description and implementation, Mon. Wea. Rev., 129, 569–585, 2001.

Chou, M.-D., and M. J. Suarez, 1994: An efficient thermal infrared radiation parameterization for use in general circulation models, NASA Tech. Memo, 104606, 3, 85.

Corbett, J.J., Fischbeck, P.S.: Emissions from ships. Science, 278, 823–824, 1997.

Cooper, O. R., Parrish, D. D., Stohl, A., Trainer, M., Nedelec, P., Thouret, V., Cammas, J. P., Oltmans, S. J., Johnson, B. J., Tarasick, D., Leblanc, T., McDermid, I. S., Jaffe, D., Gao, R., Stith, J., Ryerson, T., Aikin, K., Campos, T.: A. Weinheimer and M. A. Avery: Increasing springtime ozone mixing ratios in the free troposphere over western North America, Nature, 463, 2010, doi:10.1038/nature08708.

Cox, P., Delao, A., Komorniczak, A., and Weller, R.: The California almanac of emissions and air quality 2009 edition. http://www.arb.ca.gov/aqd/almanac/almanac09/almanac2009all.pdf, 2009

Dillon, M. B., Lamanna, M. S., Schade, G.W., Goldstein, A. H., and Cohen, R. C.: Chemical evolution of the Sacramento urban plume: Transport and oxidation, J. Geophys. Res., 107(D5), 4045, doi: 10.1029/2001JD000969, 2002.

Fiore, A., Jacob, D. J., Liu, H., Yantosca, R. M., Fairlie, T. D. and Li, Q.: Variability in surface ozone background over the United States: Implications for air quality policy, J. Geophys. Res., 108(D24), 4787, doi: 10.1029/2003JD003855, 2003.

Fuelberg, H. E., Harrigan, D. L., and Sessions, W.: A meteorological overview of the ARCTAS 2008 mission, Atmos. Chem. Phys., 10, 817–842. http://www.atmos-chem-phys.net/10/817/2010/, 2010.

Giglio, L., Descloitres, J., Justice, C. O., Kaufman, Y. J.,: An Enhanced Contextual Fire Detection Algorithm for MODIS. Remote Sensing of Environment, 87, 273-282, 2003.

Hong, S.-Y., Dudhia, J., and Chen, S.-H.: A Revised Approach to Ice Microphysical Processes for the Bulk Parameterization of Clouds and Precipitation, Mon. Wea. Rev., 132, 103–120, 2004.

IPCC: Contribution of Working Group I to the Fourth Assessment Report of the Intergovernmental Panel on Climate Change. . Climate Change 2007: The

Physical Science Basis. Cambridge, United Kingdom and New York, NY, USA, Cambridge University Press, 2007.

Jacob, D. J., Crawford, J. H., Maring, H., Dibb, J. B., Clarke, A. D., Ferrare, R. A., Hostetler, C. A., Russell, P. B., Singh, H. B., Thompson, A. M., Shaw, G. E., McCauley, E., Pederson, J. R., and Fisher, J. A.: The ARCTAS aircraft mission: Design and execution, Atmos. Chem. Phys. Discuss., 9, 17073–17123, 2009, http://www.atmos-chem-phys-discuss.net/9/17073/2009/.

Jaffe, D. A., Parrish, D., Goldstein, A., Price H., and Harris, J.: Increasing background ozone during spring on the west coast of North America, Geophys.Res Letts, 30(12), 1613, doi:10.1029/2003GL017024, 2003.

Janjic, Z. I.: Comments on "Development and Evaluation of a Convection Scheme for Use in Climate Models", J. Atmos. Sci., 57, 3686, 2000.

Janjic, Z. I.: Nonsingular Implementation of the Mellor–Yamada Level 2.5 Scheme in the NCEP Meso model, NCEP Office Note, No. 437, 61, 2002.

Kim, Y. P., and Seinfeld, J. H.: Atmospheric Gas–Aerosol Equilibrium: III. Thermodynamics of Crustal Elements Ca^{2+}, K^{+}, and Mg^{2+}, Aerosol Science and Technology, 22(1): 93-110, 1995.

Kurata, G., Carmichael, G. R., Streets, D. G., Kitada, T., Tang, Y., Woo, J. H., and Thongboonchoo, N.: Relationships between emission sources and air mass characteristics in East Asia during the TRACE-P period, Atmospheric Environment, 38(40), 6977-6987, 2004.

Lathiere, J., Hauglustaine, D. A., Friend, A. D., De Noblet-Ducoudre, N., Viovy, N., and Folberth, G. A.: Impact of climate variability and land use changes on global biogenic volatile organic compound emissions, Atmos. Chem. Phys, 6, 2129–2146, 2006, www.atmos-chem-phys.net/6/2129/2006/, 2006.

Law, K., Atmospheric chemistry: More ozone over North America, Nature, 463, 307-308, 2010.

Lefohn, A. S., Oltmans, S. J., Dann, T., and Singh, H. B.: Present-day variability of background ozone in the lower troposphere, J. Geophys. Res., 106(D9), 9945 – 9958, 2001.

Lin, C-Y. C., Jacob, D. J., Munger, J. W. and Fiore, A. M.: Increasing background ozone in surface air over the United States, Geophys. Res. Lett., 27(21), 3465-3468, 2001.

Madronich, S., Flocke, S., Zeng, J., Petropavlovskikh, I., and Lee-Taylor, J.: The Tropospheric Ultra-violet Visible (TUV) model Manual, http://www.acd.ucar.edu/TUV, 2002.

McKendry, I. G., Background concentrations of $PM_{2.5}$ and ozone in British Columbia, Canada, http://www.bcairquality.ca/reports/pdfs/background_pm25_ozone.pdf, 2006.

Mesingera, F., DiMego, G., Kalnay, E., Mitchell, K., Shafran, P. C., Ebisuzaki, W., Jovic, D., Woollen, J., Rogers, E., Berbery, E. H., Ek, M. B., Fan, Y., Grumbine, R., Higgins, W., Li, H., Lin, Y., Manikin, G., Parrish, D. and Shi, W.: (2006), North American Regional Reanalysis. Bull. Amer. Meteor. Soc., 87(3), 343–360, DOI: 10.1175/BAMS-87-3-343, 2006.

Mlawer, E. J., S. J. Taubman, P. D. Brown, M. J. Iacono, and S. A. Clough: Radiative transfer for inhomogeneous atmosphere: RRTM, a validated correlated-k model for the longwave. J. Geophys. Res., 102 (D14), 16663–16682, 1997.

Molina, L. T., CalNex 2010 Final Planning Meeting, US-Mexico Collaborative Project on Air Quality and Climate Change in the California-Mexico Border Region. http://www.arb.ca.gov/research/fieldstudy2010/1420-molina.pdf, 2010

Monin, A.S. and A.M. Obukhov: Basic laws of turbulent mixing in the surface layer of the atmosphere. Contrib. Geophys. Inst. Acad. Sci., USSR, (151), 163–187 (in Russian), 1954.

NAS report, global sources of local pollution-An Assessment of Long-Range Transport of Key Air Pollutants to and from the United States, 35 - 66, 2010, http://books.nap.edu/openbook.php?record_id=12743&page=35.

Nolle, M., Ellul, R., Gusten, H., and Heinrich, G.: Long-term background ozone and carbon monoxide measurements on the Maltese Islands, Proceedings of the European Symposium on the Physico Chemical behaviour of Atmospheric Pollutants, September 2001, Turin, Italy.

Oltmans, S. J., Lefohn, A. S., Harris, J. M., and Shadwick, D. S.: Background ozone levels of air entering the west coast of the U.S. and assessment of longer-term changes, Atmos. Environ., 42, 6020-6038, 2008.

OMI O_3 column data source: ftp://toms.gsfc.nasa.gov/pub/omi/data/ozone/Y2008/, 2008.

Parrish, D. D., Millet, D.B., and Goldstein, A. H.: Increasing ozone in marine boundary layer air inflow at the west coasts of North America and Europe, Atmospheric Chemistry and Physics, 9, 1303–1323, www.atmos-chem-phys.net/9/1303/2009/, 2009.

Parrish, D. D., Aikin, K., Oltmans, S. J., Johnson, B., Ives, M.: Impact of Transported Background Ozone on Air Quality in California, ARCTAS California workshop, Preliminary Data Analysis, www.arb.ca.gov/research/ARCTAS/presentations/15_parrish_arctas_july09.pdf, 2009.

Pierce, R. B., Schaack, T., Al-Saadi, J. A., Fairlie, T. D., Kittaka, C., Lingenfelser, G., Natarajan, M., Olson, J., Soja, A., Zapotocny, T., Lenzen, A., Stobie, J., Johnson, D., Avery, M. A., Sachse, G. W., Thompson, A., Cohen, R., Dibb, J. E., Crawford, J., Rault, D., Martin, R., Szykman, J., and Fishman, J. : Chemical data assimilation estimates of continental U.S. ozone and nitrogen budgets during the Intercontinental Chemical Transport Experiment–North America, J. Geophys. Res., 112, D12S21, doi: 10.1029/2006JD007722, 2007.

Real-time, global, sea surface temperature (RTG_SST) analysis data source: ftp://polar.ncep.noaa.gov/pub/history/sst/, 2008.

Skamarock, W. C., Klemp, J. B., Dudhia, J., Gill, D., Barker, D. M., Wang, W., and Powers, J. G.: A Description of the Advanced Research WRF Version 2, www.mmm.ucar.edu/wrf/users/docs/arw_v2.pdf, 2007.

Tang, Y., Carmichael, G. R., Horowitz, L. W., Uno, I., Woo, J.-H., Streets, D. G., Dabdub, D., Kurata, G., Sandu, A., Allan, J., Atlas, E., Flocke, F., Huey, L. G., Jakoubek, R. O., Millet, D. B., Quinn, P. K., Roberts, J. M., Worsnop, D. R., Goldstein, A., Donnelly, S., Schauffler, S., Stroud, V., Johnson, K., Avery, M. A., Singh, H. B., and Apel, E. C.: Multi-scale simulations of tropospheric chemistry in the eastern Pacific and on the U.S. West Coast during spring 2002, J. Geophys. Res., 109, D23S11, doi: 10.1029/2004JD004513, 2004.

Tang, Y. H., Carmichael, G. R., Thongboonchoo, N., Chai, T. F., Horowitz, L. W., Pierce, R. B., Al–Saadi, J. A., Pfister, G., Vukovich, J. M., Avery, M. A., Sachse, G. W., Ryerson, T. B., Holloway, J. S., Atlas, E. L., Flocke, F. M., Weber, R. J., Huey, L. G., Dibb, J. E., Streets, D. G., and Brune, W. H.: Influence of lateral and top boundary conditions on regional air quality prediction: A multi-scale study coupling regional and global chemical transport models, J. Geophys. Res.-Atmos., 112, D10S18, doi: 10.1029/2006JD007515, 2007.

Tang, Y., Lee, P., Tsidulko, M., Huang, H., McQueen, J. T., DiMego, G. J., Emmons, L. K. , Pierce, R. B, Thompson, A. M., Lin, H, Kang, D., Tong, D., Yu, S., Mathur, R., Pleim, J. E., Otte, T. L., Pouliot, G., Young, J. O., Schere, K. L., Davidson, P. M., Stajner, I.: The impact of chemical lateral boundary conditions on CMAQ predictions of tropospheric ozone over the continental United States, Environ Fluid Mech, 9:43–58 doi: 10.1007/s10652-008-9092-5, 2009.

U.S. Environmental Protection Agency: Air quality criteria for ozone and related photochemical oxidants (final), Volumes I, II, and III, EPA 600/R-05/004aF-cF, 2006.

U.S. Census Bureau, Annual Estimates of the Population for the United States, Regions, States, and Puerto Rico: April 1, 2000 to July 1, 2009, http://www.census.gov/popest/states/NST-ann-est.html, 2009

VanCuren, T.: Sulfur in southern California: A CalNex 2010 Special Study. CalNex 2010 Final Planning Meeting, http://www.arb.ca.gov/research/fieldstudy2010/1310-vancuren.pdf, 2010.

Vingarzan, R.: A review of surface ozone background levels and trends, Atm. Env, 38(21), 3431 – 3442, doi:10.1016/j.atmosenv.2004.03.030, 2004.

Vutukuru, S., Dabdub, D.: Modeling the effects of ship emissions on coastal air quality: A case study of southern California. Atmospheric Environment, 42, 3751–3764, 2008.

WRF/Chem Version 3.1 User's Guide, http://ruc.noaa.gov/wrf/WG11/Users_guide.pdf, 2009.